5-2016

Design of a Wide Area Controller Using Eigenstructure Assignment in Power Systems

Parimal Saraf
Clemson University, psaraf@g.clemson.edu

DESIGN OF A WIDE AREA CONTROLLER USING EIGENSTRUCTURE ASSIGNMENT IN POWER SYSTEMS

A Dissertation
Presented to
the Graduate School of
Clemson University

In Partial Fulfillment
of the Requirements for the Degree
Doctor of Philosophy
Electrical and Computer Engineering

---

by
Parimal Saraf
May 2016

Accepted by:
Dr. Elham B. Makram, Committee Chair
Dr. Richard Groff
Dr. Taufiqar Khan
Dr. Anthony Martin
Dr. Ramtin Hadidi

ABSTRACT

Small signal stability has become a major concern for power system operators around the world. This has resulted from constantly evolving changes in the power system ranging from increased number of interconnections to ever increasing demand of power. In highly stressed operating conditions, even a small disturbance such as a load change can make the system unstable resulting in small signal instability. The main reason for small signal instability in power systems is an inter-area mode/s becoming unstable. Inter-area modes involve a group of generators oscillating against each other. Traditionally, power system stabilizers installed on the synchrous machines were used to damp the inter-area modes. However, they may not be very suitable to perform the job since they use local I/O signals which do not have a good controllability/observability of the inter-area modes. Recent advancements in phasor measurement technology has resulted in fast acquisition of time-synchronized measurements throughout the system. Thus, instead of using local controllers, an idea of a wide area controller (WAC) was proposed by the power systems community that would use global signals. This dissertation demonstrates the design of a WAC using eigenstructure assignment technique. This technique provides the freedom to assign a few eigenvalues and corresponding left or right eigenvectors for Multi-Input-Multi-Output (MIMO) systems. This technique forms a good match for designing a WAC since a WAC usually uses multiple I/O signals and a power system only has a few inter-area modes that might lead to instability. The last chapter of this dissertation addresses an important aspect of controller design, i.e., robustness of the controller to uncertainties in operating point and time delay of feedback signals. The operating point of a power system is highly variable in nature and thus the designed

WAC should be able to damp the inter-area modes under these variations. Also, a transmission delay is associated due to routing of remote signals. This time delay is known to deteriorate the performance of the controller. A single controller will be shown to achieve robustness against both these uncertainties.

Dedication

This dissertation is dedicated to my grand parents, parents and sister.

Acknowledgements

I wish to express my gratitude to my adviser, Dr. Elham Makram for her technical guidance, support, kindness and patience throughout the period of research and study at Clemson University.

I want to thank Dr. Ramtin Hadidi for providing valuable technical inputs and always being supportive as a teacher and a friend.

I want to thank Dr. Richard Groff, Dr. Taufiqar Khan and Dr. Anthony Martin for agreeing to be on my committee.

I thank all the fellow students in my group, especially Karthikeyan Balasubramaniam and Puspal Hazra, with whom I had a lot of fruitful discussions throughout the course of my period at the university. Many thanks go to my friends Prateek Kaul, Natraj Chandrasekharan, Rohan Galgalikar, Saurabh Prabhu, Sara Touchet for their constant support and encouragement.

I thank the Department of Electrical and Computer Engineering and the professors with whom I worked through the course of my degree. They helped develop and improve my knowledge of electrical engineering.

Last but not the least I want to thank my parents, grandparents and sister who have always been encouraging and patient. A very special thanks to my lovely wife, Sumedha. Her love and support has made this journey less strenuous.

Contents

List of Figures

List of Tables

1.Introduction

Deregulation and evolution of power markets has led to increased interconnections in the power system leading to complex power flows. The aim of these interconnections is primarily to increase the reliability of operation of the system and allow trading of power between the interconnected areas. Certain operating conditions involve large amounts of power are transferred over these interconnections which results in the system being operated very close to instability. Moreover, the load in the system is continuously increasing without installation of new infrastructure. Thus it is very important to utilize the existing resources efficiently to ensure reliable and stable operation of the grid.

An interconnected power system is composed of multiple dynamic components such a rotating machines, flexible A.C transmission systems (FACTS) devices, dynamic loads etc. Similar to any dynamic system, the response of a power system to disturbances is governed by the modes present in the system. These modes can be categorized into the following four types:

a) Local modes: These modes involve a machine swinging against the rest of the system. The oscillations associated with these modes are localized to one machine or a small portion of the system.

b) Inter-area modes: These modes involve a group of machines oscillating against another group of machines connected through a weak transmission system. These modes are more complex to study and control as they involve multiple machines participating in these modes.

c) Control modes: These modes are associated with poorly tuned controllers in the system such as exciters, governors etc.

d) Torsional modes: These modes are associated with turbine-generator shaft system rotational components.

When a disturbance happens in a system, these modes are excited. These disturbances can be either small changes in the system such as a load change or large changes such a fault. In order for a system to be small-signal stable, all these modes have to be well-damped. If any of the modes is poorly damped, appropriate control action has to be taken. The challenges involved in damping inter-area modes as opposed to the other modes are that multiple synchronous machines participate in them and under stressed conditions even a small disturbance can make them unstable. Some major systems across the world known to have low frequency inter-area oscillations are: Hydro-Quebec (0.6 Hz) [1], Western Interconnected System (0.4 - 1 Hz) [2], Brazilian system (0.15-0.25 Hz) [3], UCTE interconnection in Europe (0.19 - 0.36 Hz) [4]. An important aspect associated with inter-area modes is that they are sensitive to operating conditions. As a result, they have been a major reason for blackouts across the world. The 1996 WECC blackout was a result of a 0.22 Hz inter-area mode becoming unstable due a fault in an already stressed system [5]. The recent 2003 Eastern Interconnect blackout also had an unstable 0.6 Hz inter-area mode after a set of contingencies in the system [6]. Due to the implications of these low frequency modes on the stability of the system, they also limit the amount of power that can be transmitted from one region to another.

1.1. Damping of Inter-area oscillations

Traditionally, Power system stabilizers (PSS), installed on top of the excitation system of the synchronous generators were used for damping electromechanical oscillations in a power system. PSSs were tuned to ensure the damping of local modes. The damp-

ing of these modes is achieved by providing damping torque in phase with speed of the synchronous machines at the natural frequency of the mode through utilization of their excitation systems. The feedback signals used for PSSs were local speed, acceleration or power output signals [7]. In a lot of systems, the I/O signals to the PSS do not have a good controllability/observability of the inter-area modes. Therefore, multiple PSSs need to be coordinated to enhance the damping of these modes. In [8], the impact of parameters and locations of a PSS on the local as well as inter-area modes has been presented. It is invariably the case that a few chosen PSSs are required to participate in the damping of poorly damped inter-area modes. In [9], residue analysis of the stabilizing control loop has been used to select the most effective PSSs in the system and then a Newton Raphson algorithm has been implemented to achieve partial pole assignment for assigning poorly damped modes at better locations. One issue with using PSSs for damping these low frequency oscillations is that they traditionally use local signals that may not have good observability of these modes. Also, it is predicted that with the advent of new technologies, the local modes in the system are expected to be in the range of 4 Hz [10]. Thus, utilizing a PSS for damping local as well as inter-area modes would require them to operate in a wider bandwidth.

The advent of high speed FACTS devices has enabled better control of these oscillations as they are installed close to the tie lines. Series FACTS devices are used to regulate the power flows on tie lines whereas shunt devices regulate bus voltages by injecting reactive power at a bus. A previous work has compared the performance of Static VAr Compensator (SVC), Static Synchronous Compensator (STATCOM) and PSS for damping power system oscillations [11]. In [12, 13], the integration of the dynamic models of FACTS into the power system and the tuning of the parameters of FACTS devices to achieve damping of oscillations has been shown. In [14], a non-linear control technique applied on a Unified Power Flow Controller (UPFC) has

been used to damp the inter-area oscillations. In [15], a unified model of a system comprising of three different types of FACTS devices is developed and their effectiveness in suppressing oscillations is studied using the damping torque analysis. In [16], a supplementary power oscillation damping (POD) loop, comprising of set of lead-lag blocks, on a Thyristor Controlled Switched Capacitor (TCSC) has been tuned to damp the inter-area oscillations in a power system.

Similar to PSSs, POD control loop on FACTS devices can be coordinated with other local controllers in the system. In [17], a nonlinear optimization based framework for simultaneous coordination of supplementary power oscillation damping (POD) control loop on FACTS devices and PSSs has been detailed. The objective function consists of minimizing a cumulative damping index with the constraint that the optimizing variables are within minimum and maximum limits. Another work uses a Quasi-Newton algorithm to minimize a quadratic performance index over a period of time [18]. The method again involves coordination of PSSs and POD loops on FACTS devices to minimize the deviations in tie-line powers as well as generator power outputs. The objective function used is a non-explicit function and thus the algorithm is integrated to a simulation platform to optimize the parameters of the controllable devices. Reference [19] presents an iterative optimization technique that coordinates PSSs and FACTS devices in the system to iteratively relocate the poorly damped eigenvalues to better locations.

Based on the references presented, it is clear that local controllers are not very effective in damping inter-area oscillations. They have a positive impact on damping only when coordinated with other local controllers in the system which might not be the best available option. Further, reference [20] presents a concept of nearly decentralized fixed modes (NDFM) that are inter-area modes that cannot be appreciably shifted using any sort of local controllers in the system. This is because as

mentioned earlier inter-area modes are not very controllable/observable using local signals. In [21], it has been shown that a detrimental interaction is possible between various local controllers such as PSSs, FACTS POD due to lack of knowledge of the global state variables.

1.2. Wide Area Measurement and Control

In order to address the issues faced by local controllers in damping inter-area oscillations, a WAC that utilizes global signals and operates on top of the local controllers has been proposed in [22]. The advantage of using this approach is that it gives the freedom to select the I/O signals of the controller such that inter-area modes have a good controllability/observability metric. In [22], it has been mentioned that under certain scenarios an inter-area mode might be controllable from one area and observable from another. In [23], it has been shown that remote signals rather than local signals give better controllability of the inter-area modes. A majority of previous works use methods based on residuals or/and geometric measures to select I/O signals for the WAC [24–26]. Other available techniques for selecting I/O signals are based on Hankel singular values (HSV) and relative gain array (RGA) [27].

New measurement technology utilizing Phasor Measurement Units (PMU) has made it possible to get fast measurements of various system variables such as voltages, currents, frequencies etc. at sampling rates ranging between 30 samples/sec to 120 samples/sec [28]. The unique feature of this technology is that the measurements throughout the network are time synchronized which enables obtaining a wider picture of the system. Due to a constraint on the number of PMUs that can be installed in the system, they are only deployed at certain strategic locations. These time synchronized measurements from different parts of the system can be fed as

remote signals for designing WACs. In [29], a PSS utilizing local as well as a remote signal obtained from a PMU is tuned to damp inter-area oscillations. In [30], a decentralized/hierarchical MIMO WAC to damp oscillations is designed using an optimization framework utilizing a modal performance measure over a period of time. In [31], a multi-agent based framework is used where a supervisory PSS having an H-infinity control loop is coordinated with local PSSs in each area to damp oscillations in an effective way. A fuzzy logic based rule is used to switch the supervisory PSS robust control loop. In [32], an optimal controller design with structural constraints is proposed with a two-level control structure. However, model order reduction is required to achieve faster convergence of the algorithm presented. Also, one of the important factors considered in this paper is signal transmission delay when using remote signals. In [33], a mixed-objective, output feedback H2/H-infinity synthesis with regional pole placement is presented for designing a WAC for damping inter-area oscillations. The work adopts a hierarchical control structure where the WAC operates on top of the local controllers such as PSSs. A model order reduction technique is employed when using frequency domain robust control techniques in order to save time on computation.

1.3. Eigenstructure Assignment

A WAC designed for a realistic sized power system typically involves selecting multiple I/O signals to make the inter-area modes controllable/observable. Reference [30] has presented a very detailed description of a procedure for designing a MIMO WAC for a large power system. The paper starts with a detailed discussion on selecting the feedback signals and the local controllers that participate in the global control scheme. The parameters of the centralized controller are obtained as a solution to a nonlin-

ear optimization problem that minimizes a modal performance index over time. The paper also presents a comparison of using a decentralized or a global hierarchical control scheme. Even though the work is based on using a modal performance measure, it does not exploit the design freedom available for MIMO systems to modify specific eigenvectors along with the corresponding eigenvalues for improving the dynamic performance of the system. In [34], it was identified that state feedback for MIMO systems provides additional design freedom on top of assigning closed-loop eigenvalues. This controller design method that exploits the degrees of freedom provided by both eigenvalues and eigenvectors for MIMO systems is known as eigenstructure assignment and has been extensively used in aerospace applications [35]. According to [36], all the closed-loop eigenvalues of a MIMO dynamic system can be assigned using output feedback if the sum of the number of inputs and outputs is more than the number of state variables in the system. However, in a realistic power system, this condition will never be satisfied. Furthermore, it would be a worthless activity to assign all the eigenvalues in a power system since only a few of them dominate the dynamic behavior.

There are only a few existent applications of eigenstructure assignment technique for designing controllers in power systems. In [37], a framework for implementing a decentralized control scheme (proportional output feedback based PSSs on machines) based on eigenstructure assignment has been successfully used to damp inter-area oscillations as well as reduce the participation of these modes in certain machine speeds. However, power systems throughout the world have lead-lag type PSSs installed on them. Therefore, replacing them with proportional feedback type PSSs is not a viable option. In [38], a partial left eigenstructure assignment has been presented to design a controller for a doubly fed induction generator (DFIG) in order to reduce the excitation of an inter-area mode and a shaft mode. A dynamic compensator

has been employed to increase the degrees of freedom available for eigenstructure assignment. A multi-objective optimization problem with parametric vectors associated with selected left eigenvectors as the optimizing variables is formulated. In [39], partial right eigenstructure assignment technique has been used to design a robust power system stabilizer. Similar to [38], parametric vectors associated with certain right eigenvectors are used as optimizing variables. The optimization algorithm incorporates multiple operating points in order to attain robustness against operating point changes. Both of these references deal with the design of a local controller on a machine.

The main focus of this dissertation is to study the application of eigenstructure assignment for designing a hierarchical WAC for enhancing the damping of poorly located inter-area modes. The core objectives of this thesis can be sub-divided into two parts:

1) The controller should be capable of assigning the poorly damped inter-area modes to user-specified locations while also assigning the corresponding closed-loop right eigenvectors. The number of I/O signals utilized for achieving the assignment should be less but at the same time should have sufficient controllability/observability of the poorly damped inter-area modes. Since a WAC uses remote I/O signals, the issue of time delay of feedback signals should be addressed in the controller design algorithm. The controller should not only perform for a fixed time delay but should also be robust to uncertainty in time-delay of feedback signals.

2) The operating conditions of a power system constantly vary throughout the day. Therefore, it is very important that the controller should be robust to changes in operating conditions. In other words, the controller should be capable of improving the damping of inter-area modes of interest under varying operating conditions. This performance requirement should be satisfied in addition to the controller being robust

to uncertainty in time-delay of feedback signals.

1.4. Dissertation Contents

Chapter 2 provides a basic background of modeling various dynamic components in a power system and describes the small-signal analysis of a linearized power system model around an operating point. Chapter 3 presents a detailed description of eigenstructure assignment technique applied to the design of a WAC. A quadratic programming based approach has been used to obtain the dynamic compensator based controller. Two projection techniques have been presented and compared for assigning the closed-loop right eigenvectors corresponding to the poorly damped inter-area modes. A multi-model optimization scheme has been presented in the later part of the chapter that makes the designed controller robust to uncertainty in time delays of feedback signals. The algorithm has been applied on the IEEE 68 bus system and the performance of the controller in improving the damping of poorly located inter-area modes has been validated.

Chapter 4 addresses the issue of robustness of the controller to changing operating conditions. A multi-model optimization approach, different from the one presented in chapter 3, has been used to tune a WAC obtained from chapter 3 in order to make it robust. Two different approaches have been presented to select the models to be included in the multi-model optimization. The first approach uses models that are known to be stressed operating conditions of the system. The second approach presents a method to select models such that the designed controller is robust to changes in a specific parameter of the system. The second approach also accounts for variability in time delay of feedback signals. Two different methods based on eigenstructure assignment and first order eigenvalue sensitivity have been used to

formulate the optimization problem. At the end of chapter 4, a controller that is robust to operating point changes as well as uncertainty in time-delay of feedback signals is obtained. Similar to chapter 3, this controller has been designed, tested and validated for the IEEE 68 bus system.

Chapter 5 provides the conclusions of this dissertation and presents the avenues for future research in this area. There is an appendix that aids in understanding some of the material presented in this dissertation.

2.Power System Modeling and Small Signal Stability

The main focus of this chapter is to provide a background on modeling and stability of interconnected power systems. Since the essence of this dissertation is the analysis and control of inter-area oscillations, more focus is placed on small-signal stability of the system.

An interconnected power system comprises of a number of dynamic devices that need to be modeled and combined together to obtain a unified non-linear dynamic model of the system. This non-linear model is linearized around an operating point to obtain the state space model of the system and an eigen-analysis is performed on this model to determine the eigenvalues and eigenvectors of the dynamic system. The relationship of eigenvalues and eigenvectors with the dynamic response of the system will form the foundation for the future chapters.

2.1. Dynamic Modeling

Synchronous Machine

Synchronous machines form the primary source of electric energy in the system. They form the basis of power system stability since they govern the dynamics of the system. Power system stability is the ability of keeping the interconnected synchronous machines in synchronism. Therefore, the understanding of their modeling and dynamic behavior is of utmost importance. The number of dynamic equations (dynamic order) describing the behavior of the synchronous machine can be chosen by the user

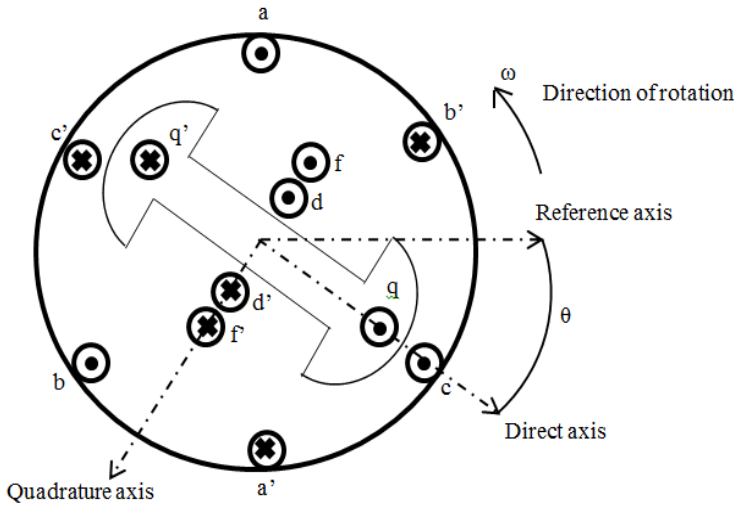

Figure 2.1.: Schematic of a synchronous machine with two poles

depending upon the purpose of study. In this work, a sixth order model has been used [40].

The dynamic equations of the sixth order model used in this work are given below in (2.1) – (2.6).

$$\dot{\delta} = \Omega_b(\omega - \omega_s) \tag{2.1}$$

$$\dot{\omega} = \frac{1}{2H}(P_m - P_e - D(\omega - \omega_s)) \tag{2.2}$$

$$\dot{e'_q} = (-e'_q - (x_d - x'_d - \gamma_d)i_d + (1 - \frac{T_{AA}}{T'_{d0}})e_{fd})/T'_{d0} \tag{2.3}$$

$$\dot{e'_d} = (-e'_d + (x_q - x'_q - \gamma_q)i_q)/T'_{q0} \tag{2.4}$$

$$\dot{e''_q} = (-e''_q + e'_q - (x'_d - x''_d + \gamma_d)i_d + \frac{T_{AA}}{T'_{d0}}e_{fd})/T''_{d0} \tag{2.5}$$

$$\dot{e''_d} = (-e''_d + e'_d + (x'_q - x''_q + \gamma_q)i_q)/T''_{q0} \tag{2.6}$$

The stator side electric equations are given by:

$$0 = r_a i_d + \psi_q + v_d \tag{2.7}$$

$$0 = r_a i_q - \psi_d + v_q \tag{2.8}$$

where:

$\gamma_d = \frac{T''_{d0}}{T'_{d0}} \frac{x''_d}{x'_d}(x_d - x'_d)$, $\gamma_q = \frac{T''_{q0}}{T'_{q0}} \frac{x''_q}{x'_q}(x_q - x'_q)$

δ is the machine rotor angle

ω is the machine angular speed

e'_q is the transient quadrature axis voltage

e'_d is the transient direct axis voltage

e''_q is the sub-transient quarature axis voltage

e''_d is the sub-transient direct axis voltage

H, D are the machine inertia and damping respectively

$e_{fd}$is the field voltage

x_d, x'_d, x''_d are the direct axis synchronous, transient and sub-transient reactances respectively

x_q, x'_q, x''_q are the quadrature axis synchronous, transient and sub-transient reactances respectively

T'_{d0}, T''_{d0} are the direct axis transient and sub-transient field winding time constants respectively

T'_{q0}, T''_{q0} are the quadrature axis transient and sub-transient field winding time constants respectively

T_{AA} is the d-axis additional leakage time constant

P_m, P_e are the input mechanical power and output electrical power respectively

The initial values of v_d and v_q are obtained using the power flow solution that yields

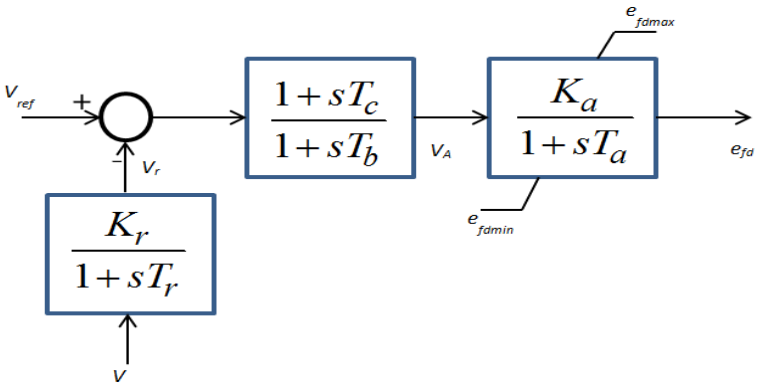

Figure 2.2.: Block diagram of a simple excitation system

P_g,Q_g, $V\angle\theta$ at the generator bus.

$$I = \left(\frac{P_g + i * Q_g}{V}\right)^* \tag{2.9}$$

$$\delta = \angle(V + (r_a + i * x_q)I) \tag{2.10}$$

$$v_d = Vsin(\delta - \theta) \tag{2.11}$$

$$v_q = Vcos(\delta - \theta) \tag{2.12}$$

The voltages v_d and v_q are obtained by converting the bus voltage V from network reference frame to machine reference frame. The current I is also rotated by an angle $(\frac{\pi}{2} - \delta)$ to convert it to the machine reference frame.

Excitation Systems

The basic function of the excitation system is to provide direct current to the field winding of the synchronous machine. The excitation system controls the voltage and reactive power and aids in enhancing system stability. Excitation system can be D.C, A.C or static [41]. A block diagram of a simple excitation system has been shown in fig. 2.2. The dynamic equations representing the system have been given in (2.13) -

(2.15).

$$\dot{V}_r = \frac{(K_r V - V_r)}{T_r} \tag{2.13}$$

$$\dot{V}_{as} = \left(\left(1 - \frac{T_c}{T_b}\right)(V_{ref} - V_r) - V_{as}\right)/T_b \tag{2.14}$$

$$\dot{e}_{fd} = \frac{(K_a V_A - e_{fd})}{T_a} \tag{2.15}$$

where V_{as} is the internal state variable associated with the lead-lag block.

Governor

The governor has the responsibility to control the power output of the synchronous machine and thus the frequency. The droop controls the amount of change in power with change in frequency. The purpose of droop is to enable parallel operation of multiple generators. The time constants associated with governor controls are small and are slow acting. Governor is used for relatively slower control actions such as automatic generation control (AGC). The block diagram of a simple governor has been shown in fig. 2.3. The dynamic equations associated with the governor have been given in (2.16) – (2.18).

$$\dot{x}_{g1} = \frac{(P_{in} - x_{g1})}{T_1} \tag{2.16}$$

$$\dot{x}_{g2} = \left(\left(1 - \frac{T_3}{T_2}\right)x_{g1} - x_{g2}\right)/T_2 \tag{2.17}$$

$$\dot{x}_{g3} = \left(\left(1 - \frac{T_5}{T_4}\right)\left(x_{g2} + \frac{T_3}{T_2}x_{g1}\right) - x_{g3}\right)/T_4 \tag{2.18}$$

where x_{g1}, x_{g2} and $x_{g3}$are the internal state variables of the governor control blocks.

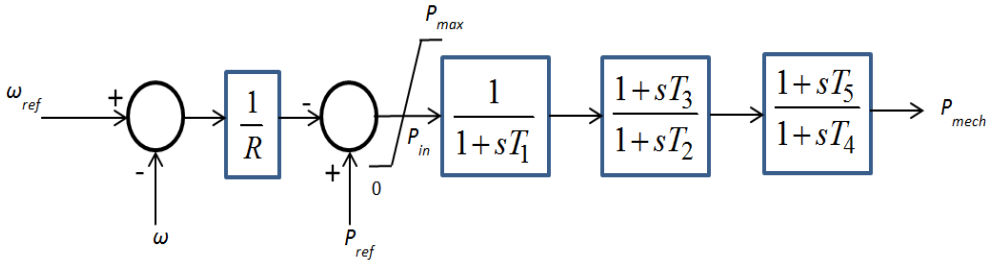

Figure 2.3.: Block diagram of a simple governor-turbine system

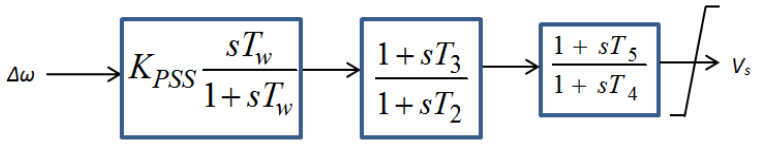

Figure 2.4.: Block diagram of a PSS

Power System Stabilizer (PSS)

The main purpose of PSS is to add a supplementary damping signal to the excitation system. PSS uses feedback signals such as generator speed, generator power or generator acceleration to produce the supplementary signal. PSS produces a damping torque in phase with the rotor speed deviations in order to aid in oscillation damping. The basic block diagram of PSS has been shown in fig. 2.4.

The dynamic equations associated with the PSS are given in (2.19) - (2.21)

$$\dot{v}_1 = \frac{(P_{in} - x_{g1})}{T_1} \tag{2.19}$$

$$\dot{v}_2 = \left(\left(1 - \frac{T_3}{T_2}\right)(K_{PSS}\Delta\omega + v_1) - v_2\right)/T_2 \tag{2.20}$$

$$\dot{v}_3 = \left(\left(1 - \frac{T_5}{T_4}\right)\left(v_2 + \left(\frac{T_3}{T_2}(K_{PSS}\Delta\omega + v_1)\right)\right) - v_3\right)/T_4 \tag{2.21}$$

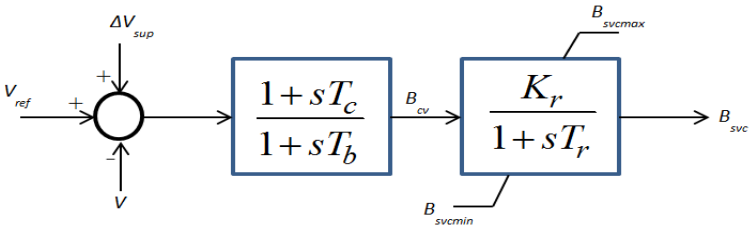

Figure 2.5.: Block diagram of a SVC

Static VAR Compensator (SVC)

A SVC is a shunt FACTS device that injects reactive power at the point of connection. It is mainly used to support voltages in the system. It can also be utilized for damping inter-area oscillations by providing a supplementary signal to the voltage reference through a supplementary control loop. The basic block diagram of PSS has been shown in fig. 2.5.

$$\dot{B}_{con} = \left(\left(1 - \frac{T_c}{T_b} \right) (V_{ref} + \Delta V_{sup} - V) - B_{con} \right) / T_b \tag{2.22}$$

$$\dot{B}_{svc} = \frac{(K_r B_{cv} - B_{svc})}{T_r} \tag{2.23}$$

where $B_{con}$is the internal state variable of the lead-lag block. ΔV_{sup} is the signal that comes from a supplementary control loop to enable SVC to participate in damping of oscillations.

2.2. Small Signal Stability and Linearized Model of a Power System

As mentioned earlier, a power system is a highly interconnected dynamic system. In order to analyze the stability of this system as a whole, a non-linear differential

algebraic model is obtained by combining the differential equations of various components enlisted in the previous section and the algebraic equations associated with the network [41]. The differential algebraic equations of the power system have been given in (2.24) - (2.26) [40].

$$\dot{x} = f(x, x_a, u) \tag{2.24}$$

$$0 = g(x, x_a, u) \tag{2.25}$$

$$y = h(x, x_a, u) \tag{2.26}$$

where x are the state variables of the system, x_a is the vector of algebraic variables, u is a vector of input variables, f is a vector of differential equations, g is a vector of algebraic equations, h is a vector of output equations and y is the output vector of the system. Small signal stability deals with the analysis of equilibrium points where $\dot{x} = 0$. The primary step towards small signal analysis is to determine the state space matrices of the power system around an equilibrium point. The equilibrium point is obtained by running a load flow of the system. Following load flow, there are two methods to obtain the state space matrices of the system around an equilibrium point:

1) Using analytic jacobian.

2) Numerical approximation.

The modeling and control implementation presented in this dissertation have been carried out in a MATLAB based toolbox called power system toolbox (PST) [42]. PST uses the numerical perturbation approach for obtaining the state space matrices. A partitioned explicit approach is used where the differential and algebraic variables are updated separately [43]. The method involves perturbing the variable x and u and obtaining the matrices $\frac{\Delta f}{\Delta x}$, $\frac{\Delta f}{\Delta u}$, $\frac{\Delta h}{\Delta x}$, $\frac{\Delta h}{\Delta u}$. Thus the state space representation of the system is given as:

$$\dot{x} = Ax + Bu \tag{2.27}$$

$$y = Cx + Du \tag{2.28}$$

where $A \in R^{n \times n}$, $B \in R^{n \times m}$, $C \in R^{r \times n}$ and $D \in R^{r \times m}$ is the output vector. The matrix D is always a zero matrix since the transfer functions associated with different dynamic components of a power system are proper. Once the linearized model of the power system is obtained, its stability and response around that operating point is governed by the eigenvalues. The n eigenvalues of the system can be determined by finding the roots of the characteristic equation given in (2.29).

$$det(A - \lambda_i I) = 0 \tag{2.29}$$

where $I^{n \times n}$ is an identity matrix. The eigenvalues can be represented as $\sigma_i \pm j\kappa_i$ where $\kappa_i = 0$ for purely real ones and $\sigma_i = 0$ for purely imaginary ones. The system is stable iff all $\sigma_i \leq 0$. Two important parameters associated with any eigenvalue are the damping, ζ_i and frequency, f_i of that eigenvalue. These are given as:

$$\zeta_i = \frac{-\sigma_i}{\sqrt{\sigma_i^2 + \kappa_i^2}} \tag{2.30}$$

$$f = \frac{\kappa_i}{2\pi} \tag{2.31}$$

The right and left eigenvectors, v_i and u_i, are determined using (2.32) and (2.33) respectively.

$$Av_i = \lambda_i v_i \tag{2.32}$$

$$w_i A = w_i \lambda_i \tag{2.33}$$

The significance of right eigenvector is that its elements indicate the relative activity of a state variable in a mode whereas the elements of left eigenvector indicate the contribution of a state variable to a mode. In order to normalize the relationship between state variables and modes, a matrix called as *participation matrix* P is defined [41]. The i^{th} column of P has been shown in (2.34).

$$p_i = \begin{bmatrix} p_{1i} \\ p_{2i} \\ . \\ . \\ p_{ni} \end{bmatrix} = \begin{bmatrix} v_{1i}w_{i1} \\ v_{2i}w_{i2} \\ . \\ . \\ v_{ni}w_{in} \end{bmatrix} \tag{2.34}$$

Electromechanical modes are the system modes associated with machine rotor state variables (angle and speed). As mentioned in chapter 1, electromechanical modes normally lie in the low frequency range ranging from 0.2 Hz to 2.5 Hz. The electromechanical modes that have a high participation in a specific machine's rotor state variables (angle and speed) are the local modes associated with that machine. On the other hand, an inter-area mode involves multiple machine rotor state variables participating in it. Participation factor analysis aids in choosing the location of installing a controller in case an electromechanical mode is poorly damped.

The poorly damped electromechanical modes in the system are known as the critical modes. This dissertation specifically involves the study and control of critical inter-

area modes. Using the analysis presented till now, the main challenges associated with the damping of inter-area modes are that:

1) In a large power system, since multiple machines participate in inter-area modes, usually there is no one location where a local controller can alleviate the problem.

2) In a stressed operating condition, even a small disturbance can make them migrate into the right half plane or in other words make the system unstable.

Therefore, a centralized WAC has been proposed in the literature and implemented in this work for enhancing the damping of critical inter-area modes. The rapid development in phasor measurement technology has made possible the use of remote feedback signals for control. A generic schematic of a WAC has been shown in fig. 2.6. It is worth noting that the WAC can be either designed as a state feedback or an output feedback controller. However, since the number of state variables in a realistic power system is large, state feedback controller is not a feasible choice. Therefore, this dissertation studies and implements an output feedback WAC and that is what has been shown in fig. 2.6.

The first step towards designing the WAC involves selecting appropriate I/O signals such that inter-area modes are controllable/observable. The participation factor does not link the system modes to system input and outputs (only depends on the state matrix). Therefore, the residue method has been used in this work [24]. Residue provides a combined metric of controllability and observability of a mode using the chosen I/O signals. The transfer function $G(s)$ of the power system can be written in terms of the residues as:

$$G(s) = \frac{y(s)}{u(s)} = \sum_{i=1}^{n} \frac{R_i}{s - \lambda_i} \tag{2.35}$$

where,

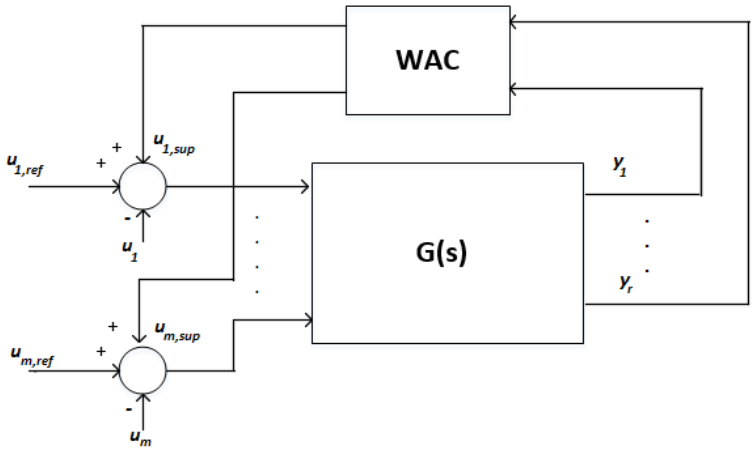

Figure 2.6.: Schematic of a WAC

$$R_i = ||Cv_i u_i^T B|| \tag{2.36}$$

The residue R_i for the i^{th} mode is also the sensitivity of that mode to a general feedback gain K or in other words, the impact that a small change in a proportional feedback gain K will have on the eigenvalue λ_i.

Therefore, in fig. 2.6, the signals $u_{1,sup}$,...,$u_{m,sup}$ are supplementary signals provided by the WAC. The user selects the dimension m and r by choosing the signals that enable control of the critical inter-area mode. Once, the appropriate I/O signals are selected, the next step is to design the controller that improves the damping of the critical inter-area mode/s without impacting the rest of the modes in a negative way.

The rest of the dissertation targets the design of a WAC for enhancing the damping of critical inter-area modes using eigenstructure assignment.

3.Design of a Wide Area Controller

This chapter demonstrates the application of partial right eigenstructure assignment for designing an output-feedback based WAC in a power system. The unique feature of the controller is that it utilizes the additional design freedom provided by right eigenvectors along with eigenvalue placement to improve the dynamic behavior of the system. The fact that multi-input-multi-output (MIMO) systems provide more design freedom than just manipulating the eigenvalues of the system has been exploited for controller design. Supplementary loops on two static VAR compensators (SVC) have been utilized to achieve the damping of oscillations. The advantage of using SVC (or any other FACTS devices) is that it is better suited for damping of inter-area oscillations since it is installed directly on the tie-line and it ensures low interaction with the local electromechanical modes of the system. A very important aspect of designing a WAC is its robustness against time delay of feedback signals. This chapter also presents a multi-model optimization strategy to deal with uncertainty in time delays.

A number of existing techniques involve coordinating the decentralized controllers (PSSs, FACTS PODs) in the system using optimization techniques such that all the eigenvalues of the system follow the minimum damping criterion (normally set to be 5%) [9], [44], [45] . These methods are based on moving poorly damped poles to well damped locations. However, it is a well-known fact that the transient response of a system is governed by not only the eigenvalues but also the eigenvectors. In [34], it was first shown that MIMO systems provide more design freedom than assignment of eigenvalues for the case of state feedback. In [36], the necessary and sufficient conditions for exploiting additional degrees of freedom on top of assigning the eigenvalues

was presented for the case of output feedback. Depending upon the number of inputs and outputs of the MIMO systems, a limited number of eigenvalues and associated right or left eigenvector can be appropriately assigned. In a typical power system, there are only a few inter-area modes that are of concern. Therefore, eigenstructure assignment forms a suitable technique to assign these critical inter-area modes along with the corresponding right eigenvectors. Feedback signal selection plays an important role to ensure that the critical inter-area modes are controllable (have a good I/O controllability metric/residue) while the local modes have a low I/O controllability metric.

This chapter presents the design of a hierarchical, WAC that operates on top of local controllers in order to damp inter-area oscillations. The unique feature of the algorithm is that it formulates the controller design problem as a quadratic optimization problem which can be solved in a single step (being a convex problem) [46, 47]. Unlike [38], a transfer function representation of the dynamic compensator has been used where the numerator coefficients of the elements of the compensator form the optimizing variables. The denominator poles as well as closed-loop right eigenvectors corresponding to the inter-area modes have to be pre-assigned in order to formulate the controller design problem as a quadratic optimization problem. For this purpose, a SVD based technique is used to determine the basis vectors for each achievable (or assignable) closed-loop right eigenvector [46]. This is followed by determining the weights to be used with these basis vectors to obtain the closed-loop right eigenvectors using projection techniques [48, 49] . Two projection techniques utilizing open-loop right eigenvector projection and weighted open-loop eigenvector projection using participation factors of the state variables in the inter-area modes have been employed and compared. Reference [49] has shown that utilization of open-loop right eigenvector projection to obtain the closed-loop right eigenvector results in a robust

closed-loop system (small condition number of the closed loop modal matrix). It has to be noted that although the system under study already consists of local controllers, it is still considered as an open-loop for the purpose of eigenvector projection since a hierarchical control structure has been adopted.

An important aspect involved in the design of a WAC is the time delay of feedback signals. In [50, 51], it has been shown that communication latency or time delay of feedback signals degrades the performance of the controller. Design of a WAC considering time delays has been addressed using robust control techniques [52], incorporation of time delay into system model using Pade approximation [32] and using delay-dependent stability analysis [53]. In [54], a mu synthesis approach has been used to design a robust controller with time delay as an uncertain parameter. In this chapter, a multi-model optimization problem based on partial right eigenstructure assignment has been formulated to design a WAC robust to uncertain time delays. Pade approximation has been used to approximate the time delay as a rational transfer function [32].

3.1. Controller Design Using Quadratic Programming

Partial Right Eigenstructure Assignment

Consider the linearized model of a power system around an operating point as:

$$\dot{x} = Ax + Bu \tag{3.1}$$

$$y = Cx + Du \tag{3.2}$$

where $x \in R^{n\times 1}$ is the state vector, $u \in R^{m\times 1}$ and $y \in R^{r\times 1}$ is the output vector. The free response of the system from an initial state without any inputs is given as:

$$x_i(t) = \sum_{i=1}^{n} v_{ji} c_j e^{\lambda_j t} \tag{3.3}$$

$$c_j = \sum_{k=1}^{n} w_{jk} x_k(0) \tag{3.4}$$

where v_i, w_i are the right and left eigenvectors of eigenvalue λ_i respectively and $x(0)$ is the initial state vector. Therefore, the eigenvalues control the rate of decay whereas the right eigenvector determines the shape of response.

The elements of right eigenvector determine the relationship between the state variables and the associated mode. For a MIMO system, a few selected eigenvalues and eigenvectors can be appropriately manipulated in order to improve the dynamic performance of the system. In the case of proportional feedback, partial right eigenstructure assignment technique is capable of assigning r eigenvalues and corresponding r eigenvectors [38]. Let a proportional output feedback controller, $u = Ky$, be connected to the system in (3.1) and (3.2). This results in the closed-loop state matrix being $(A + BKC)$. Assume $i = 1...q \leq r$ controllable eigenvalues are to be assigned to locations λ_i . Then, the closed loop system has to satisfy (3.5).

$$(A + BKC)v_i = \lambda_i v_i \tag{3.5}$$

where $v_i \in \mathbb{C}^{(n)\times 1}$ is the corresponding closed-loop right eigenvector. The problem of eigenstructure assignment can be presented as the determination of controller K that achieves the assignment of λ_i and v_i. Once the location of λ_i is selected, the next step is to determine v_i that can be assigned. **Unlike a SISO system, a MIMO system can have multiple options for selecting a right eigenvector associated to an**

eigenvalue. The equation (3.5) can be restructured into equations (3.6) and (3.7) shown below.

$$\begin{bmatrix} A - \lambda_i I & B \end{bmatrix} \begin{bmatrix} v_i \\ f_i \end{bmatrix} = 0 \tag{3.6}$$

$$where,\ KCv_i = f_i \tag{3.7}$$

The vector $f_i \in \mathbb{C}^{m\times 1}$ is known as the input-direction. It should be noted that the eigenvector, v_i, to be assigned cannot be chosen arbitrarily. It can be inferred from (5) that the achievable vector $\begin{bmatrix} v_i & f_i \end{bmatrix}^T$ can only belong to the null-space of the matrix $\begin{bmatrix} A - \lambda_i I & B \end{bmatrix}$. In other words, the achievable $\begin{bmatrix} v_i & f_i \end{bmatrix}^T$ corresponding to an eigenvalue is some linear combination of the basis vectors of the null space of matrix $\begin{bmatrix} A - \lambda_i I & B \end{bmatrix}$. The rank of this null-space is the same as the dimension of B. Therefore, higher the dimension of B, the more is the degree of freedom available for eigenvector assignment. Singular value decomposition (SVD) is used to determine the null space of $\begin{bmatrix} A - \lambda_i I & B \end{bmatrix}$ and obtain the basis vectors for the achievable closed-loop right eigenvector. The right singular matrix can be split into sub-matrices as given in (3.8).

$$Z = \begin{bmatrix} Z_{11} & Z_{12} \\ Z_{21} & Z_{22} \end{bmatrix} \tag{3.8}$$

The columns of $Z_{12} \in \mathbb{C}^{n\times m}$ form the basis vectors for achievable v_i and columns of $Z_{22} \in \mathbb{C}^{m\times m}$ form the basis vectors for the achievable f_i. Let $\eta_i \in \mathbb{C}^{m\times 1}$ be the weights to be used with the basis vectors to obtain the achievable $\begin{bmatrix} v_i & f_i \end{bmatrix}^T$. The vector η_i can be determined by projecting a desired eigenvector v_d onto the subspace spanned by the columns of as shown in (3.9) [55].

$$\eta_i = \left(Z_{12}^T Z_{12}\right)^{-1} Z_{12}^T v_d \tag{3.9}$$

Then the achievable v_i and f_i are obtained as shown in (3.10).

$$v_i = Z_{12}\eta_i,\ f_i = Z_{22}\eta_i, \tag{3.10}$$

Traditionally in power systems, v_d is selected such that the participation of certain machine speeds in inter-area modes is reduced [37,38]. Here two options of obtaining η_i have been compared:

1) $\eta_i = \left(Z_{12}^T Z_{12}\right)^{-1} Z_{12}^T v_{i,ol}$ where $v_{i,ol}$ is the open-loop right eigenvector.

2) $\eta_i = \left(Z_{12}^T P Z_{12}\right)^{-1} Z_{12}^T P v_{i,ol}$ where P is a diagonal matrix consisting of the participation factors of mode i.

The elements of the right eigenvector determine the impact on respective system state variables if the corresponding mode is excited. Thus, the aim of using open loop right eigenvector projection is to avoid a drastic change in the dynamic behavior of system when closing the feedback loop. This projection technique is also known to result in robust design and small control gains [49]. The second projection technique scales the open-loop right eigenvector by the participation factor. The logic behind this approach is that all the state variables do not participate equally in a mode. Therefore, weights are introduced in the projection problem of (3.9) by utilizing the participation factor of the respective mode. Results using both the options will be presented and compared.

Once v_i and f_i are determined, the feedback gain required for assignment of eigenvalue/eigenvector pairs can be obtained using (3.7) and is given in (3.11):

$$K = \begin{bmatrix} f_1 & \dots & f_q \end{bmatrix} \left(L^T L\right)^{-1} L^T \tag{3.11}$$

where $L = C \begin{bmatrix} v_1 & \dots & v_q \end{bmatrix}$.

Dynamic Compensator

Previous section dealt with partial right eigenstructure assignment for the case of proportional feedback. However, since this work uses a dynamic compensator, new necessary and sufficient conditions have to be enlisted. The dynamic extension causes the state space of the closed-loop system to belong to $R^{(n+n_a)\times 1}$ where $x_c \in R^{n_a \times 1}$ are the state variables added by the compensator. Therefore, the closed-loop right eigenvector can be expressed as $\begin{bmatrix} \mathtt{v_i} & \mathtt{v_{ci}} \end{bmatrix}$ where $\mathtt{v_i}$ represents the right sub-eigenvector belonging to $\mathbb{C}^n$ and $\mathtt{v_{ci}}$ represents the right sub-eigenvector belonging to $\mathbb{C}^{n_a}$. The main reason for utilizing a dynamic compensator is that it increases the number of eigenvalues and eigenvectors that can be assigned to $r + n_a$ [38].

An important result used in this paper is that even though the dynamic order of the closed-loop system increases to $r + n_a$, the assignment problem still depends on the right sub-eigenvector $\mathtt{v_i}$ [47]. Let's assume that the compensator in the state space form is represented by matrices (A_c, B_c, C_c, D_c). The controller transfer function is shown in (3.12).

$$K(s) = C_c(sI - A_c)^{-1}B_c + D_c \tag{3.12}$$

The closed-loop state space matrix obtained by applying (A_c, B_c, C_c, D_c) on the system given in (3.1) and (3.2) is given in (3.13).

$$A_{cl} = \begin{bmatrix} A + BD_cC & BC_c \\ B_cC & A_c \end{bmatrix} \tag{3.13}$$

where $A_c \in R^{n_a \times n_a}$, $B_c \in R^{n_a \times r}$, $C_c \in R^{m \times n_a}$, $D_c \in R^{m \times r}$. Let's assume that the closed-loop eigenvalues are represented by $\lambda_{i,cl}$. Then A_{cl} has to satisfy (3.14).

$$\begin{bmatrix} A + BD_cC & BC_c \\ B_cC & A_c \end{bmatrix} \begin{bmatrix} \mathtt{v_i} \\ \mathtt{v_{ci}} \end{bmatrix} = \lambda_{\mathtt{i,cl}} \begin{bmatrix} \mathtt{v_i} \\ \mathtt{v_{ci}} \end{bmatrix} \tag{3.14}$$

This matrix representation can be split into two equations given in (3.15) and (3.16).

$$(A + BD_cC)\mathtt{v_i} + BC_c\mathtt{v_{ci}} = \lambda_{\mathtt{i,cl}}\mathtt{v_i} \tag{3.15}$$

$$(BC_c)\mathtt{v_i} + A_c\mathtt{v_{ci}} = \lambda_{\mathtt{i,cl}}\mathtt{v_{ci}} \Rightarrow \mathtt{v_{ci}} = (\lambda_{i,cl}I - A_c)^{-1}B_cC\mathtt{v_i} \tag{3.16}$$

Substitution of $\mathtt{v_{ci}}$ obtained in (3.16) into (3.15) results in the relationship shown in (3.17).

$$(A + BD_cC + BC_c(\lambda_{i,cl}I - A_c)^{-1}B_cC)\mathtt{v_i} = \lambda_{\mathtt{i,cl}}\mathtt{v_i} \tag{3.17}$$

Utilization of (3.12) in (3.17) results in (3.18).

$$(A + BK(\lambda_{\mathtt{i,cl}})C)\mathtt{v_i} = \lambda_{\mathtt{i,cl}}\mathtt{v_i} \tag{3.18}$$

The above relationship proves that even though the compensator adds some state variables to the system, the assignment still depends on the first n elements ($\mathtt{v_i}$) of the closed-loop right eigenvector. In other words, (3.7) still holds with the exception that K is replaced by $K(\lambda_{\mathtt{i,cl}})$. This is an important result that is used in the formulation

of the eigenstructure assignment problem in later sections. An eigenvalue/eigenvector pair $(\lambda_{\mathtt{i,cl}}, \mathtt{v_i})$ can be assigned by dynamic feedback $K(s)$ iff (3.19) is satisfied.

$$K(\lambda_{\mathtt{i,cl}})C\mathtt{v_i} = \mathtt{f_i} \tag{3.19}$$

If $\lambda_{\mathtt{i,cl}}$ is a complex eigenvalue (as will be in the case of an inter-area mode), a similar constraint corresponding to complex conjugates $(\overline{\lambda}_{\mathtt{i,cl}}, \overline{\mathtt{v}}_{\mathtt{i}}, \overline{\mathtt{f}}_{\mathtt{i}})$ has to be satisfied.

Quadratic Programming

The design objectives of partial right eigenstructure assignment comprise of assigning some critical eigenvalues and corresponding closed-loop right eigenvectors using (3.6) - (3.10). Then (3.19) and its conjugate equivalent are the constraints that the gain has to satisfy in order to assign the complex eigenvalue/eigenvector pair. Furthermore, bounds can be imposed on the numerator coefficients. Thus a quadratic programming based optimization is formulated utilizing the dynamic compensator. This paper uses a transfer function representation of the dynamic compensator. The quadratic programming formulation is made possible by specifying the denominator coefficients of the compensator *a priori*. Thus, the optimization variables are the numerator coefficients. The degree of the numerator determines the number of optimizing variables in the system. If the algorithm does not converge with a specific order of the numerator, the order can be increased with the constraint that the degree of numerator cannot be greater than the denominator. A general k^{th} order dynamic compensator matrix is given in (3.20).

$$\begin{bmatrix} \frac{b_{111}s^k+.....+b_{(k+1)11}}{s^k+a_{111}s^{k-1}+.....+a_{k11}} & \cdots & \frac{b_{11r}s^k+.....+b_{(k+1)1r}}{s^k+a_{11r}s^{k-1}+.....+a_{k1r}} \\ \cdots & \cdots & \cdots \\ \cdots & \cdots & \cdots \\ \frac{b_{1m1}s^k+.....+b_{(k+1)m1}}{s^k+a_{1m1}s^{k-1}+.....+a_{km1}} & \cdots & \frac{b_{1mr}s^{k-1}+.....+b_{(k+1)mr}}{s^k+a_{1mr}s^{k-1}+.....+a_{kmr}} \end{bmatrix} \tag{3.20}$$

where $b_{1mr}.....b_{(k+1)mr}$ represent the numerator coefficients and $a_{1mr}.....a_{kmr}$ represent the denominator coefficients of the element (m, r) of the compensator. The constraint (3.19) is made linear by pre-assigning the pair $(\mathtt{v_i}, \mathtt{f_i})$ using projection methods already presented. The optimization problem can be stated as shown below [47, 56].

Quadratic cost function: The cost function consists of minimizing the sum of Frobenius norm of the compensator at l different frequencies typically around the eigenvalues to be shifted as shown in (3.21). This norm of the controller at a given frequency signifies the amount of energy required for the control action at that particular frequency [44, 57]. Therefore, minimizing J ensures reduction in average control energy over frequencies $i = 1....l$ and it can be expressed as a quadratic function in terms of the optimizing variables (numerator coefficients).

$$Minimize\, J = \sum_{i=1}^{l} ||K(j\omega_i)||_F^2 \tag{3.21}$$

Equality constraints: For $i = 1....q$ complex eigenvalue/eigenvector assignments, the $2q$ equality constraints are given in (3.22) and (3.23).

$$K(\lambda_{\mathtt{i,cl}})C\mathtt{v_i} = \mathtt{f_i} \tag{3.22}$$

$$K(\overline{\lambda}_{\mathtt{i,cl}})C\overline{\mathtt{v}}_{\mathtt{i}} = \overline{\mathtt{f}}_{\mathtt{i}} \tag{3.23}$$

Numerator coefficient bounds: The supplementary control signals from the controller

are dependent on the magnitude of the feedback. Therefore, it is necessary to put a bound on the elements of the feedback matrix in order to limit the control effort. The optimization variables, i.e., numerator coefficients can be bounded as shown in (3.24).

$$b_{min} \leq b_{ijk} \leq b_{max} \tag{3.24}$$

Once the cost function and the equality constraints are obtained in terms of the numerator coefficients, quadratic programming is used in MATLAB to solve the problem. The formation of all the matrices that are required to be fed to *quadprog* can be found out in detail in [58]. A flowchart explaining the algorithm for controller design using partial right eigenstructure assignment has been shown in fig. 3.1.

3.2. I/O Signal Selection and Time Delay of Feedback Signals

Selection of appropriate I/O signals for the controller is important to ensure that all the poorly damped modes to be relocated are controllable and observable. Poor choice of signals might result in unreasonably high gains and thus an infeasible controller. In this work, the locations of SVCs have been pre-assigned. The SVCs are installed close to the tie lines which is the followed practice in an actual power system. The challenge here is to select the appropriate feedback signals given the locations of SVCs are fixed. The residual method explained briefly in chapter 2 is used for selecting the feedback signals for the WAC. As was mentioned earlier, the residual method also represents the first order sensitivity of an open-loop eigenvalue $\lambda_{i,ol}$ with respect to a controller K. The metric based on the first order perturbation of an eigenvalue has been used and given in (3.25) [59,60].

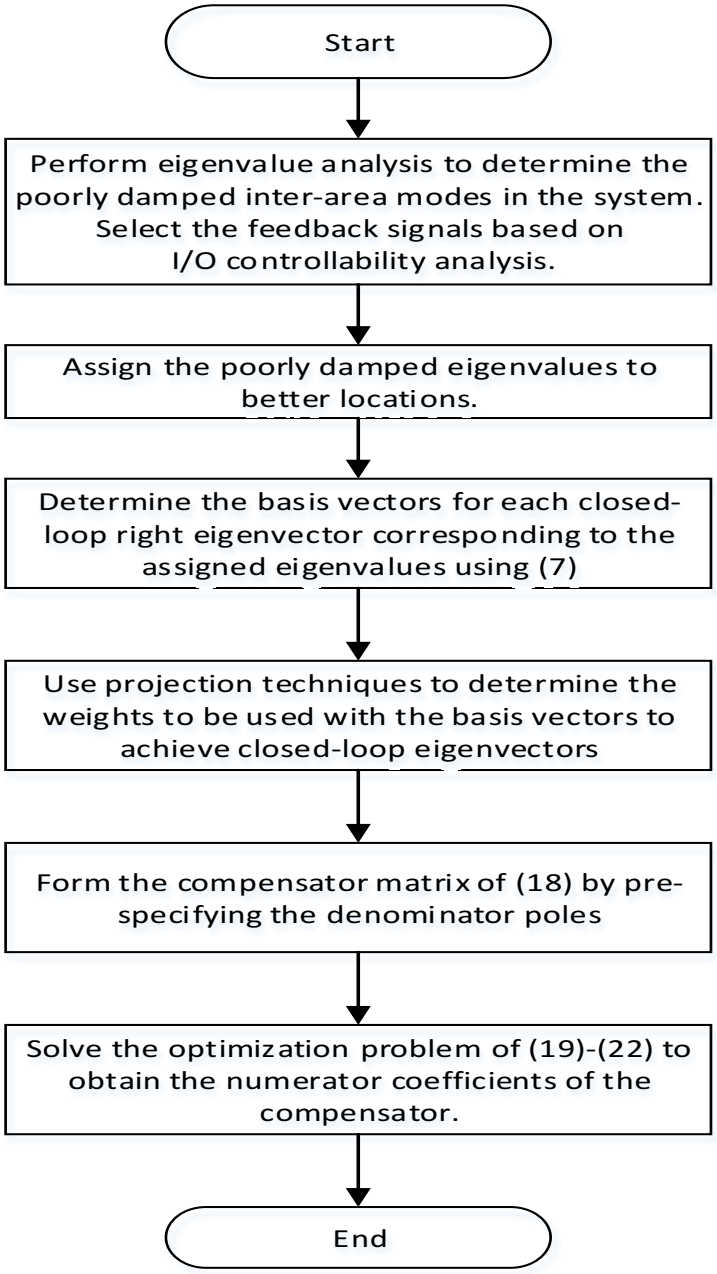

Figure 3.1.: A flowchart explaining the controller design algorithm

$$\frac{d\lambda_{i,ol}}{dK} = ||Cv_i u_i^T B|| \tag{3.25}$$

The primary reason for using SVCs is to ensure that the local modes in the system are minimally affected. On the other hand if PSS/s were chosen to be a part of the WAC scheme, the control interaction might result in a local mode becoming unstable or moving towards the right half plane as the inter-area modes are moved to better locations. As will be shown in the results, utilizing SVCs and the selected feedback signals results in the local modes being non-controllable. Also, the modes other than the inter-area modes that are controllable using the chosen I/O signals are well into the left half plane. This is the reason that no constraint is put on the other eigenvalues (other than the assigned ones) in the optimization process to ensure that none of them becomes unstable.

An important factor while using remote feedback signals is to account for the time delay. Time delay has been approximated by utilizing the second order Pade approximation as given in (3.26) [32].

$$e^{-\tau s} = \frac{\tau^2 s^2 - 6\tau s + 12}{\tau^2 s^2 + 6\tau s + 12} \tag{3.26}$$

The state space representation of the dynamics of delay can be written as shown in (3.27) and (3.28). The time delay block connected to the plant has been shown in fig. 3.2.

$$\dot{x_d} = A_d x_d + B_d u_d \tag{3.27}$$

$$y_{1d} = C_d x_d + D_d u_d \tag{3.28}$$

where y_{1d} is one of the delayed outputs of the plant. A similar representation can be used for other inputs. The input u_d to the time delay block is one of the outputs

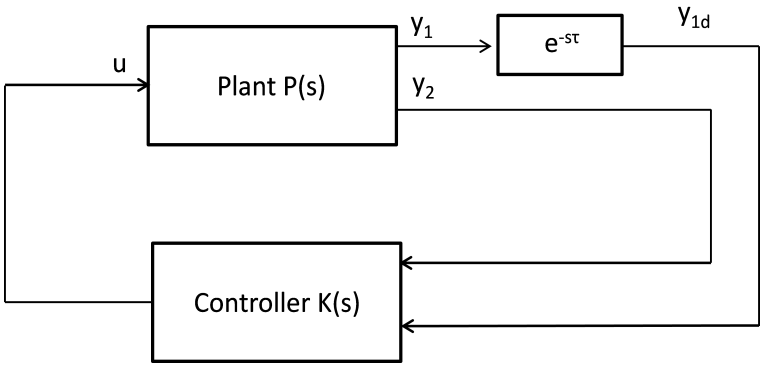

Figure 3.2.: time delay in one of the output signals

from the plant. Thus u_d can be substituted with y_1 using (3.2). The final state space representation of the system including the time delay can be written as given in (3.29) and (3.30).

$$\dot{x_{td}} = A_{td}x_{td} + B_{td}u_{td} \tag{3.29}$$

$$y_{td} = C_{td}x_{td} + D_{td}u_{td} \tag{3.30}$$

where $x_{td} = \begin{bmatrix} x \\ x_d \end{bmatrix}$, $y_{td} = \begin{bmatrix} y_{1d} \\ y_2 \end{bmatrix}$, $A_{td} = \begin{bmatrix} A & 0 \\ B_dC_{r1} & A_d \end{bmatrix}$, $B_{td} = \begin{bmatrix} B \\ B_dD_{r1} \end{bmatrix}$, $C_{td} = \begin{bmatrix} D_dC_{r1} & C_d \\ C_{r2} & 0 \end{bmatrix}$, $D_{td} = \begin{bmatrix} D_dD_{r1} \\ D_{r2} \end{bmatrix}$. C_{r1}, C_{r2}, D_{r1} and D_{r2} represent the respective rows of C and D matrices.

The impact of time delay on the performance of a WAC employing remote signals has been presented in numerous works [29, 50]. Local control typically experiences time delay of the order of 10ms. However, in a wide area control scheme, the remote signals might have a delay of the order of 100ms. If a larger number of signals are to be routed, a delay of more than 100ms is expected. Moreover, transmitting multiple signals introduces variability in the amount of time delay. Therefore, accounting for

an uncertain time delay is very important to ensure that the controller is robust to uncertainty in time delay. A multi-model optimization approach has been followed to incorporate the impact of time delay and has been presented in the next section.

3.3. Multi-model Optimization for Controller Design

As mentioned in the previous section, time delays of feedback signals degrade the performance of a WAC. A constant time delay can be accounted into controller design by using a lead-lag compensation block [53]. However, the challenge is the uncertainty in time delay. In a recent work, a mu-synthesis based approach has been used where the time delay has been considered as an uncertain parameter for determining the linear fractional transformation of the system [54]. This work proposes to use a modal multi-model method for incorporating the uncertainty in time delay into the controller design. A quadratic optimization problem utilizing the system model with and without the time delay is setup. The time delay is included in the system model by using (3.26) - (3.30). A specific value of time delay, τ, is chosen and the design algorithm results in a controller that is robust to multiple values of time delays up to τ. Let's assume that the system model with and without the delay is termed as the delayed model and the nominal model respectively. The multi-model optimization problem formulation will be presented below.

Let the controller designed for the nominal model be termed as $K_{nom}(s)$. The aim is to design a controller, $K_{robust}(s)$, that ensures the damping of the inter-area modes for the varying values of time delay of feedback signals. Let $\lambda_{i1,cl}$ be the $i1$ eigenvalues that were assigned by $K_{nom}(s)$ for the nominal model. Also, assume

that the nominal and delayed system models are represented as $(A_1, B_1, C_1, 0)$ and $(A_2, B_2, C_2, 0)$ respectively. The steps for robust controller design are listed below:

- Apply the controller, $K_{nom}(s)$ on the delayed system model. Determine the eigenvalues that violate the minimum damping criteria (5% damping).
- The design objective for $K_{robust}(s)$ is to assign the eigenvalues obtained from the previous step to better locations, $\lambda_{i2,cl}$, while preserving the eigenvalues, $\lambda_{\mathtt{i1,cl}}$, assigned by $K_{nom}(s)$ for the nominal model. The optimization problem involving the assignment of $(\lambda_{\mathtt{i1,cl}}, \mathtt{v_{i1}}, \mathtt{f_{i1}})$ and $(\lambda_{\mathtt{i2,cl}}, \mathtt{v_{i2}}, \mathtt{f_{i2}})$ for the nominal and the delayed system model respectively is shown in (3.31) - (3.34) [61].

$$Minimize\, J = \sum_{i=1}^{l} ||K_{nom}(j\omega_i) - K_{robust}(j\omega_i)||_F^2 \tag{3.31}$$

such that,

$$K_{robust}(\lambda_{\mathtt{i1,cl}})C_1\mathtt{v_{i1}} = \mathtt{f_{i1}} \tag{3.32}$$

$$K_{robust}(\lambda_{\mathtt{i2,cl}})C_2\mathtt{v_{i2}} = \mathtt{f_{i2}} \tag{3.33}$$

$$b_{min} \leq b_{ijk} \leq b_{max} \tag{3.34}$$

where $\lambda_{i1} = 1...q_1 \leq r + n_a$, $\lambda_{i2} = 1...q_2 \leq r + n_a$. The objective function in (27) ensures that the controller $K_{robust}(s)$ is as close as possible to $K_{nom}(s)$ [58]. Also, the objective function can be expressed as a quadratic function in terms of the numerator coefficients of $K_{robust}(s)$. Therefore, the optimization is solved using quadratic programming in MATLAB. The matrices required for quadratic programming formulation have been given. There are two important factors to be considered while

incorporating multiple models for controller design using eigenstructure assignment:

1. Similar to sub-section 3.1.3, the constraints of (3.32) and (3.33) can be linearized iff $(\mathtt{v_{i1}}, \mathtt{f_{i1}})$ and $(\mathtt{v_{i2}}, \mathtt{f_{i2}})$ are pre-assigned. The equations (3.9) and (3.10) are used to determine the vectors $(\mathtt{v_{i1}}, \mathtt{f_{i1}})$ and $(\mathtt{v_{i2}}, \mathtt{f_{i2}})$. The matrices required for determination of these vectors are Z_{12} and $v_{i,ol}$. Z_{12} for the two state space models is obtained using $null(\begin{bmatrix} A_1 - \lambda_{i1} I & B_1 \end{bmatrix})$ and $null(\begin{bmatrix} A_2 - \lambda_{i2} I & B_2 \end{bmatrix})$. The next important step is to select $v_{i,ol}$. The eigenvalues being treated in this subsection are the ones obtained by the application of $K_{nom}(s)$ on the nominal and the delayed model. Therefore, the eigenvector $v_{i,ol}$ corresponding to these eigenvalues belong to the space $\mathbb{C}^{(n+n_a)\times 1}$(application of $K_{nom}(s)$ increases the dynamic order). This would result in the matrices Z_{12} and $v_{i,ol}$ needed in (3.9) being dimensionally incompatible ($Z_{12} \in \mathbb{C}^{n\times m}$ whereas $v_{i,ol} \in \mathbb{C}^{(n+n_a)\times 1}$) . This problem is solved by exploiting the concept presented in (3.12) - (3.18). Therefore only the first n elements of $v_{i,ol}$ are used for projection.

2. It is possible to have constraints treating the same type of mode in two different models. This would result in high sensitivity of that eigenvalue and thus lower robustness [61]. Care should be taken to remove a constraint for the nominal model if a similar constraint is being added for the delayed model. This point will also be demonstrated in the results section more clearly.

It has to be noted that the dynamic order of $K_{nom}(s)$ and $K_{robust}(s)$ has been selected to be the same in this work. However, the orders can be chosen to be different.

3.4. Results and Discussion

The algorithm presented in this chapter has been applied to the IEEE 68 bus system. The system has been built and simulated in matlab based power system toolbox (PST) [42]. A modified version of the system presented in [62] has been used. The details of the system have been provided in appendix A. A schematic showing the system with the WAC has been shown in fig. 3.3. The system has two SVCs rated 200 MVA located at buses 40 and 50. The damping has been achieved by providing a supplementary signal to the SVC reference voltage signals. The reason for using two SVCs is to provide enough degrees of freedom for eigenvector assignment as explained in section 3.1. The dynamic model of the system in PST consists of 186 state variables. Sixth order model has been used for synchronous machines and the loads have been modeled as constant impedance loads. PSSs and governors have been installed only on machines 1 – 12 considering the fact that the generators 13-16 are equivalent areas.

Controller Design for the Nominal Model

The initial step consists of performing a small signal stability analysis on the nominal model to determine the inter-area modes in the system. The next step involves selecting the I/O signals that have a good controllability metric for the poorly damped eigenvalues (damping ratio less than 5%). Since the output signal of the controller is fixed to be the SVC supplementary voltage control signal, the aim is just to find the appropriate input signals. The feedback signals based on the controllability metric were chosen to be the real power flows in the lines 49-52 and 52-42. The selection of these feedback signals also ensured that none of the local modes were controllable. The other possible options for tie lines (42-41, 50-52) were also successfully used for

controller design but the results have not been presented here due to limited space. The I/O controllability of the top ten controllable modes using the selected I/O signals has been presented in table I. It can be observed that except the inter-area modes, majority of the other controllable modes have a high, negative real part. The next step is to choose the locations to be assigned to the poorly damped eigenvalues. The approach followed here is to keep the imaginary part the same and change the real part such that the damping ratio becomes 10%. It has been noted that the damping ratio of the eigenvalue $-0.308 \pm 2.392i$ is already above the minimum damping criterion. Therefore, it is assigned at the same location. The open-loop and assigned eigenvalues have been shown in table II.

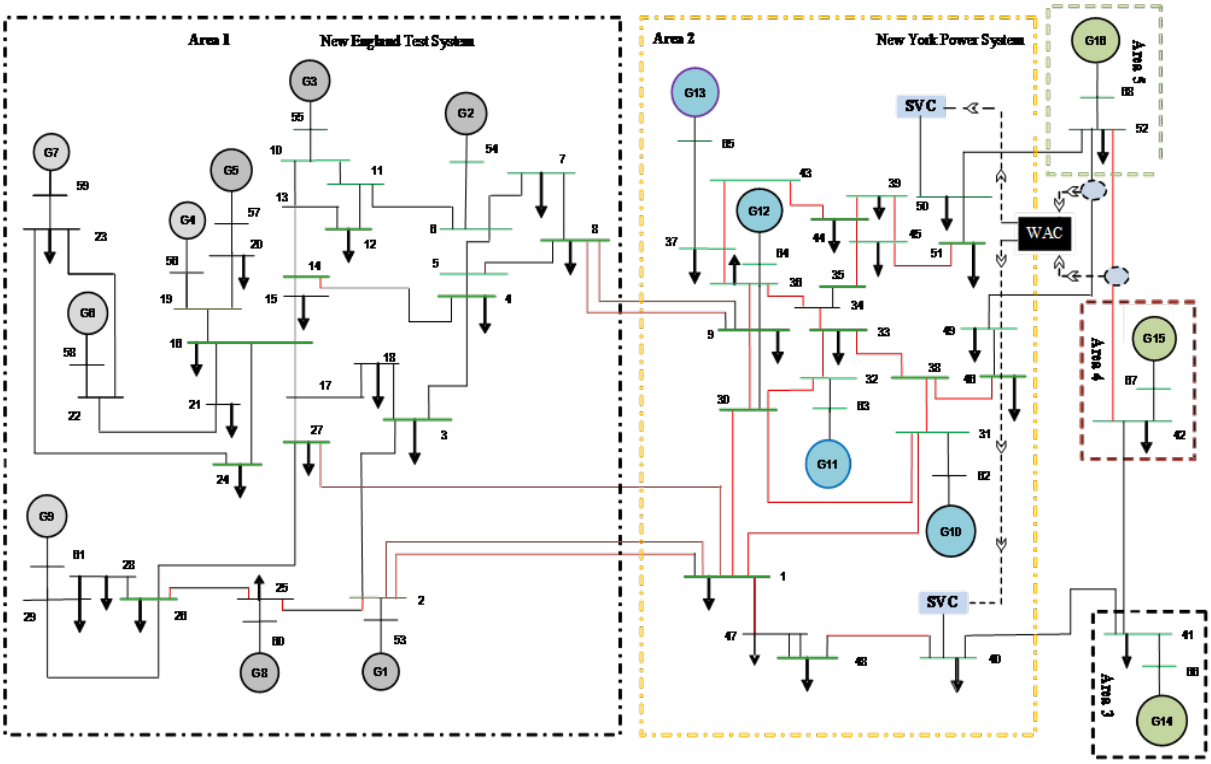

Figure 3.3.: IEEE 68 bus system with the WAC

Table 3.1.: Residues of top 10 controllable eigenvalues using the selected I/O signals

Open-loop eigenvalues	Residues
-61.66	21.8
-68.73	6.63
-67.77	2.78
-0.117+3.329i	2.2
-0.178+4.889i	1.19
-0.308+2.392i	1.17
-9.05+11.61i	1.14
-28.67	0.64
-7.59+19.73i	0.53
-7.95+14.86i	0.43

Table 3.2.: Assigned eigenvalues and their damping ratios

Open-loop eigenvalues	Closed-loop eigenvalues	Open-loop damping ratio	Closed-loop damping ratio
-0.308+2.392i	-0.308+2.392i	12.8%	12.8%
-0.117+3.329i	-0.334+3.329i	3.54%	10%
-0.178+4.889i	-0.491+4.889i	3.65%	10%

The achievable closed-loop right eigenvectors corresponding to each eigenvalue are determined using (3.9) and (3.10) using either of the eigenvector projection techniques mentioned in section 3.1. Once, the closed-loop right eigenvectors are determined, the optimization problem utilizing equations (3.21) - (3.24) is setup. The order of the dynamic compensator is chosen to be three and the compensator poles are chosen to be $(-4, -5, -6)$. It has to be noted that the controllability metric defined in (3.25) is based on a proportional output feedback. However, using a dynamic compensator adds new poles into the system. The location of these poles will have a marginal effect on some of the system eigenvalues. Therefore, the closed-loop system eigenvalue plot will have a few other eigenvalues displaced marginally than expected from the controllability metric of table I. Choice of complex compensator poles has the least

impact on other system eigenvalues and is the best choice. It has to be noted that these system eigenvalues being marginally displaced are the ones that lie into the far left half plane. The local modes were not affected at all in any of the cases that were studied. The degree of numerator has been chosen to be equal to that of the denominator. The cost function is formulated to minimize the sum of the Frobenius norm of the compensator at frequencies ranging from 0 to 7 rad/s in increments of 1 rad/s. The numerator coefficients in the optimization problem are bounded to be within -120 and 120. In this paper, both the projection techniques presented in section 3.1 have been used for designing the controller. The controllers designed using open-loop eigenvector projection and weighted open-loop eigenvector projection are termed as $K_{nom1}(s)$ and $K_{nom2}(s)$ respectively. The performance of $K_{nom2}(s)$ is found out to be superior to $K_{nom1}(s)$. Thus, $K_{nom2}(s)$ is used for the design of $K_{robust}(s)$ presented in the next subsection. The controllers $K_{nom1}(s)$ and $K_{nom2}(s)$ are found to be [63]:

$$K_{nom1}(s) = \begin{bmatrix} \frac{-0.327s^3+2.847s^2-11.454s-36.123}{s^3+15s^2+74s+120} & \frac{1.181s^3+6.82s^2+12.27s+59.956}{s^3+15s^2+74s+120} \\ \frac{0.118s^3-1.417s^2+2.723s+14.5}{s^3+15s^2+74s+120} & \frac{0.441s^3-0.24s^2+2.371s-12.85}{s^3+15s^2+74s+120} \end{bmatrix} \tag{3.35}$$

$$K_{nom2}(s) = \begin{bmatrix} \frac{0.0818s^3+0.890s^2-1.265s-36.44}{s^3+15s^2+74s+120} & \frac{0.215s^3-0.211s^2-1.671s-33.98}{s^3+15s^2+74s+120} \\ \frac{0.420s^3+3.843s^2+3.193s+37.41}{s^3+15s^2+74s+120} & \frac{1.075s+9.169s^2+10.77s+62.62}{s^3+15s^2+74s+120} \end{bmatrix} \tag{3.36}$$

The eigenvalues of the system with and without the output feedback controller have been shown in fig. 3.4. Fig. 3.4 shows that the controller selectively assigns the poorly damped modes to better locations while preserving the well damped inter-area mode at the same location. Furthermore, the rest of the eigenvalues are minimally impacted. The time domain results have been shown for three different operating

conditions to justify the inherent robustness of the controller as shown in table III. The operating condition, OP1, is the *base-case* condition. The operating condition, OP2, involves increasing the output of generator 15 by 10 per unit (on 100 MW base) while reducing the output of generator 14 by the same amount. This operating point stresses the tie line $42-41$ and worsens the damping of the eigenvalue of the nominal system. The operating point, OP3, consists of the line $46-49$ being disconnected. A ten cycle, three phase fault at bus 49 has been used to demonstrate the performance of the controller under different operating conditions.

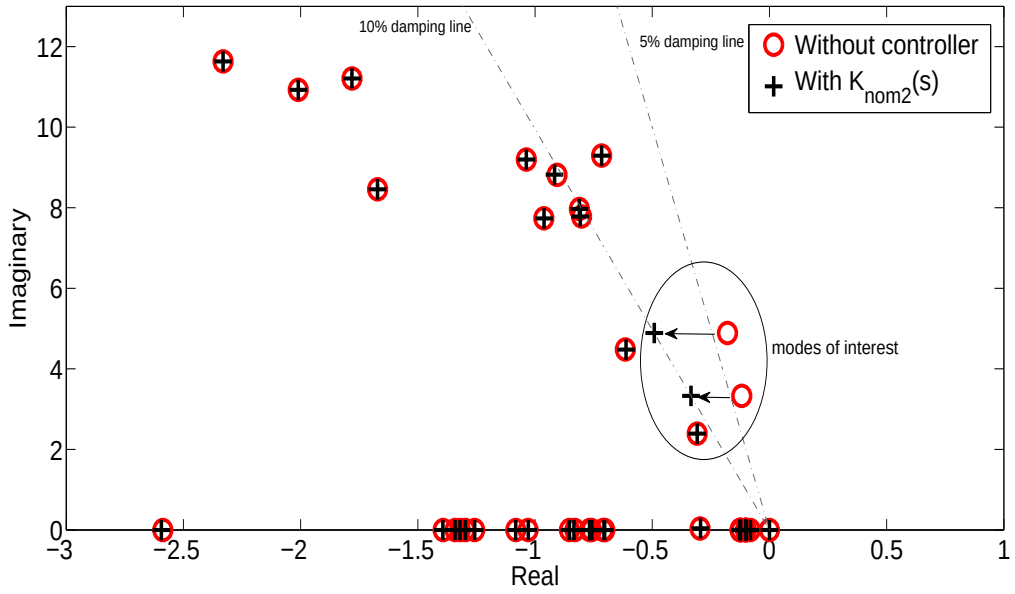

Figure 3.4.: IEEE 68 bus system with the WAC

Table 3.3.: Operating points used for validating the robustness of the controller

Operating Point	Operating Condition
OP1	*base-case*
OP2	increase the output of generator 15 by 10 p.u while reduce the output of generator 14 by 10 p.u
OP3	line 46-49 disconnected

The plot showing the rotor angle difference between generators 15 and 16 for different faults and operating conditions have been shown in fig. 3.5. The results clearly indicate the significance of eigenvector assignment in the design of the controller. As seen from the results, $K_{nom2}(s)$ is more robust to operating point changes in the system as compared to $K_{nom1}(s)$. Fig. 3.6 shows the susceptance of the SVCs during fault for all the three operating conditions when using $K_{nom2}(s)$. This figure validates that control objective is achieved with bounded control effort.

Multi-model optimization for controller design

Once the controller for the nominal system model, $K_{nom2}(s)$ is obtained, the next step is to determine, the next step is to determine $K_{robust}(s)$ robust to time delay uncertainty of the feedback signals. The delayed system model is obtained by using a value of $\tau = 400ms$. The controller, $K_{nom2}(s)$, is applied to the delayed system. Two eigenvalues, $(-0.1073 \pm 3.555i)$ and $(-0.0436 \pm 5.172i)$ are found to violate the minimum damping criterion. A multi-model optimization problem is formulated using equations (3.31) - (3.34) to improve the damping of these eigenvalues while preserving the performance of $K_{nom2}(s)$ for the nominal model. Ideally, the eigenvalues assigned in the previous subsection are re-assigned at the same location to form the constraints associated with the nominal model. Similarly, the eigenvalues $(-0.1073 \pm 3.555i)$ and $(-0.0436 \pm 5.172i)$ associated with the delayed model are assigned to better locations to form the constraints relative to the delayed system model. However, it has to be noted that two eigenvalues associated with the delayed model are similar in nature to the ones assigned for the nominal model. Therefore, the constraints associated with the re-assignment of $(-0.334 \pm 3.329i)$ and $(-0.491 \pm 4.889i)$ at the same location are removed for the nominal model. The utilization of the idea of eigenvector projection

ensures that the removal of these constraints does not affect these eigenvalues drastically while improving the damping of $(-0.1073 \pm 3.555i)$ and $(-0.0436 \pm 5.172i)$ for the delayed model. The two poorly damped eigenvalues associated with the delayed model are assigned to have a damping ratio of 7%. Similar to previous subsection, this is achieved by keeping the imaginary part constant and varying the real part. The assigned locations are found to be $(-0.249 \pm 3.555i)$ and $(-0.362 \pm 5.172i)$. The eigenvalue plot showing the comparison of $K_{nom2}(s)$ and $K_{robust}(s)$ on the nominal and delayed system models has been shown in fig. 3.7. Similar to previous subsection, the numerator coefficients in the optimization problem are bounded to be within -120 and 120. The controller $K_{robust}(s)$ is given to be [63]:

$$K_{robust}(s) = \begin{bmatrix} \frac{-1.411s^3+10.039s^2-21.75s+118.63}{s^3+15s^2+74s+120} & \frac{2.274s^3-2.47s^2+22.57s-37.52}{s^3+15s^2+74s+120} \\ \frac{-3.346s^3-2.19s^2-56.5s-61.72}{s^3+15s^2+74s+120} & \frac{4.436s^3+13.511s^2+44.37s+98.53}{s^3+15s^2+74s+120} \end{bmatrix} \tag{3.37}$$

The eigenvalue plots presented in fig. 3.7 show that the controller, $K_{robust}(s)$ is able to meet the minimum damping criterion for the nominal as well the delayed system model. Two controller induced poles also come into the picture as shown in fig. 3.7(b). However, they do not pose any problem as they are well into the left half plane. Moreover, the local modes in both the eigenvalue plots are not affected at all.

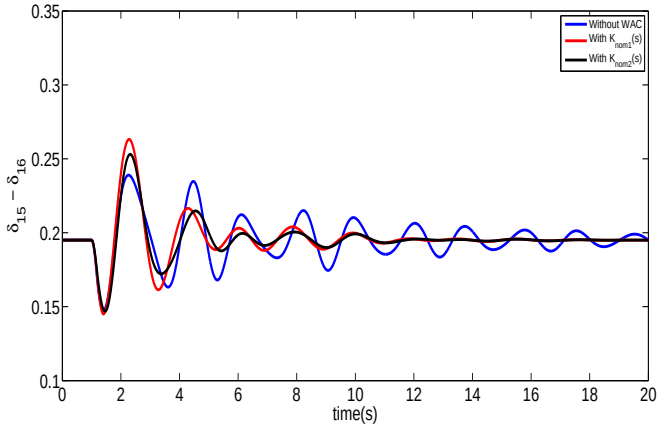

(a) Angle difference for OP 1, fault at bus 49

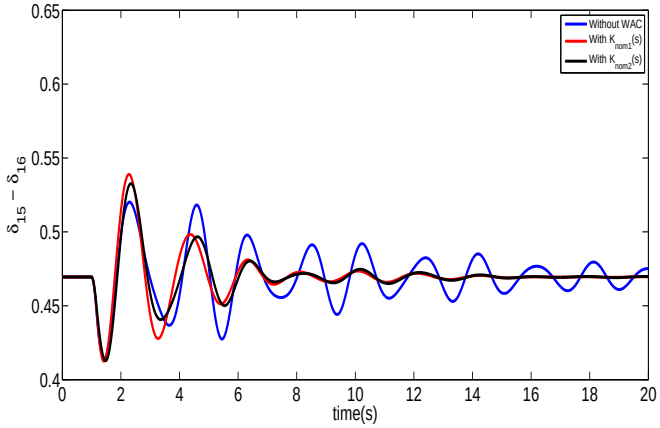

(b) Angle difference for OP 2, fault at bus 49

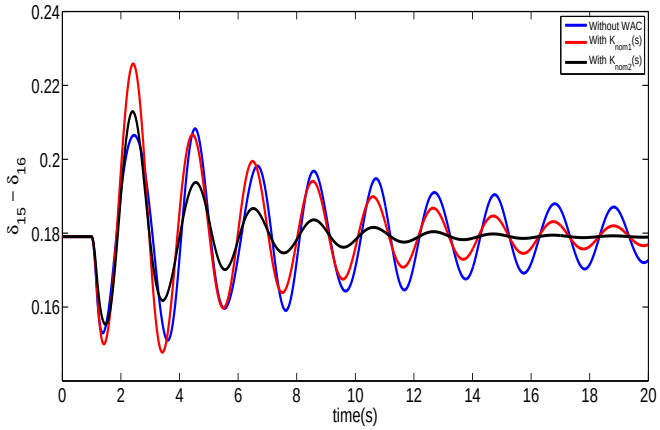

(c) Angle difference for OP3, fault at bus 49

Figure 3.5.: Comparison of performance of $K_{nom1}(s)$ and $K_{nom2}(s)$

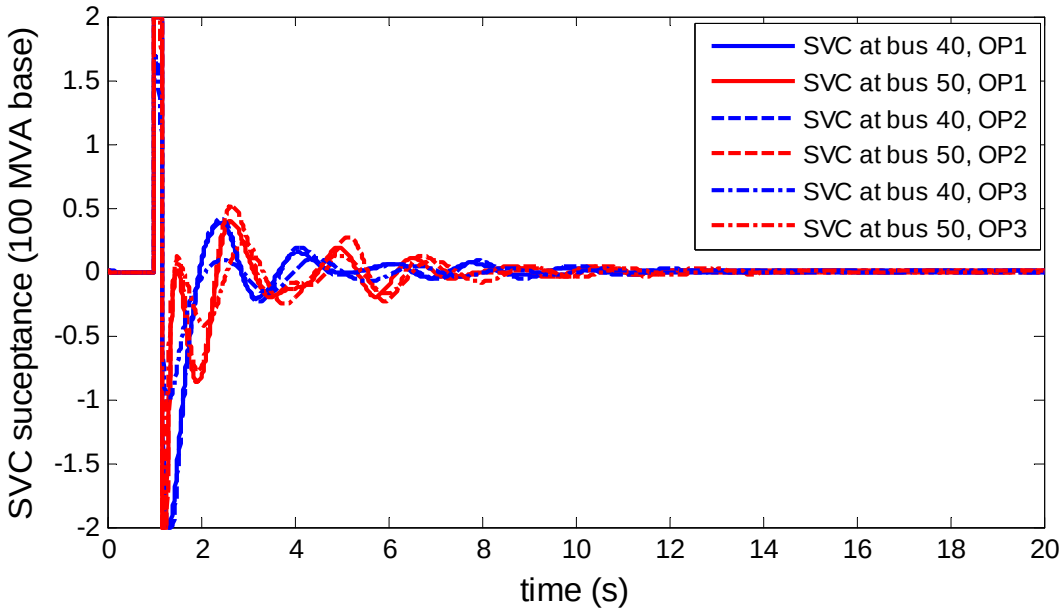

Figure 3.6.: Susceptance of the SVCs during fault for all three operating conditions when using $K_{nom2}(s)$

The Time domain results showing the rotor angle differences between generators 15 and 16 for different values of time delay of feedback signals have been shown in figs. 3.8 - 3.10. The disturbance applied in the system is a ten cycle, three phase fault at bus 49. It has to be noted that the results shown incorporate delay in both the feedback signals. The results show the robustness of the controller, $K_{robust}(s)$, to varying values of time delays under different operating conditions.

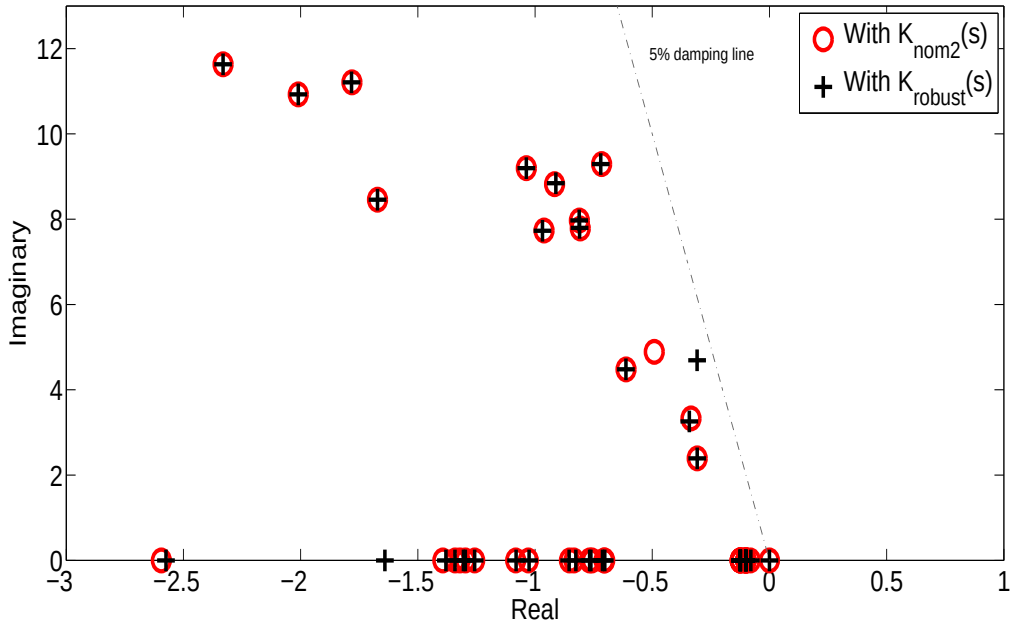

(a) Comparison of eigenvalues with $K_{nom2}(s)$ and $K_{robust}(s)$ connected to the nominal system

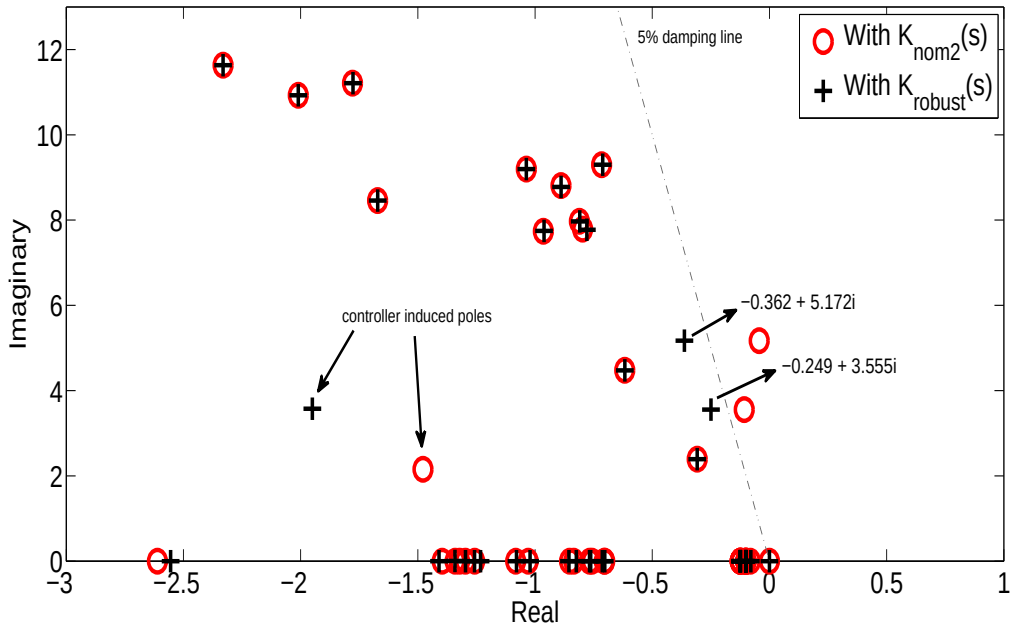

(b) Comparison of eigenvalues with $K_{nom2}(s)$ and $K_{robust}(s)$ connected to the delayed system

Figure 3.7.: Comparison of the performance of $K_{nom2}(s)$ and $K_{robust}(s)$ connected to the nominal and delayed system

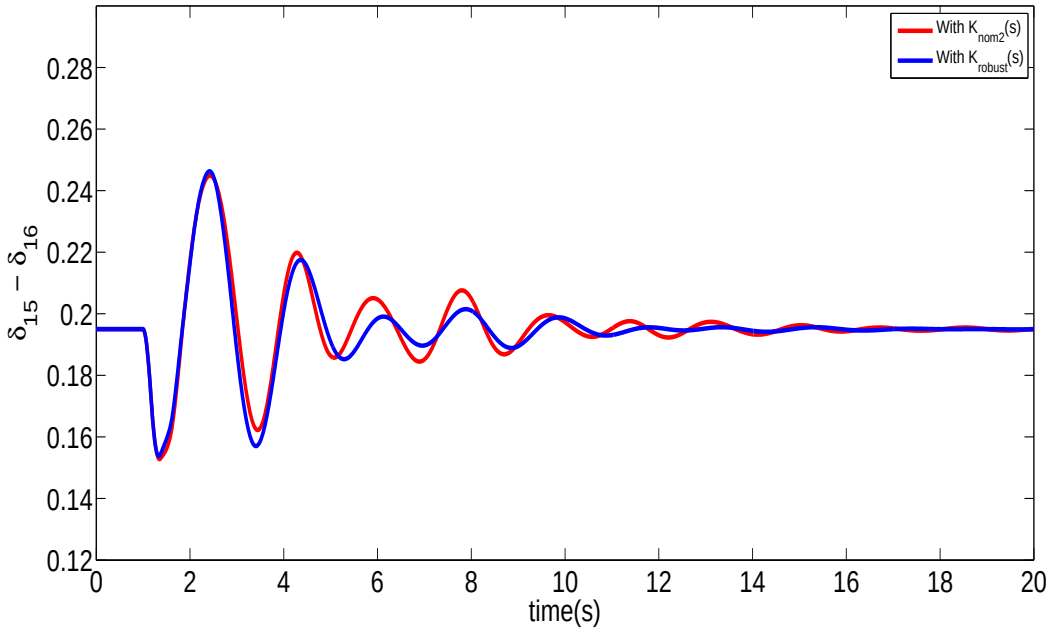

(a) Angle difference for OP 1 with a feedback delay of 200ms

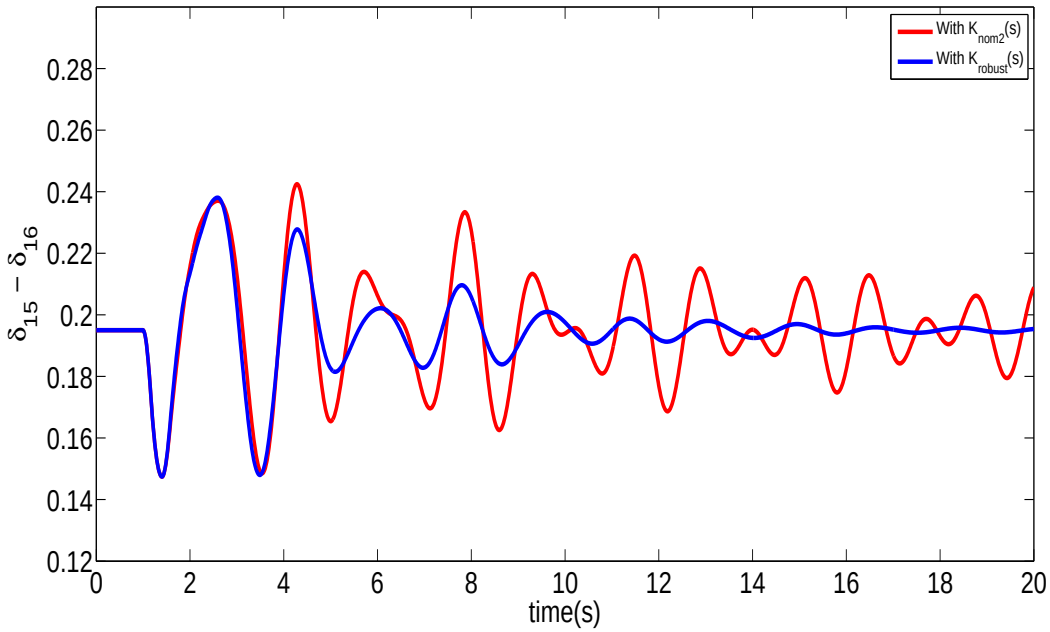

(b) Angle difference for OP 1 with a feedback delay of 400ms

Figure 3.8.: Comparison of the performance of $K_{nom2}(s)$ and $K_{robust}(s)$ for OP1 and different values of time delays

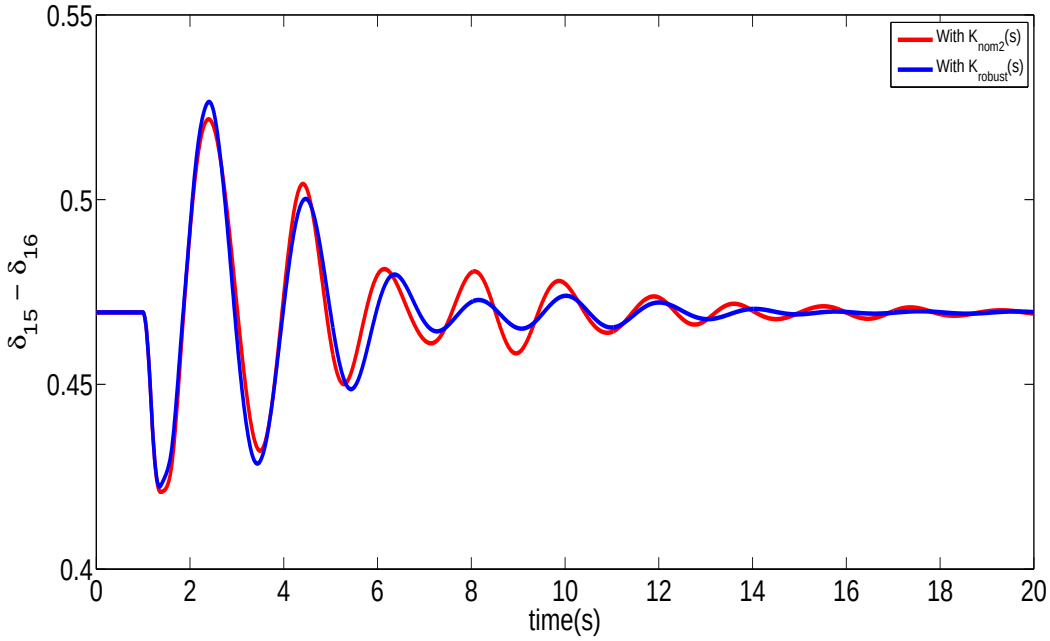

(a) Angle difference for OP 2 with a feedback delay of 200ms

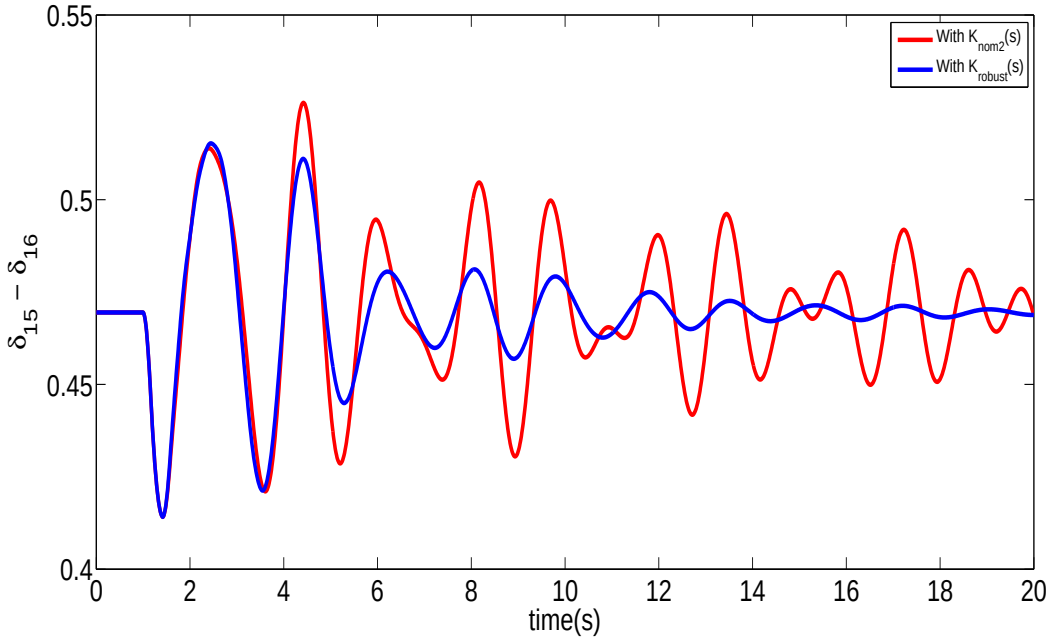

(b) Angle difference for OP 2 with a feedback delay of 400ms

Figure 3.9.: Comparison of the performance of $K_{nom2}(s)$ and $K_{robust}(s)$ for OP2 and different values of time delays

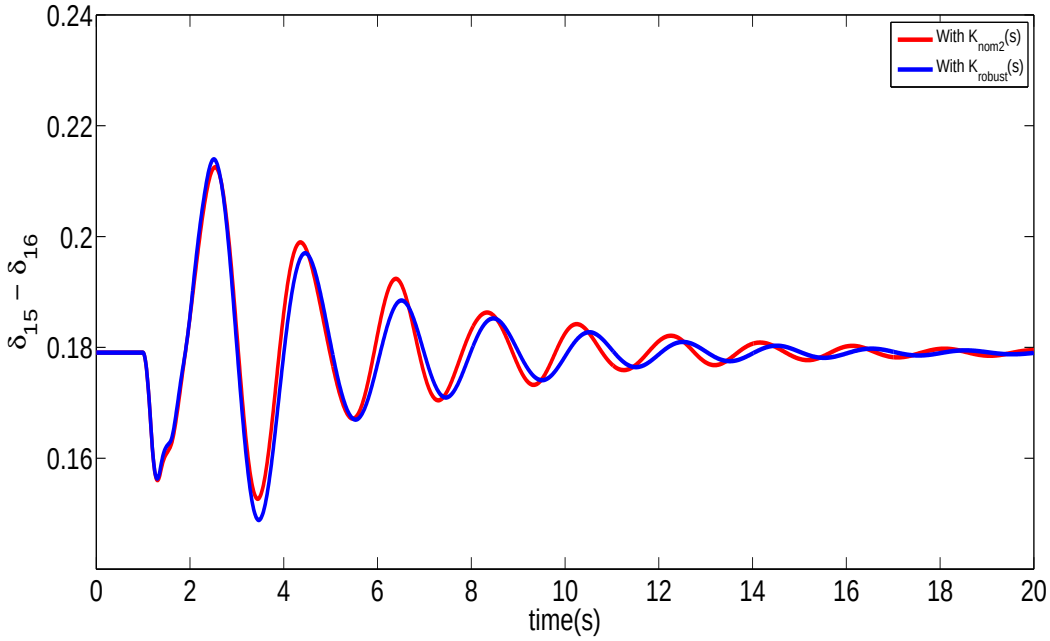

(a) Angle difference for OP 3 with a feedback delay of 200ms

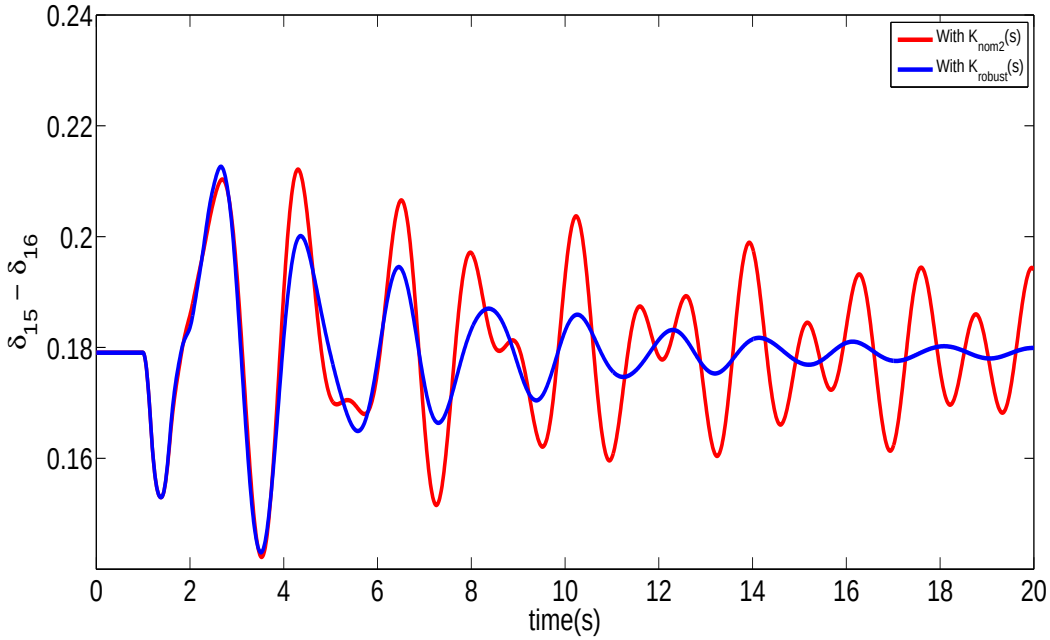

(b) Angle difference for OP 3 with a feedback delay of 400ms

Figure 3.10.: Comparison of the performance of $K_{nom2}(s)$ and $K_{robust}(s)$ for OP3 and different values of time delays

3.5. Discussion

There are certain aspects of the method that can be improved and have been addressed in the next chapter. These are:

1. The method uses projection techniques to assign the closed-loop right eigenvectors. However, the weights η_i to be used with the basis vectors can be used as optimizing variables along with the eigenvalue locations since they are degrees of freedom. This idea will be demonstrated in the next chapter to formulate the controller design problem.

2. The controller was designed based on a linearized model around an operating point. However, a power system experiences variability in operation throughout the day. Therefore, robustness of the controller forms an important aspect. In order to address this issue, a multi-model optimization formulation will be presented in the next chapter. The multi-model optimization strategy presented in this chapter is not particularly suited for scenarios where more than two models are involved.

3. In the next chapter, a constraint on the damping of rest of the eigenvalues of the system, other than the critical eigenvalues, will be incorporated.

4.Robustification of a Wide Area Controller

One of the primary objectives of this thesis is to design a WAC that is robust to operating point changes in the system as well as time-delay uncertainties of the feedback signals. As mentioned earlier, power systems experience varying operating conditions throughout the day. Thus, robustness forms a very important aspect of designing a WAC.

In control systems terminology, robustness can be subdivided into frequency domain and real parametric uncertainties. There has been extensive research and literature on addressing the issue of frequency domain uncertainty (mainly model uncertainties) in power system using H-infinity optimization technique [64]. The conventional H-infinity optimization technique involves selection of weighting filters to define the frequency range of interest for optimization which is not a very straightforward procedure. A better method of finding the H-infinity norm involves solving a linear matrix inequality (LMI) where the eigenvalue constraints can be specified more easily [65]. On the other hand, the approach for addressing robustness against real parametric uncertainties is totally different. Two different approaches have been used previously in power systems to design a controller robust to real parametric uncertainties namely: μ synthesis (frequency domain) [66] and pole placement involving multiple models of the system (time-domain) [45]. As the name suggests, robustness against real parametric uncertainty involves studying the robustness of the system to any variable parameter/s in the system. The μ-synthesis technique is a frequency domain technique that uses a metric known as structured singular value (SSV) to analyze the

robust stability of the system. In [45], a pole placement technique has been presented that uses a multi-model optimization approach with the tunable parameters of various local controllers (PSSs) being the optimizing variables [45]. The control objective is to ensure that eigenvalues across all the selected models satisfy the minimum damping criterion.

This chapter presents formulation of multi-model optimization problems using two different methods such that eigenvalues across all the selected models satisfy the minimum damping criterion. This is achieved by tuning the initial controller $K(s)$ obtained using the technique presented in section 3.1. However, It should be noted that $K(s)$ can be any generic WAC. The uniqueness of the tuning procedure lies in the way the multi-model optimization problem is formulated. Two different approaches have been used to select the models to be incorporated in the optimization problem:

1. Approach `I` - This approach involves selecting stressed operating points based on system information. In power systems, these operating points are usually known to the operator. A lot of existing literature follows this approach to address the issue of robustness against operating point changes [39, 45, 67].

2. Approach `II` - The first approach cannot address the issue of robustness of the designed controller to the variation of a specific parameter of the system as well as uncertain time delay of feedback signals. Approach `II` presents a method to appropriately select models such that the resulting controller is robust to uncertainties in operating points as well as time delays.

Two different methods have been used to setup the multi-model optimization problem used in both the approaches:

1. `Method 1` : This method is based on eigenstructure assignment technique. The essence of the technique was explained in detail in the last chapter. However in

this chapter, the optimization problem is setup in a totally different way utilizing a different set of optimizing variables as well as the optimization algorithm.

2. `Method 2:` This method makes use of the first order sensitivity of an eigenvalue with respect to a proportional feedback controller to slowly move the critical eigenvalues associated with each of the selected models inside the 5% damping line.

Both these methods will be explained in detail in the following sections.

The first step towards tuning $K(s)$ is to transform the uncompensated system/s connected to $K(s)$ into a form that can be incorporated into the multi-model optimization algorithms. This has been shown in the next section.

4.1. Obtaining the Extended Dynamic System

The initial closed-loop system available is given as:

$$\dot{x} = Ax + Bu \tag{4.1}$$

$$y = Cx \tag{4.2}$$

$$u = K(s)y \tag{4.3}$$

where (4.1) and (4.2) represent the *base-case* system model. The controller $K(s)$ is given in state-space form as:

$$\dot{x}_c = A_c x_c + B_c y \tag{4.4}$$

$$u = C_c x_c + D_c y \tag{4.5}$$

where $x_c \in R^{n_a \times 1}$. The transformation of the uncompensated system connected to

dynamic compensator into an extended dynamic system connected to proportional feedback is given in (4.6) - (4.8) [39].

$$\dot{x_a} = A_a x_a + B_a u_a \tag{4.6}$$

$$y_a = C_a x_a \tag{4.7}$$

$$u_a = K_a y_a \tag{4.8}$$

where $x_a = \begin{bmatrix} x \\ x_c \end{bmatrix} \in R^{(n+n_a)\times 1}, u_a = \begin{bmatrix} u \\ \dot{x}_c \end{bmatrix} \in R^{(m+n_a)\times 1}, y_a = \begin{bmatrix} y \\ x_c \end{bmatrix} \in R^{(r+n_a)\times 1}.$

$$A_a = \begin{bmatrix} A & 0 \\ 0 & 0 \end{bmatrix} \qquad B_a = \begin{bmatrix} B & 0 \\ 0 & I_{n_a \times n_a} \end{bmatrix}$$

$$C_a = \begin{bmatrix} C & 0 \\ 0 & I_{n_a \times n_a} \end{bmatrix} \qquad K = \begin{bmatrix} D_c & C_c \\ B_c & A_c \end{bmatrix}$$

Once, this extended dynamic system has been obtained, the proportional feedback controller, K_a, can be tuned using the multi-model optimization techniques to meet the control objectives. As the optimization terminates, the extended dynamic system connected to proportional feedback is converted back to the original form (uncompensated system connected to tuned dynamic compensator). Let the extended dynamic models associated with the chosen models be referred to as $mod_{a,bc}$, $mod_{a,1m}$.....$mod_{a,nm}$.

4.2. Setting the Optimization Problem

Method 1

The feedback gain K_a connected to $mod_{a,1m}.....mod_{a,nm}$ (more stressed operating conditions) will result in certain eigenvalues being outside the 5% damping line. However, since K_a was designed for $mod_{a,bc}$, the closed loop system $mod_{a,bc} - K_a$ will have all the eigenvalues on or to the left of the 5% damping line. The control objective using the eigenstructure assignment technique is to re-assign selected inter-area modes (already well-damped) of the closed-loop system, $mod_{a,bc} - K_a$, to $(\lambda_{a,i}, v_{a,i}, f_{a,i})$ by tuning K_a such that the closed-loop eigenvalues associated with all the models ($mod_{a,bc}$, $mod_{a,1m}.....mod_{a,nm}$ connected to the tuned controller) satisfy the minimum damping criterion. A nested optimization strategy has been adopted where the objective of the outer loop is to minimize the distance of the critical eigenvalues from the 5% damping line and the objective of the inner loop is to minimize the deviation of the designed controller from K_a. The outer and inner loops have been described below:

1) *Outer loop*:

The connection of the proportional feedback controller to the extended dynamic system results in the closed loop state matrix to be $(A_a + B_a K_a C_a)$. Let $\lambda_{c,i}$, where $i = 1....q_a \leq (r + n_a)$, be the eigenvalues of the closed-loop system given in (4.6) - (4.8) that are selected to be re-assigned. Similar to (3.6) - (3.7), the closed-loop eigenvalue-eigenvector relationship can be restructured as:

$$\begin{bmatrix} A_a - \lambda_{a,i} I & B_a \end{bmatrix} \begin{bmatrix} v_{a,i} \\ f_{a,i} \end{bmatrix} = 0 \tag{4.9}$$

$$where,\ K_a C_a v_{a,i} = f_{a,i} \tag{4.10}$$

The basis vectors for each assignable $\begin{bmatrix} v_{a,i} & f_{a,i} \end{bmatrix}^T$ span the null-space of the matrix $\left(\begin{bmatrix} A_a - \lambda_{a,i} I & B_a \end{bmatrix}\right)$. The rank of this nullspace is the same as the column space of $B_a \in R^{(n+n_a)\times(m+n_a)}$. It is evident that the degrees of freedom available for assigning the closed-loop right eigenvector can be increased by either increasing the number of inputs (m) or increasing the order of the compensator (n_a). **It has to be noted that only relationship in (4.9) is used for the outer loop and the relationship in (4.10) is utilized in the inner-loop.**

In section 3.1, the location of closed-loop eigenvalue was selected by the user. However, in this formulation, the location of the closed-loop eigenvalue is treated as an independent variable. The location $\lambda_{a,i}$ can be given as:

$$\lambda_{a,i} = \lambda_{c,i} - \triangle\lambda_{c,i} \tag{4.11}$$

where, $\triangle\lambda_{c,i}$ is the change in location of $\lambda_{c,i}$. Similar to section 3.2, once $\lambda_{a,i}$ is known, the matrices $Z_{a,12}$ and $Z_{a,22}$ are determined using $svd(\begin{bmatrix} A_a - \lambda_{a,i} I & B_a \end{bmatrix})$ [46]. The right singular matrix, Z_a is given in (4.12).

$$Z_a = \begin{bmatrix} Z_{a,11} & Z_{a,12} \\ Z_{a,21} & Z_{a,22} \end{bmatrix} \tag{4.12}$$

The columns of $Z_{a,12} \in \mathbb{C}^{(n+n_a)\times(m+n_a)}$ form the basis vectors for $v_{a,i}$ and columns of $Z_{a,22} \in \mathbb{C}^{(m+n_a)\times(m+n_a)}$ form the basis vectors for $f_{a,i}$. Let $\eta_{a,i} \in \mathbb{C}^{(m+n_a)\times 1}$ be the weights to be used with the basis vectors. Then the $v_{a,i}$ and $f_{a,i}$ can be obtained using (4.13).

$$\begin{bmatrix} v_{a,i} \\ f_{a,i} \end{bmatrix} = \eta_{a,i_1} \begin{bmatrix} Z_{a,12_1} \\ Z_{a,22_1} \end{bmatrix} + ... + \eta_{a,i_{(m+n_a)}} \begin{bmatrix} Z_{a,12_{(m+n_a)}} \\ Z_{a,22_{(m+n_a)}} \end{bmatrix} \quad (4.13)$$

where, $\eta_{a,i_1}, ..., \eta_{a,i_{(m+n_a)}}$ are the elements of the vector $\eta_{a,i}$ and $Z_{a,12_1}.....Z_{a,12_{(m+n_a)}}$, $Z_{a,22_1}.....Z_{a,22_{(m+n_a)}}$ are the columns of matrices $Z_{a,12}$ and $Z_{a,22}$ respectively. The vector of optimizing variables θ is given as:

$$\theta = (re(\triangle\lambda_{c,i}),\, im(\Delta\lambda_{c,i}),\, re(\eta_{a,i_1}),\, im(\eta_{a,i_1}).....,\, re(\eta_{a,i_{(m+n_a)}}),\, im(\eta_{a,i_{(m+n_a)}}))$$

In each iteration, a different θ results in a new $(\lambda_{a,i}, v_{a,i}, f_{a,i})$ which is fed as an input to the inner loop. The objective function for the outer loop comprises of minimizing $J_1(\theta)$ given in (4.14).

$$J_1(\theta) = \sum_{mo=1}^{nm+1} \sum_{i=1}^{q_d} (0.05 - \xi_{i,mo}) \quad (4.14)$$

where θ refers to the optimizing variables, mo refers to the specific model out of all the models, q_d refers to the eigenvalues of the mo^{th} model that violate the minimum damping criterion and $\xi_{i,mo}$ refers to the damping of i^{th} eigenvalue, where $i = 1...q_d$ for the mo^{th} model. A derivative-free, direct search optimization algorithm known as mesh adaptive direct search (MADS) method has been used in MATLAB to solve the unconstrained optimization problem. The bounds on the optimizing variables are

given below in (4.15) - (4.18).

$$0 \leq re(\Delta\lambda_{c,i}) \leq \alpha_{\lambda_i,max} \tag{4.15}$$

$$\beta_{\lambda_i,min} \leq im(\Delta\lambda_{c,i}) \leq \beta_{\lambda_i,max} \tag{4.16}$$

$$\alpha_{\eta_i,min} \leq re(\eta_{a,i}) \leq \alpha_{\eta_i,max} \tag{4.17}$$

$$\beta_{\eta_i,min} \leq im(\eta_{a,i}) \leq \beta_{\eta_i,max} \tag{4.18}$$

In the first iteration K_a is connected to all the selected models and the value of $J_1(\theta)$ is computed. If $J_1(\theta)$ is more than zero or a certain threshold selected by the user, $(\lambda_{a,i}, v_{a,i}, f_{a,i})$ are initialized from zero and passed as input to the inner loop.

2) *Inner loop*: The purpose of the inner loop is to determine a $\triangle K_a$ such that $K_a + \triangle K_a$ achieves the assignment $(\lambda_{a,i}, v_{a,i}, f_{a,i})$ while minimizing the deviation from K_a. A quadratic optimization problem with $\triangle K_a$ as the optimizing variable is formulated with the objective of minimizing $||\triangle K_a||_F^2$. The constraint for the problem is setup using (4.10). As new $(\lambda_{a,i}, v_{a,i}, f_{a,i})$ is obtained as input every iteration, the objective is to determine $\triangle K_a$ such that $K_a + \triangle K_a$ satisfies (4.10) [68, 69]. This relationship is given in (4.19).

$$(K_a + \Delta K_a)C_a v_{a,i} = f_{a,i} \Rightarrow (\Delta K_a)C_a v_{a,i} = f_{a,i} - K_a C_a v_{a,i} \tag{4.19}$$

The matrix equality of (4.19) can be split into $(m+n_a)$ linear equations. Lets assume that the product of matrix C_a with the vector $v_{a,i}$ (elements all complex) in (4.19) results in a vector $\mathcal{M}_i \in \mathbb{C}^{(r+n_a)\times 1}$. Then, the linear constraints can be written as below:

$$(\Delta K_a) re(\mathcal{M}_i) = re(f_{a,i}) - K_a(re(\mathcal{M}_i)) \tag{4.20}$$

$$(\Delta K_a) im(\mathcal{M}_i) = im(f_{a,i}) - K_a(im(\mathcal{M}_i)) \tag{4.21}$$

The next step is to represent the constraints in (4.20) and (4.21) in $H\beta = c$ form where the elements of the matrix ΔK_a (optimizing variables) form the vector β. This has been shown using an example below:

Example: Assume:

$$\Delta K_a = \begin{bmatrix} \Delta K_{11} & \Delta K_{12} & \Delta K_{13} \\ \Delta K_{21} & \Delta K_{22} & \Delta K_{23} \end{bmatrix}, \; re(\mathcal{M}_i) = \begin{bmatrix} 1 \\ 2 \\ 3 \end{bmatrix}, \; re(f_{a,i}) - K_a(re(\mathcal{M}_i)) = \begin{bmatrix} 4 \\ 5 \end{bmatrix}$$

Then (4.20) can be written as:

$$\begin{bmatrix} \Delta K_{11} & \Delta K_{12} & \Delta K_{13} \\ \Delta K_{21} & \Delta K_{22} & \Delta K_{23} \end{bmatrix} \begin{bmatrix} 1 \\ 2 \\ 3 \end{bmatrix} = \begin{bmatrix} 4 \\ 5 \end{bmatrix}$$

This can be represented in $H\beta = c$ form as follows:

$$\begin{bmatrix} 1 & 2 & 3 & 0 & 0 & 0 \\ 0 & 0 & 0 & 1 & 2 & 3 \end{bmatrix} \begin{bmatrix} \Delta K_{11} \\ \Delta K_{12} \\ \Delta K_{13} \\ \Delta K_{21} \\ \Delta K_{22} \\ \Delta K_{23} \end{bmatrix} = \begin{bmatrix} 4 \\ 5 \end{bmatrix}$$

This has been achieved in the actual implementation using the trace operator [68,69].

Once the optimization converges to give $\triangle K_a$, the controller is updated to $K_a + \triangle K_a$ and provided as input to the outer loop where the objective function in (26) is calculated. This procedure is repeated iteratively till the value of $J_1(\theta)$ reaches zero (all the closed-loop eigenvalues associated with each of the three system models move to the left of the minimum damping line) or below a certain threshold specified by the user. The final obtained K_a is converted back into its dynamic form and is termed as $K_{method1}(s)$.

A flowchart showing the various steps of the algorithm has been presented in fig. 4.1.

Method 2

As mentioned in previous sub-section, K_a connected to $mod_{a,1m}.....mod_{a,nm}$ (more stressed operating conditions) will have certain eigenvalues outside the 5% damping line. The aim here is to use first order eigenvalue sensitivity to tune K_a such that the critical eigenvalues of all the selected models move inside the 5% damping line [68, 70]. Lets assume $\lambda_{c,i_{1m}}, ..., \lambda_{c,i_{nm}}$ be the critical eigenvalues associated with

$mod_{a,1m}.....mod_{a,nm}$ respectively. The first order eigenvalue sensitivity of $\lambda_{c,i_{1m}}$ with respect to K_a is given as:

$$\triangle\lambda_{c,i_{1m}} = (u_{c,i_{1m}}B_{a,1m})\triangle K_a(C_{a,1m}v_{c,i_{1m}}) \tag{4.22}$$

where $B_{a,1m}$, $C_{a,1m}$ are the input and output matrices of model $mod_{a,1m}$, $u_{c,i_{1m}}$ and $v_{c,i_{1m}}$ are left and right eigenvectors associated with $\lambda_{c,i_{1m}}$ respectively. Equation (4.22) can be written for all the critical eigenvalues of models $mod_{a,2m}.....mod_{a,nm}$.

The control objective is achieved by using an iterative procedure where each iteration solves a quadratic optimization problem. The objective function consists of minimizing a quadratic cost function, $||\triangle K_a||_F^2$. In order to setup the constraints for the problem, a trapezoid has to be defined by the user. Formulation of constraints for the optimization problem has been explained in detail as follows:

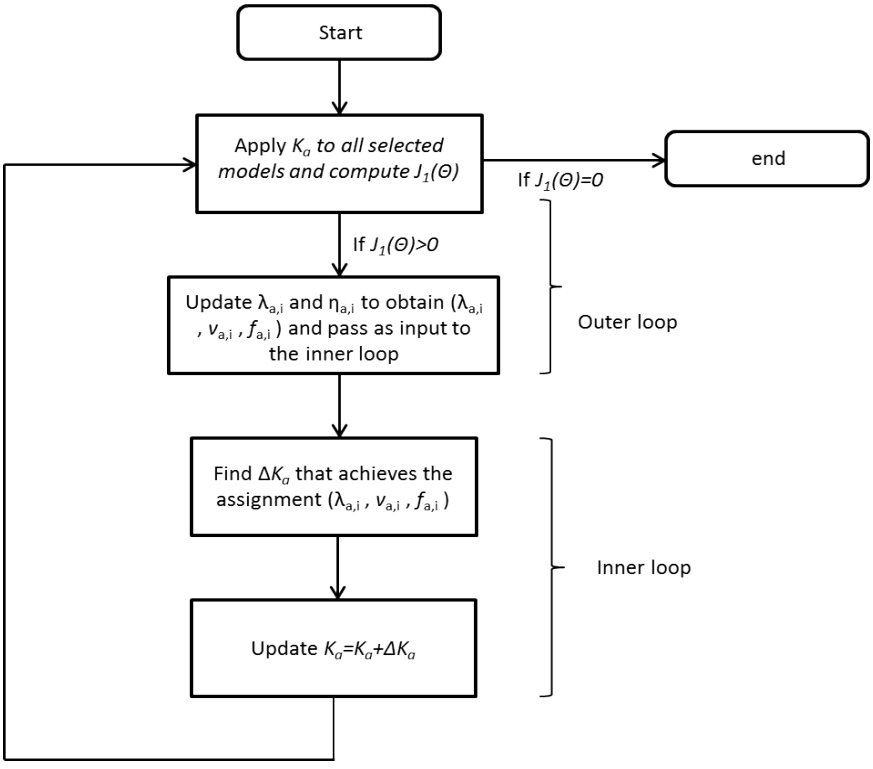

Figure 4.1.: Algorithm showing the steps to be followed in `Method 1`

In order to have a clear understanding of this part, an appropriate starting point is to understand the conditions that a point in a Cartesian plane should satisfy to be on the left or right of a line. Lets consider a line connected by points (a_1, b_1) and (a_2, b_2). Also, consider two points, (a_3, b_3) to the left-side and (a_4, b_4) to the right-side of the line. This has been shown in fig. 4.2.

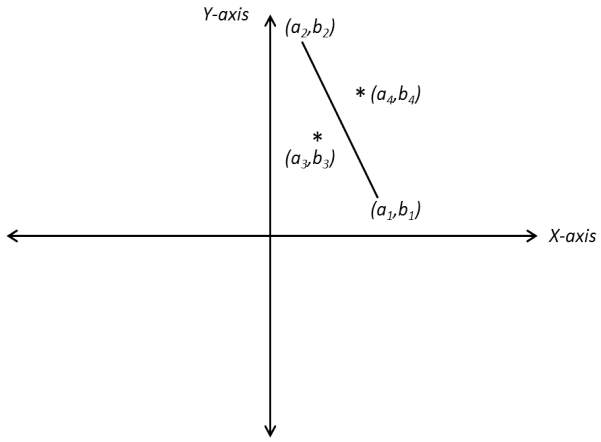

Figure 4.2.: A line to connected by two points to one point each to the left and right of the line

The equation of the line connecting (a_1, b_1) and (a_2, b_2) is given by:

$$(b_2 - b_1)x - (a_2 - a_1)y + a_2b_1 - a_1b_2 = 0 \tag{4.23}$$

The point (a_4, b_4) to the right of the line will satisfy:

$$(b_2 - b_1)a_4 - (a_2 - a_1)b_4 + a_2b_1 - a_1b_2 > 0 \tag{4.24}$$

while point (a_3, b_3) to the left of the line will satisfy:

$$(b_2 - b_1)a_3 - (a_2 - a_1)b_3 + a_2b_1 - a_1b_2 < 0 \tag{4.25}$$

In order to formulate the constraints for the optimization problem, a trapezoid is

defined by the user such that the rightmost side forms the 5% damping line (or any damping percentage based on user requirements). Then, each critical eigenvalue associated with each of the models is connected to the vertices forming the rightmost side as shown in fig. 4.3. The objective of defining this trapezoid is to limit the movement of the critical eigenvalue within the triangle defined by vertices $(0, 0)$, (x_1, y_1) and (x_2, y_2). This enables faster movement of critical eigenvalues into the trapezoid [70]. The point (x_1, y_1) represents the location of the critical eigenvalue $\lambda_{c,i_{1m}}$ (will be different for $\lambda_{c,i_{2m}}, ..., \lambda_{c,i_{nm}}$) . Since the user defines the trapezoid, it is easy to determine the equations of the lines connecting points $(0, 0)$ to (x_1, y_1) and (x_1, y_1) to (x_2, y_2).

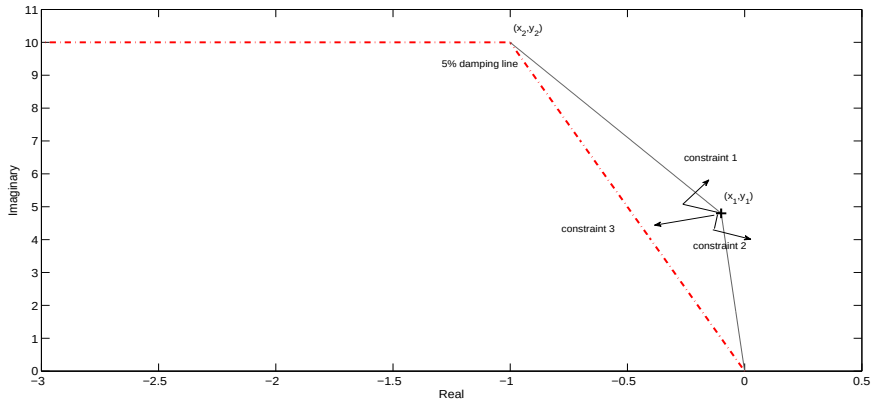

Figure 4.3.: A line to connected by two points to one point each to the left and right of the line

A perturbation ΔK_a will result in a small change $\Delta\lambda_{c,i_{1m}}$. In terms of coordinates, let this small change be represented as $(\Delta x_1, \Delta y_1)$. If the point, $(x_1 + \Delta x_1, y_1 + \Delta y_1)$ has to lie to the left of the line connected by points (x_1, y_1) and (x_2, y_2), it has to satisfy:

$$(y_2 - y_1)(x_1 + \Delta x_1) - (x_2 - x_1)(y_1 + \Delta y_1) + x_2 y_1 - x_1 y_2 < 0 \qquad (4.26)$$

Simplifying (4.26) results in (4.27). This represents constraint 1 shown in fig. 4.3.

$$(y_2-y_1)\Delta x_1-(x_2-x_1)\Delta y_1 < 0 \Longrightarrow (y_2-y_1)(re(\Delta\lambda_{c,i_{1m}}))-(x_2-x_1)(im(\Delta\lambda_{c,i_{1m}})) < 0 \tag{4.27}$$

Similarly, constraint 2 can be represented as:

$$(y_1-0)\Delta x_1-(x_1-0)\Delta y_1 < 0 \Longrightarrow (y_1)(re(\Delta\lambda_{c,i_{1m}}))-(x_1)(im(\Delta\lambda_{c,i_{1m}})) < 0 \tag{4.28}$$

Constraint 3 enables movement of the critical eigenvalue towards the trapezoid and is represented as:

$$L.B \leq re(\triangle\lambda_{c,i_{1m}}) \leq U.B \tag{4.29}$$

where $L.B$ and $U.B$ are negative numbers representing the lower and upper bounds respectively for the real part of $\triangle\lambda_{c,i_{1m}}$. In order to represent the constraints (4.27) - (4.29) in terms of the optimizing variable ΔK_a, equation (4.22) is utilized [68, 69]. The objective function used for the optimization results in $\triangle K_a$ being small which ensures that the first order eigenvalue sensitivity holds true. The method is repeated iteratively and K_a is updated in each iteration till all the critical inter-area modes move into the trapezoid. The final obtained K_a is converted back into its dynamic form and is termed as $K_{method2}(s)$. A flowchart explaining the algorithm has been shown in fig. 4.4.

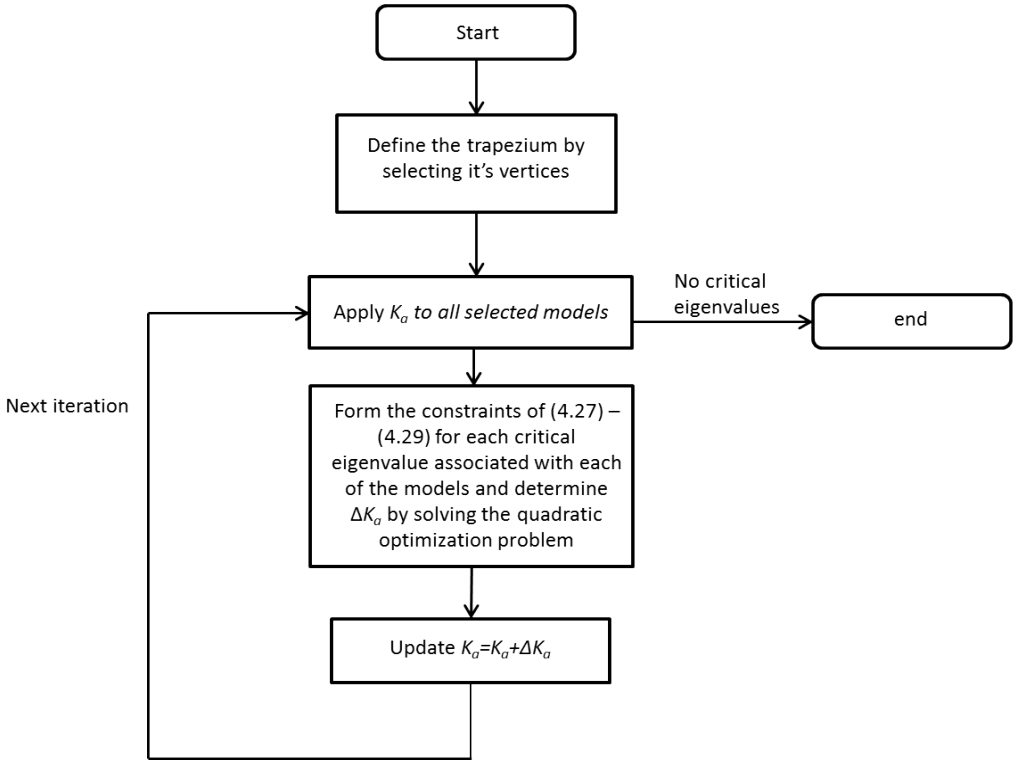

Figure 4.4.: Algorithm showing the steps to be followed in `Method 2`

4.3. Approach I

The multi-model optimization methods described in the previous section are applied on the IEEE 68 bus system described in detail in the previous chapter. However, the feedback signals have been selected to be the tie-line power flow in lines $(52-42)$ and $(42-41)$ unlike chapter 3. The *base-case* operating point is identical to the one presented in chapter 3 (also provided in appendix A). Initially, the user has knowledge about the controller $K(s)$ and a few, selected models of the system corresponding to different operating points. It should be noted that $K(s)$ used in this chapter was designed for 5% damping assignment of the critical eigenvalues of the *base-case* system. The models selected to participate in the optimization problem have been shown in table 4.1. These operating points are not selected randomly but

Table 4.1.: Different operating points for ensuring robustness

Operating point	Operating condition
OP1	*base-case* model
OP2	increase the output of generator 16 by 10 p.u (base 100 MW) and increase the load at bus 42 by 10p.u
OP3	increase the output of generator 15 by 15 p.u and reduce the output of generator 14 by 15 p.u

are chosen based on the fact that they negatively impact the damping of critical inter-area modes. The first step is to obtain the "extended dynamic system connected to proportional feedback" representation of all the selected models connected to $K(s)$. Then, `methods 1 and 2` are implemented to obtain the controllers $K_{method1}(s)$ and $K_{method2}(s)$ respectively.

- `Method 1:` The initial controller $K(s)$ assigned the poorly damped eigenvalues of the *base-case* model to $(-0.166 + 3.329i)$ and $(-0.244 + 4.889i)$ (5% damping assignment). These are the eigenvalues that are chosen to be re-assigned such that critical eigenvalues across all the models satisfy the 5% damping criterion. The bounds $\{\alpha_{\lambda_i,max}, \beta_{\lambda_i,min}, \beta_{\lambda_i,max}, \alpha_{\eta_i,min}, \alpha_{\eta_i,max}, \beta_{\eta_i,min}, \beta_{\eta_i,max}\}$ are selected to be $\{1, -1.5, 1.5, -5, 5, -5, 5\}$ and are the same for both the selected inter-area modes. The controller designed using this method is known as $K_{method1}(s)$.

- `Method 2:` This method requires the user to define the vertices of the trapezoid in order to run the optimization procedure presented in fig. 4.4. In order to attain the objective of minimum 5% damping, the vertices of the trapezoid are chosen to be $(0, 0)$, $(-200, 0)$, $(-200 + 200i)$ and $(-10.01 + 200i)$ (clockwise with respect to fig. 4.3). These vertices are selected such that only the critical

inter-area modes lie outside the trapezoid. If not, then the optimization will try to move an eigenvalue that might not be controllable and hence there would be no convergence of the optimization algorithm. The bounds $L.B$ and $U.B$ have been chosen to be -0.1 and -0.05 respectively which signifies the limits of the movement of a critical inter-area mode towards the left. The controller designed using this method is known as $K_{method2}(s)$.

Once the relevant inputs are provided to both the methods, algorithms presented in figs. 4.1 and 4.4 are run to obtain controllers, $K_{method1}(s)$ and $K_{method2}(s)$ respectively. The closed-loop eigenvalues of the selected system models connected to $K(s)$, $K_{method1}(s)$ and $K_{method2}(s)$ have been shown in fig. 4.5-4.7. It is clearly evident that $K_{method1}(s)$ and $K_{method2}(s)$ are capable of moving all the critical inter-area modes to the left of the 5% damping line. The eigenvalue plots have been corroborated by providing time domain plots showing the angular difference between generators 15 and 16 for a ten-cycle, three-phase fault at bus 52. These results have been presented in figs. 4.8-4.10 for all the selected operating points ($OP1$, $OP2$, $OP3$).

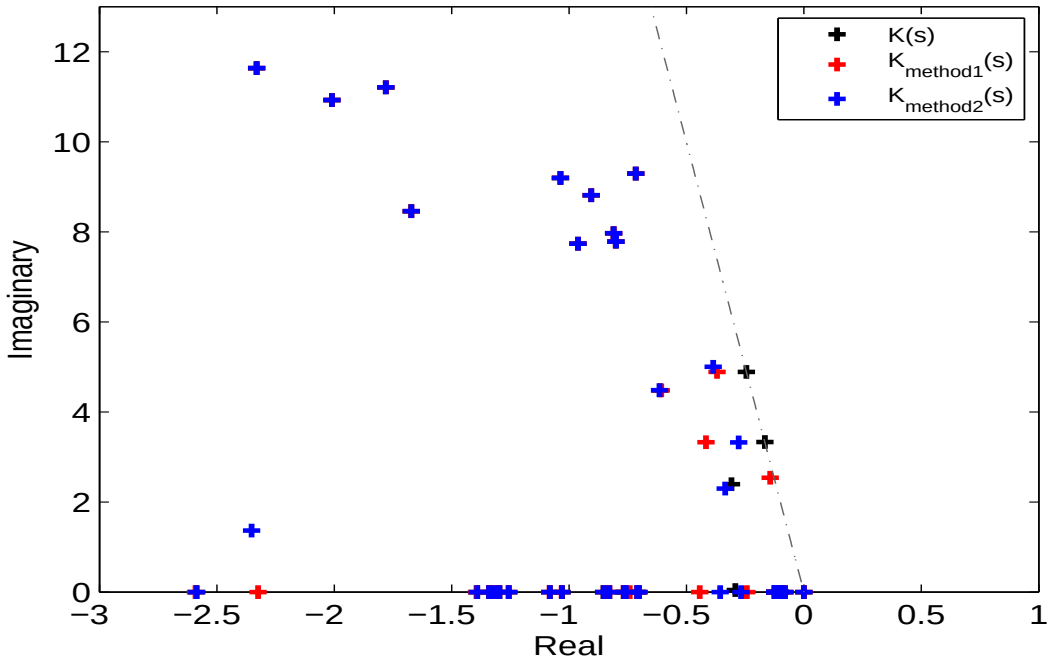

Figure 4.5.: Closed-loop eigenvalues with $K(s)$, $K_{method1}(s)$ and $K_{method2}(s)$ connected in feedback to system model $OP1$

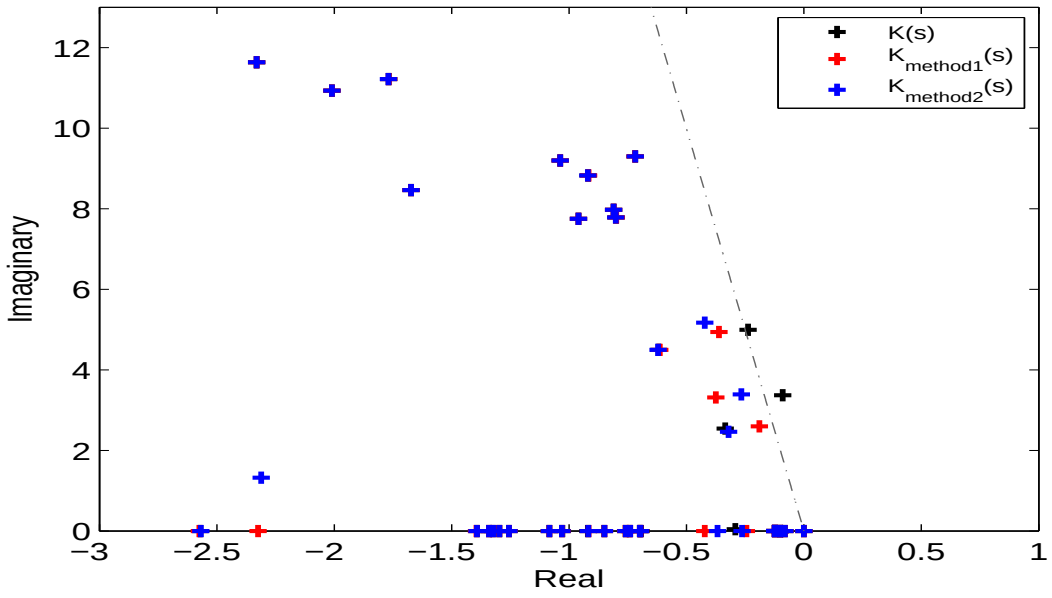

Figure 4.6.: Closed-loop eigenvalues with $K(s)$, $K_{method1}(s)$ and $K_{method2}(s)$ connected in feedback to system model $OP2$

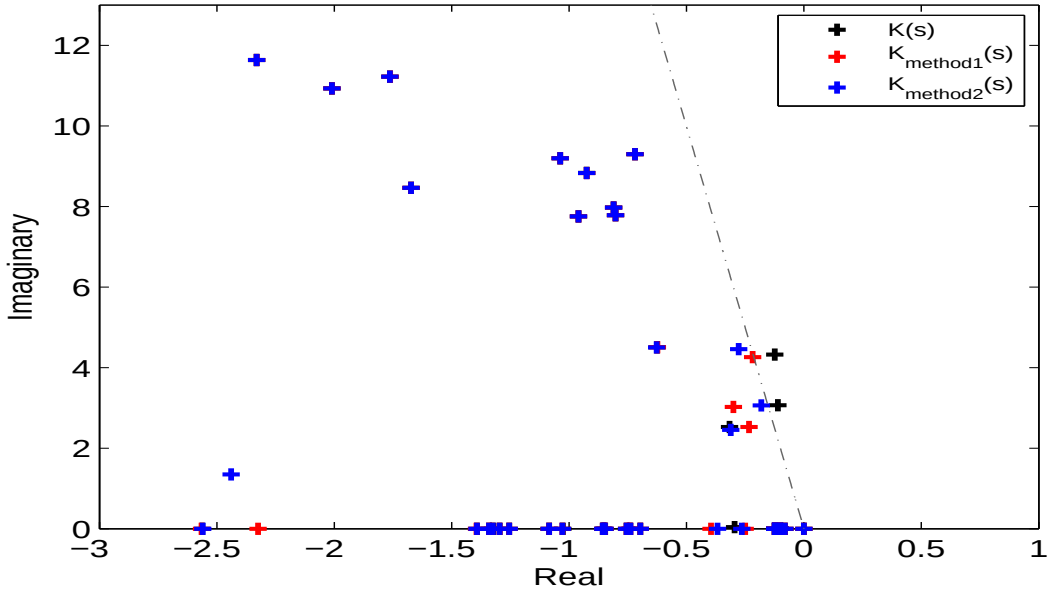

Figure 4.7.: Closed-loop eigenvalues with $K(s)$, $K_{method1}(s)$ and $K_{method2}(s)$ connected in feedback to system model $OP3$

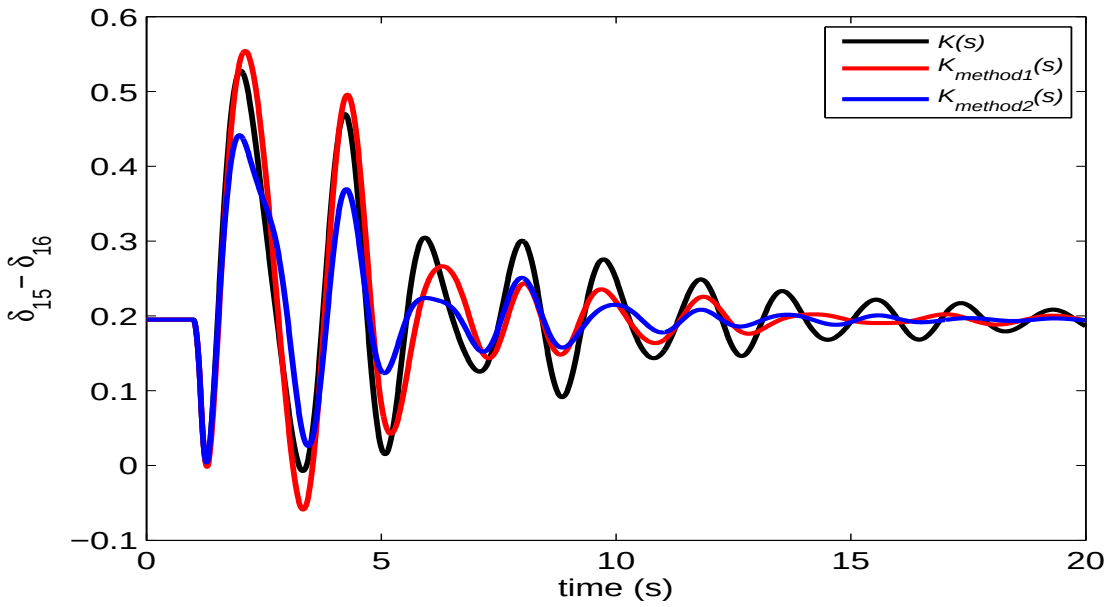

Figure 4.8.: Angle difference between machines 15 and 16 for a ten-cycle, three-phase fault at bus 52, OP1

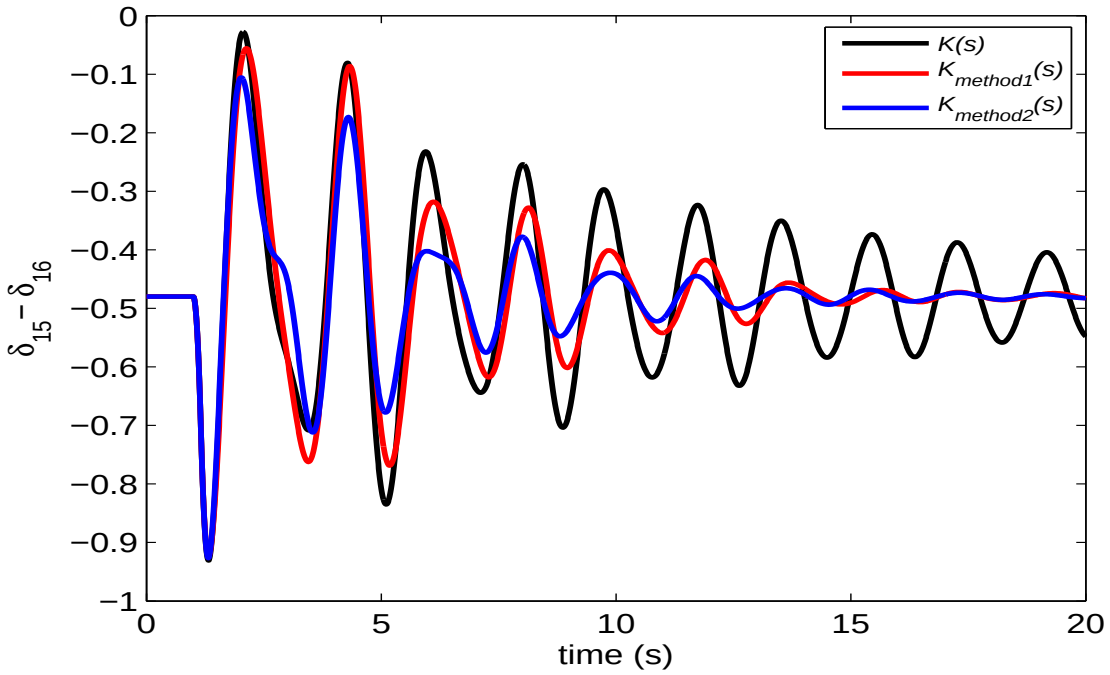

Figure 4.9.: Angle difference between machines 15 and 16 for a ten-cycle, three-phase fault at bus 52, OP2

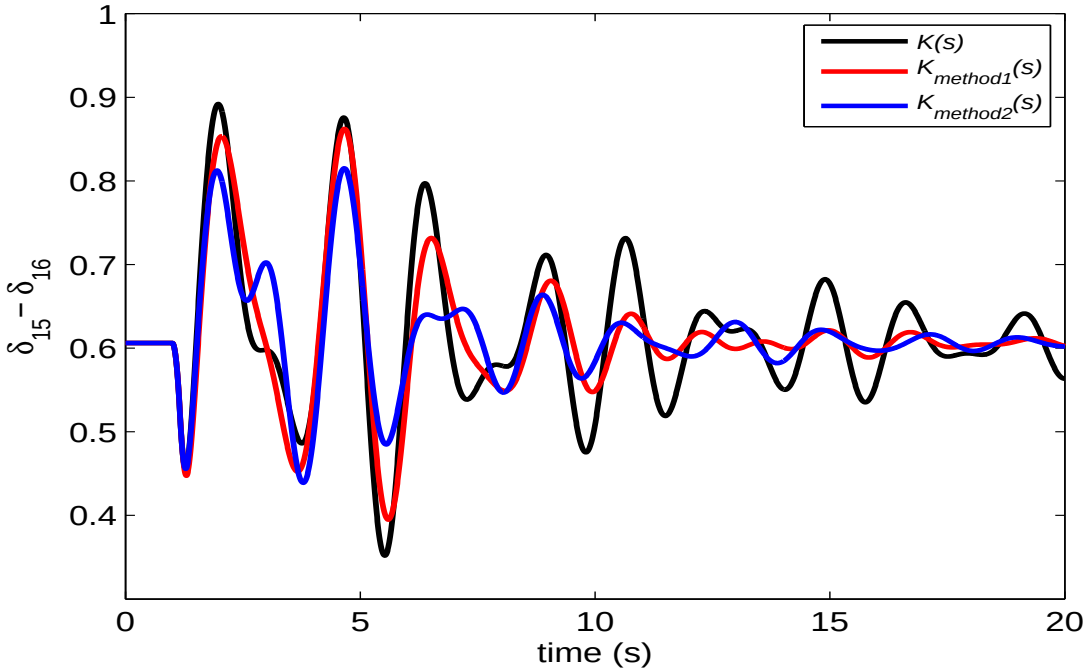

Figure 4.10.: Angle difference between machines 15 and 16 for a ten-cycle, three-phase fault at bus 52, OP3

4.4. Approach II

Approach I successfully demonstrated the design of two controllers obtained using multi-model optimization techniques. It was shown how different operating points of the system can be utilized to design controllers that are better than the one designed for the *base-case* model. Using approach II , the aim is to focus on two objectives that were not addressed using approach I:

- Robustness of the controller to variation of a specific parameter in the system.
- Robustness of the controller to uncertainty in time delays of feedback signals.

It should be noted that a single controller should be able to achieve both the goals. There are two important steps to be followed in approach II that differentiate it from approach I:

1. Selecting a parameter of the system that has a high impact on the damping of critical inter-area modes.
2. Selecting the models to be incorporated in the multi-model optimization such that the controller becomes robust to variations in the chosen system parameter.

Selecting the parameter is simple and can be selected either based on the knowledge of the system or by performing sensitivity analysis. Selection of models is the harder part and requires the linear fractional transform (LFT) representation of the uncertain system. This LFT representation of the system is provided as an input to a technique that uses first order eigenvalue sensitivity to determine the value of the uncertain parameter that causes one of the critical inter-area modes to reach the imaginary axis. This system model will be called the *worst-case* model. In order to achieve robustness against time delays, a delay τ is incorporated into the *worst-case* model to

obtain the *worst-case + time-delay* model. The "extended dynamic system connected to proportional feedback" representation of these three models connected to $K(s)$ are then provided as inputs to `methods 1` and `2` to obtain controllers $K_{robust1}(s)$ and $K_{robust2}(s)$ respectively.

Linear Fractional Transform

The essence of this procedure is to separate an uncertain system into certain and uncertain part so that the system can be used to perform robust stability and performance studies. An aspect of power systems that plays an important role in forming the LFT representation is that an uncertain operating parameter cannot be directly associated with the elements of the state matrix. Usually in control systems, real parametric uncertainty analysis involves an uncertain parameter in the state matrix. Obtaining the LFT in such a scenario is a straightforward procedure as opposed to power systems. Therefore, a numerical technique has been used to obtain the LFT [71, 72].

An uncertain state space representation of a system is given in (4.30) [72].

$$\dot{x} = A(p)x \tag{4.30}$$

where p is the uncertain parameter that varies in the range $p_{min} \leq p \leq p_{max}$. Assuming that the parameter p has a nominal value p_{nom}, the parametric uncertainty can be represented as a parametric set as given in (4.31).

$$p = p_{nom}(1 + \overline{r}\delta) \tag{4.31}$$

where $p_{nom} = \frac{p^{max}+p^{min}}{2}, \overline{r} = \frac{p^{max}-p^{min}}{p^{max}+p^{min}}$ and δ is a real scalar lying between -1 and

1. Similar to the approach followed in μ synthesis, the initial objective is to obtain the '$M-\Delta$' form to separate out the fixed part and uncertainties. In the case of operating point uncertainty, the elements of the uncertain state space matrix cannot be explicitly expressed as functions of the parameter 'p'. Therefore, a numerical technique is used to approximate the relationship [71, 72]. The parameter p is varied over a range of possible values $[p_1.....p_n]$ and the state matrix is obtained for each operating condition. A generalized variation of the element $a_{ij} \in A_i$ can be expressed as $a_{ij}^{var} \in F_{ij}(p)$ where F_{ij} is the function to be determined. According to [71, 72], a second order polynomial function is appropriate for approximating a single parameter uncertainty.

$$a_{ij}^{var} = \hat{a_{ij,0}} + \hat{a_{ij,1}}p + \hat{a_{ij,2}}p^2 \tag{4.32}$$

For $[p_1.....p_n]$, an over-determined set of equations is obtained as shown in (4.33).

$$\begin{bmatrix} 1 & p_1 & p_1^2 \\ . & . & . \\ 1 & p_n & p_n^2 \end{bmatrix} \begin{bmatrix} \hat{a_{ij0}} \\ \hat{a_{ij1}} \\ \hat{a_{ij2}} \end{bmatrix} = \begin{bmatrix} a_{ij,A_1} \\ . \\ a_{ij,A_n} \end{bmatrix} \tag{4.33}$$

where $\hat{a_{ij,0}}, \hat{a_{ij,1}}, \hat{a_{ij,2}}$ are the elements of the matrix $\hat{A}_0, \hat{A}_1, \hat{A}_2$ and can be determined using least squares method. The Substitution of (4.31) into (4.32) results in (4.34) [71].

$$A(\delta) = \overline{A}_0 + L^T[\overline{A}_1(\delta I) + \overline{A}_2(\delta^2 I)]R \tag{4.34}$$

where $\overline{A}_0$, $\overline{A}_1$ and $\overline{A}_2$ are dependent on $\hat{A}_0$, $\hat{A}_1$, $\hat{A}_2$, p_{max} and p_{min}. The L and R matrices are made up of 0's and 1's which signify the change of matrix rows and columns with change in operating conditions. The next step is to transform (4.34)

into a LFT representation shown in (4.35) - (4.37).

$$\dot{x} = T_{11}x + T_{12}w \tag{4.35}$$

$$z = T_{21}x + T_{22}w \tag{4.36}$$

$$w = \Delta z \tag{4.37}$$

where $w = \begin{bmatrix} w_1 & w_2 \end{bmatrix}$ and $z = \begin{bmatrix} z_1 & z_2 \end{bmatrix}$ are the inputs and outputs to the uncertainties respectively, $T_{11} = \overline{A}_0$, $T_{12} = \begin{bmatrix} L^T\overline{A}_1 & L^T\overline{A}_2 \end{bmatrix}$, $T_{21} = \begin{bmatrix} 0 \\ R \end{bmatrix}$, $T_{22} = \begin{bmatrix} I & 0 \\ 0 & 0 \end{bmatrix}$, $\triangle = \begin{bmatrix} \delta & 0 \\ 0 & \delta^2 \end{bmatrix}$. Fig. 4.11 depicts the LFT representation of the system for robust stability analysis. For robustness analysis, the '$\frac{1}{s}$' loop shown in fig. 4.11 is closed to obtain the '$M - \Delta$' structure.

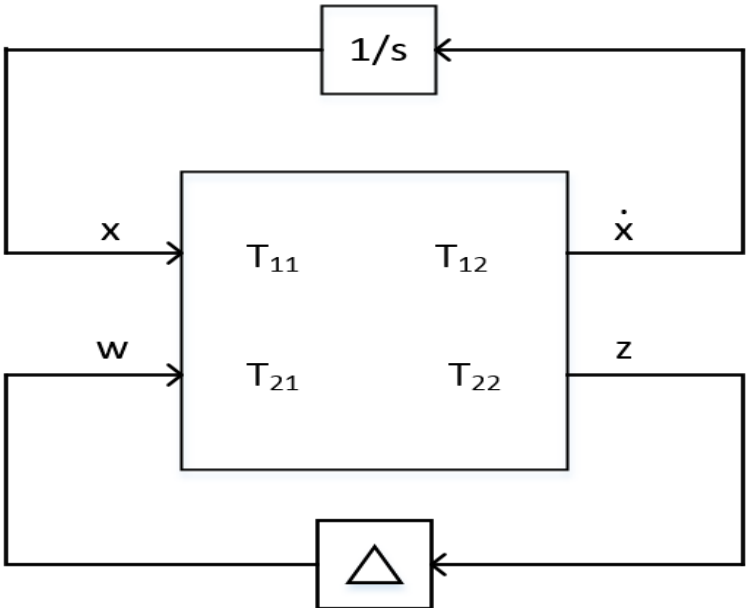

Figure 4.11.: LFT representation of the system

Destabilizing Perturbation

An algorithm presented in [73] is used to find the largest perturbation of the uncertain parameter from base-case value that destabilizes the system. The $M-\Delta$ structure obtained in the previous sub-section can be thought of as a dynamic system M connected to a feedback $\triangle$. Assume the state space representation of M to be $(A^{'}, B^{'}, C^{'}, 0)$. Then the closed-loop state matrix can be expressed as $A^{'} + B^{'}\Delta C^{'}$. The idea is to vary the perturbation Δ such that one of the poles of the closed loop system reaches the imaginary axis. However, the poles that are to be moved are unknown initially. To resolve this issue, a power algorithm used for the regularization of the real mu problem is used for finding the initial perturbation [73, 74]. Power algorithm results in an initial perturbation Δ^R that has moved one of the eigenvalues λ_0 very close to the imaginary axis. Using this initial value, an optimization algorithm is used to find an additional model perturbation $\tilde{\Delta}$ that moves one of the poles $(\lambda_0\ )$ of $A^{'} + B^{'}(\Delta^R + \tilde{\Delta})C^{'}$ to the imaginary axis [73]. The eigenvalue λ_0 is moved incrementally towards the imaginary axis using first order eigenvalue sensitivity as given in (4.38) and (4.39).

$$\alpha_i = (u_0 B^{'})(C^{'} v_0) \tag{4.38}$$

$$\Delta\lambda_0 = \textstyle\sum_{i=1}^{r} \alpha_i \tilde{\delta_i} \tag{4.39}$$

where $\tilde{\Delta} = [\tilde{\delta_1}, \tilde{\delta_2}.....\tilde{\delta_r}]$ are perturbations along different dimensions of hypercube $\tilde{\Delta}$ and u_0, v_0 are the left and right eigenvectors associated with eigenvalue λ_0. Skew-mu toolbox in matlab has been used to find the destabilizing perturbation or the *worst-case* model [75]. It is worth mentioning that the algorithm is polynomial time. The

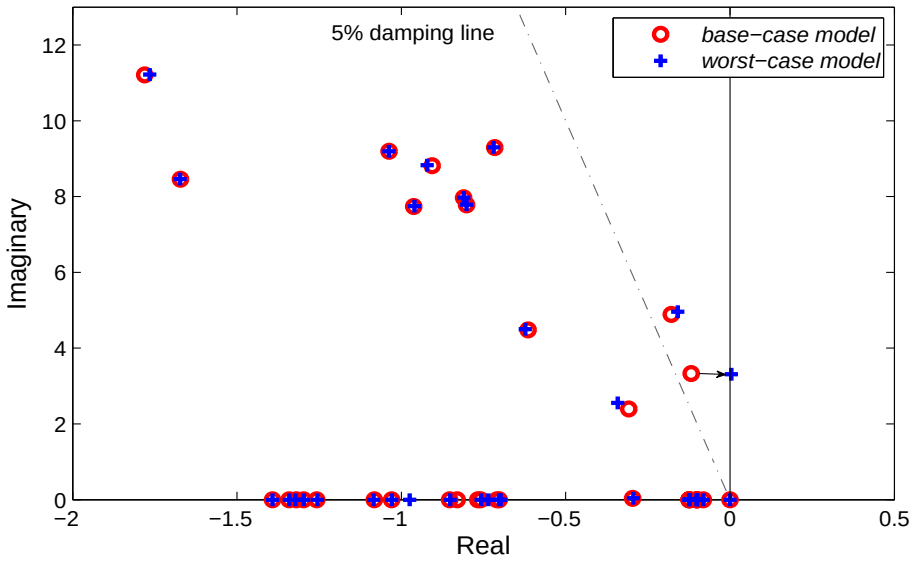

Figure 4.12.: Eigenvalues of the *base-case* and *worst-case* models

eigenvalues of a sample *base-case* and *worst-case* models have been shown in fig. 4.12.

Results

The controllers, $K_{robust1}(s)$ and $K_{robust2}(s)$, designed using the techniques presented in section 4.4 will be applied on the IEEE 68 bus system. The *base-case* system is identical to the one used in chapter 3 and section 4.3. Initially, the user has knowledge of $K(s)$ and the *base-case* system model. The poorly damped inter-area modes in the *base-case* model are known to be sensitive to the real power flow in tie-line $(52-42)$ and thus the real power flow in tie-line $(52-42)$ is chosen as the uncertain parameter for the designing the robust controllers. In order to generate the LFT representation of the uncertain system, the power flow in tie-line $(52-42)$ is varied by varying the load at bus 42 as well as the output of generator 16. Three different operating points corresponding to $P_{load,42} = \begin{bmatrix} 150MW & 350MW & 550MW \end{bmatrix}$ ($150MW$ is the base case load) are used for the purpose. Once obtained, the $M-\triangle$ representation of the uncertain system is provided as an input to the algorithm, '*mu_lb_with_freq*.m', in

the skew-mu toolbox to determine the *worst-case* model. The worst-case operating point is found to be the scenario where $P_{load,42} = 1611MW$. A time delay $e^{-\tau s}$ with $\tau = 400ms$ is incorporated into the *worst-case* model (using Pade approximation) to obtain the *worst-case+time-delay* model [32]. These models along with $K(s)$ are provided as inputs to `methods 1` and `2`. Once all the three models are known, the next step is to obtain $mod_{a,bc}$, $mod_{a,wc}$, $mod_{a,wcd}$ (extended dynamic systems associated with the *base-case, worst-case* and *worst-case+time-delay* models respectively) and K_a.

The initial inputs and bounds to be provided to `methods 1` and `2` are the same as listed in section 4.3. The closed-loop eigenvalues of the *base-case*, *worst-case* and *worst-case+time-delay* models connected to $K(s)$, $K_{robust1}(s)$ and $K_{robust2}(s)$ have been shown in figs. 4.13-4.15. The robustness of the controller is validated by showing the response of the system to a disturbance for different values of real power on line $(52-42)$ (achieved by varying the load on bus 42 and output of generator 16) and different time delays. A three-phase, ten-cycle fault has been applied on bus 52 and the angle difference between generators 15 and 16 has been shown in figs. 4.16 - 4.19.

4.5. Discussion

In this chapter, a novel technique of making a WAC robust to operating point and time delay uncertainties has been presented. The design of a robust WAC in a power system can be considered as a two stage process with the algorithm presented in chapter 3 being the first stage (can be some other technique also) and the two algorithms (`method 1 and 2`) presented in this chapter being the second stage. The robustness has been achieved by setting up a multi-model optimization problem. The aim of the multi-model optimization problem is to tune the initial controller such that all

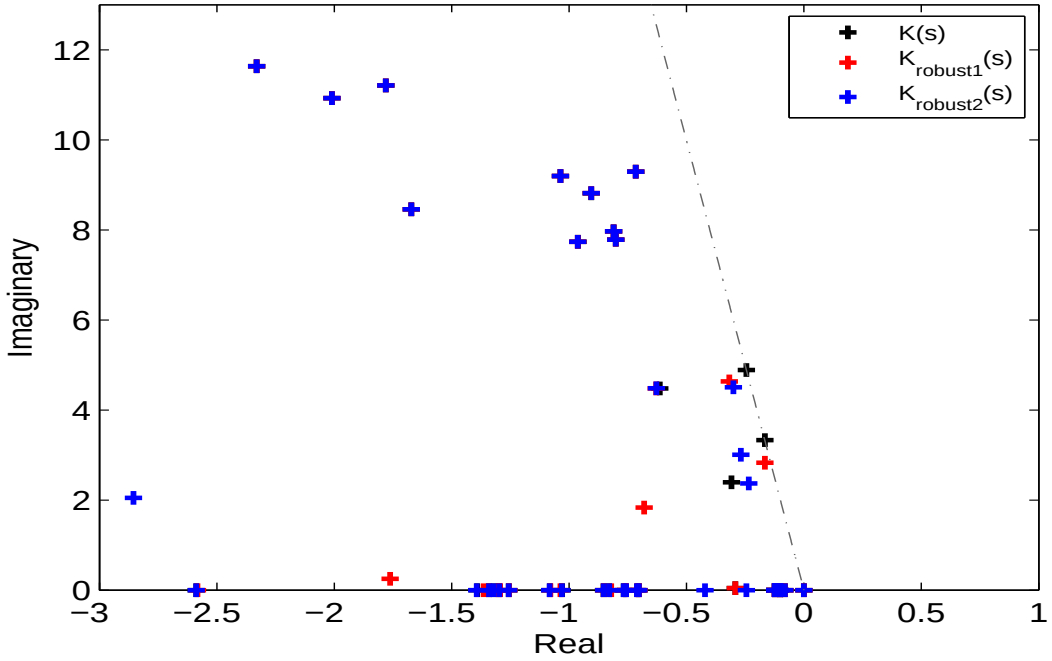

Figure 4.13.: Closed-loop eigenvalues with $K(s)$, $K_{robust1}(s)$ and $K_{robust2}(s)$ connected in feedback to system model $OP1$

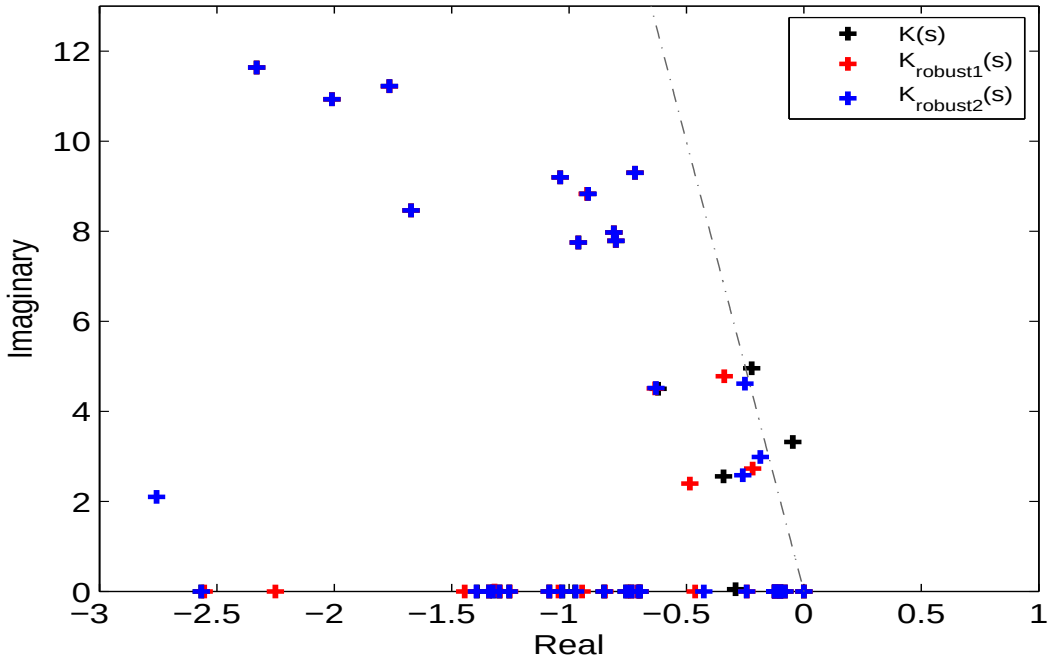

Figure 4.14.: Closed-loop eigenvalues with $K(s)$, $K_{robust1}(s)$ and $K_{robust2}(s)$ connected in feedback to system model $OP2$

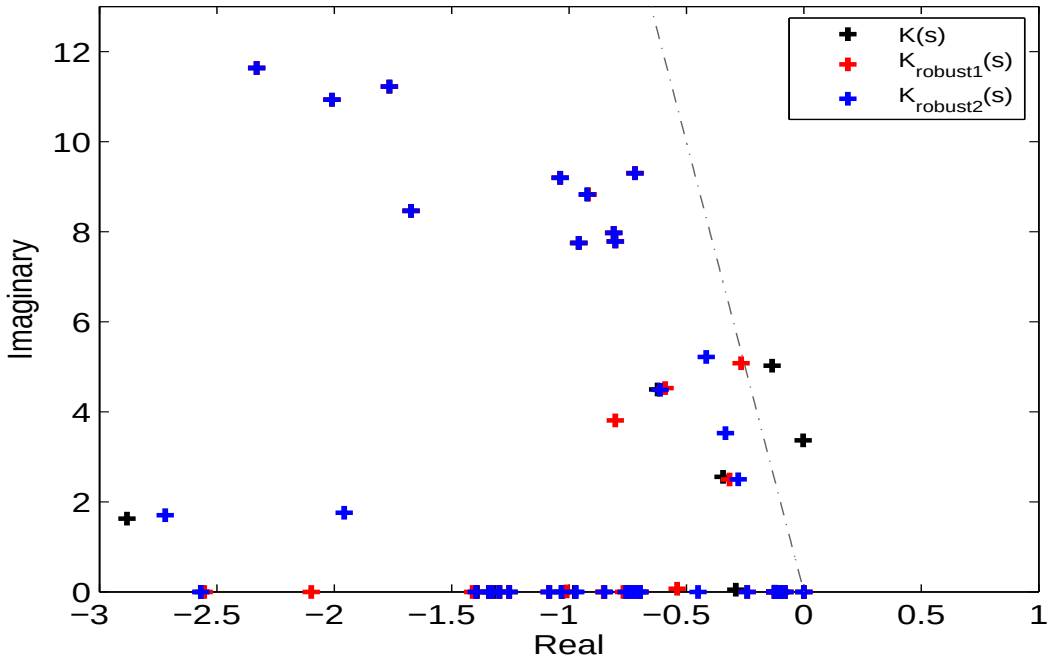

Figure 4.15.: Closed-loop eigenvalues with $K(s)$, $K_{robust1}(s)$ and $K_{robust2}(s)$ connected in feedback to system model $OP3$

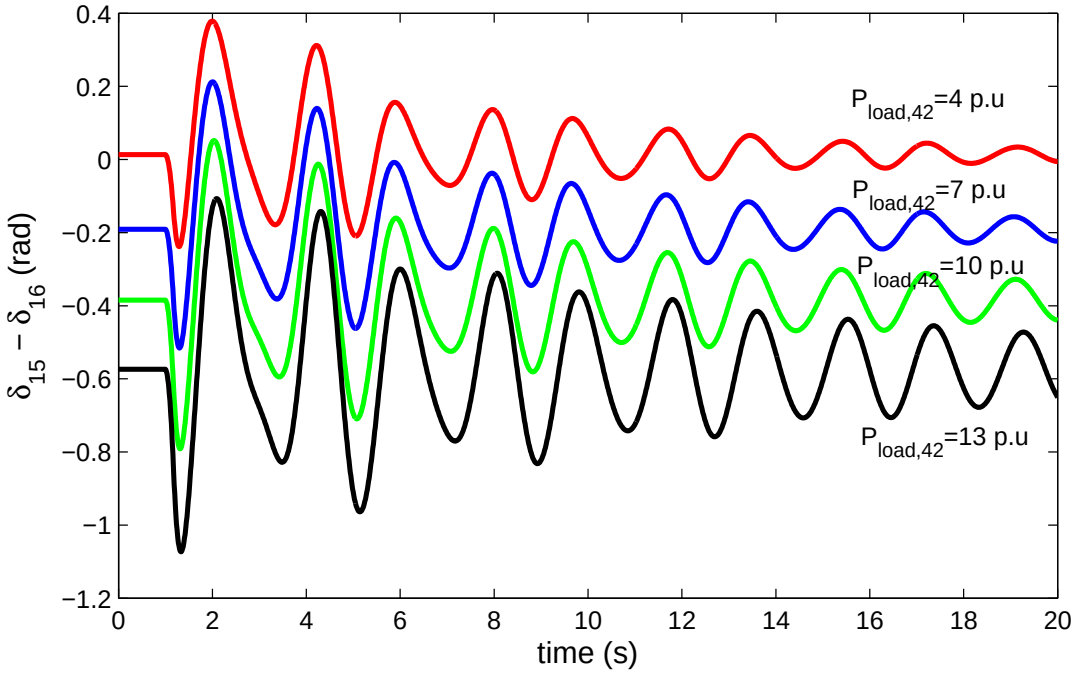

Figure 4.16.: Angle difference between machines 15 and 16 for different values of $P_{load,42}$ using $K(s)$

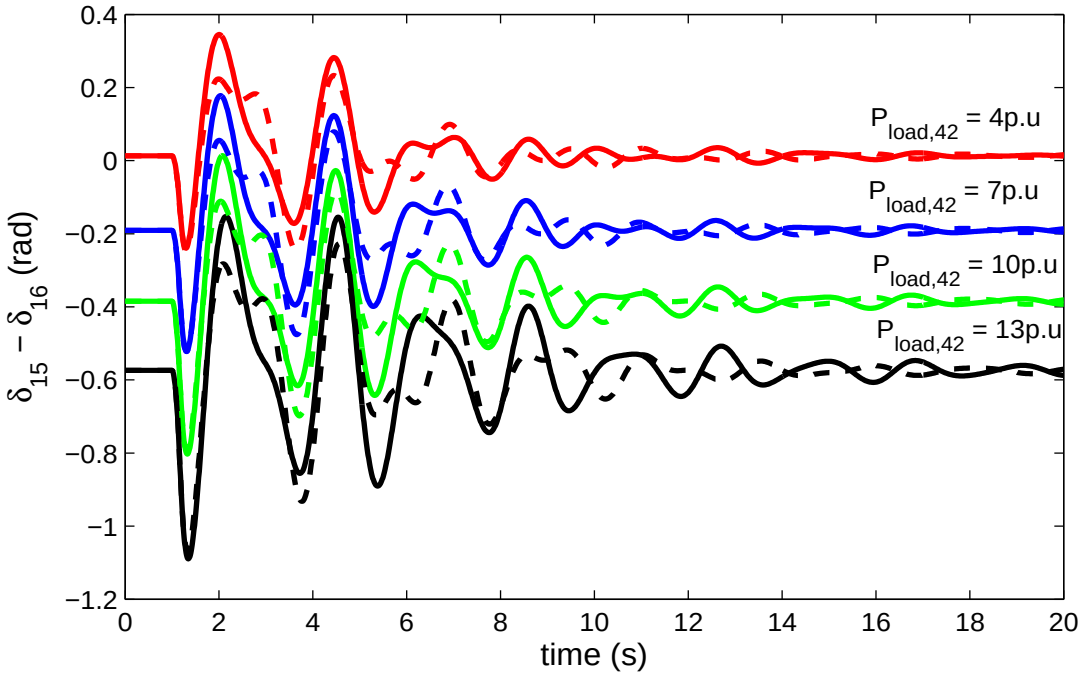

Figure 4.17.: Angle difference between machines 15 and 16 for different values of $P_{load,42}$ using $K_{robust1}(s)$ (solid) and $K_{robust2}(s)$ (dashed)

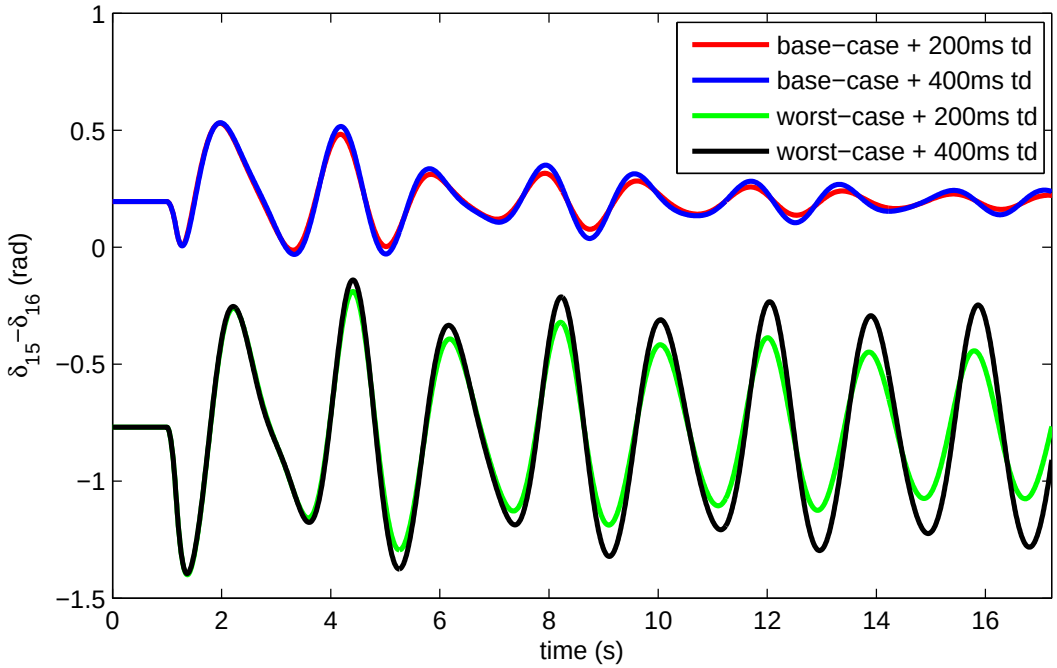

Figure 4.18.: Angle difference between machines 15 and 16 for different values of time delay using $K(s)$

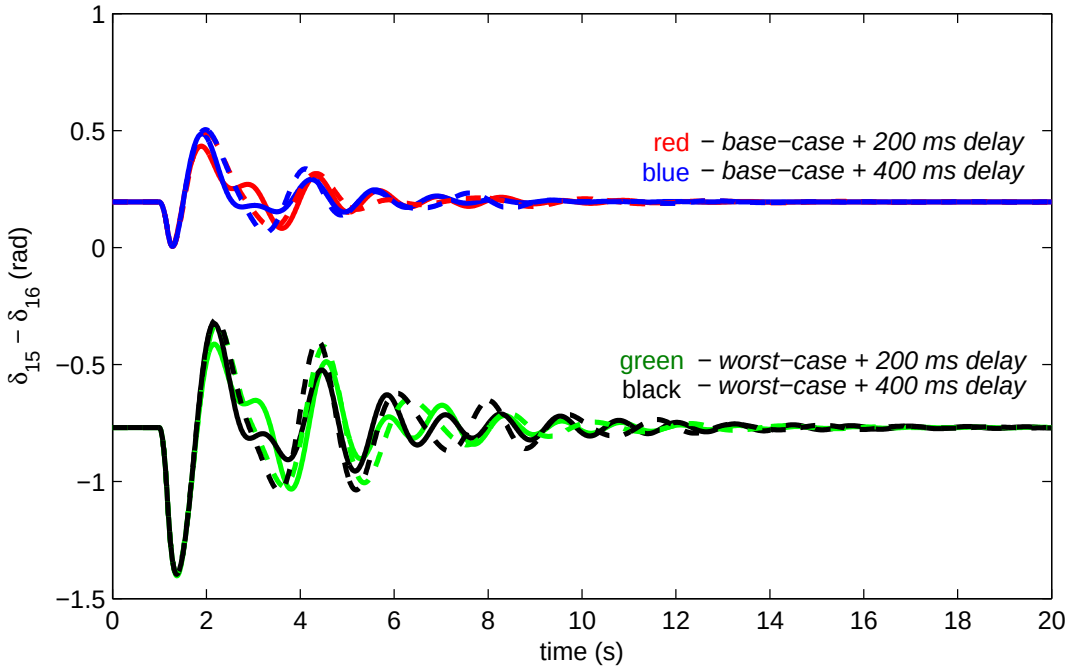

Figure 4.19.: Angle difference between machines 15 and 16 for different values of time-delays using $K_{robust1}(s)$ (solid) and $K_{robust2}(s)$ (dashed)

the critical eigenvalues move towards the left of the minimum damping line. Two different approaches, namely approach `I` and approach `II`, have been presented in this chapter that differ in the way the models to be incorporated in the optimization problem are selected. Approach `I` involves selecting a few, stressed operating points of the system based on the system information whereas approach `II` presents a technique of selecting models such that the designed controller is robust to uncertainty in a specific parameter of the system. The impact of time delay is also addressed using approach `II`. Each of the approaches uses two different methods to formulate the optimization problem. `Method 1` is based on the eigenstructure assignment technique and exploits the degrees of freedom for closed-loop right eigenvector assignment provided by MIMO systems. This method uses an unconstrained, derivative-free optimization algorithm known as MADS to solve the optimization problem. Whereas `method 2` uses an iterative scheme where a quadratic optimization problem is solved

in each iteration. The method uses first order eigenvalue sensitivity to move the critical inter-area modes to the left of the minimum damping line.

5.Conclusions and Future Work

5.1. Conclusions

This dissertation presents a methodology of designing a WAC in an interconnected power system using modal control techniques. The work exploits the development in phasor measurement technology to make use of remote measurements for control. The core contributions of this thesis can be subdivided into two main categories:

- Chapter 3 describes the design of a WAC using partial right eigenstructure assignment technique. The extra degrees of freedom provided by MIMO systems for assigning the closed-loop right eigenvectors has been exploited. A dynamic compensator based controller has been designed in order to limit the number of I/O signals used by the controller. The controller design problem has been formulated as a quadratic optimization problem with the numerator coefficients being the optimizing variables. This formulation is made possible by pre-assigning the compensator poles and the closed-loop right eigenvectors. Two projection techniques have been presented to determine the closed-loop right eigenvectors *a priori*. The closed-loop right eigenvector is dependent on the location of the assigned closed-loop eigenvalue that is selected by the user. The inputs required for the algorithm are the closed-loop eigenvalue locations, structure of the compensator matrix with the compensator poles known, bounds on the numerator coefficients. The algorithm yields a controller that is capable of assigning the critical eigenvalues associated with the *base-case* model to the user-selected locations with minimal control effort. I/O signal selection plays an important role in ensuring that the critical inter-area modes are control-

lable/observable. Later part of chapter 3 demonstrates the formulation of a multi-model optimization problem in order to address the issue of time-delay of feedback signals.

- Chapter 4 presents a novel methodology of making a WAC robust to operating point and time delay uncertainties. When a WAC designed for an operating point is connected to system models corresponding to more stressed operating conditions (in terms of critical inter-area mode damping), there will be certain critical inter-area modes associated with some system models that violate the minimum damping criterion. The main contribution of this chapter is to present multi-model optimization techniques that move critical eigenvalues associated with each of the selected models to the left of the minimum damping line. Two different approaches for selecting the models to be incorporated in the optimization problem has been presented. Approach `I` involves selecting models that are known, stressed operating points of the system whereas approach `II` details a procedure to select models such that a controller becomes robust to variation in an uncertain parameter in the system. Approach `II` also accounts for the uncertainty in time delay of feedback signals. Two different methods, `methods 1` and `2` based on eigenstructure assignment and first order eigenvalue sensitivity respectively, have been used to formulate the multi-model optimization problem.

5.2. Future Work

The work presented in this dissertation can be extended to various other applications:

1. Sensitivity of an eigenvalue with respect to a system parameter can be modi-

fied by using eigenstructure assignment technique. Eigenvalue sensitivity is a function of both the eigenvalue location as well as left and right eigenvectors. A number of times, it is required to reduce the sensitivity of a particular mode such as an inter-area mode to a specific system parameter such as a load in the system.

2. The controller tuning techniques explained in chapter 4 are not capable of obtaining structured controllers. A structured controller has some elements constrained to be a constant or a zero. It would be a challenging task to incorporate structural constraints in the tuning procedure.

3. Another interesting idea would be to combine frequency domain constraints with the modal optimization techniques presented in this dissertation. An example would be to incorporate a constraint where the controller has zero gain at $\omega = 20 rad/s$. This would add more flexibility in design.

4. All the algorithms presented in this dissertation require computation of the eigenvalues of system. Moreover, tuning procedures require computation of closed-loop eigenvalues of multiple models in each iteration. For a large size power system, this would be a computationally intensive activity. Therefore, model order reduction techniques need to be explored in conjunction with modal control techniques presented in this dissertation.

Bibliography

[1] I. Kamwa and L. Gerin-Lajoie, "State-space system identification-toward mimo models for modal analysis and optimization of bulk power systems," *Power Systems, IEEE Transactions on*, vol. 15, no. 1, pp. 326–335, 2000. 2

[2] C. W. Taylor, D. C. Erickson, K. E. Martin, R. E. Wilson, and V. Venkatasubramanian, "Wacs-wide-area stability and voltage control system: R&d and online demonstration," *Proceedings of the IEEE*, vol. 93, no. 5, pp. 892–906, 2005. 2

[3] N. Martins, A. Barbosa, J. Ferraz, M. Dos Santos, A. Bergamo, C. Yung, V. Oliveira, and N. Macedo, "Retuning stabilizers for the north-south brazilian interconnection," in *Panel session on system reliability as affected by power system stabilizers, 1999 IEEE PES Summer Meeting, Edmonton, Canada*, 1999. 2

[4] H. Breulmann, E. Grebe, M. Lösing, *et al.*, "Analysis and damping of inter-area oscillations in the ucte/centrel power system," 2000. 2

[5] K. E. Martin, "Phasor measurement systems in the wecc," in *Power Systems Conference and Exposition, 2006. PSCE'06. 2006 IEEE PES*, pp. 132–138, IEEE, 2006. 2

[6] G. Andersson, P. Donalek, R. Farmer, N. Hatziargyriou, I. Kamwa, P. Kundur, N. Martins, J. Paserba, P. Pourbeik, J. Sanchez-Gasca, *et al.*, "Causes of the 2003 major grid blackouts in north america and europe, and recom-

mended means to improve system dynamic performance," *Power Systems, IEEE Transactions on*, vol. 20, no. 4, pp. 1922–1928, 2005. 2

[7] H. Vu and J. Agee, "Comparison of power system stabilizers for damping local mode oscillations," *Energy Conversion, IEEE Transactions on*, vol. 8, no. 3, pp. 533–538, 1993. 3

[8] P. Kundur, "Effective use of power system stabilizers for enhancement of power system reliability," in *Power Engineering Society Summer Meeting, 1999. IEEE*, vol. 1, pp. 96–103, IEEE, 1999. 3

[9] J. C. Ferraz, N. Martins, and G. N. Taranto, "Simultaneous partial pole placement for power system oscillation damping control," in *IEEE Winter Power Meeting*, vol. 28, pp. 1154–1159, 2001. 3, 23

[10] I. Kamwa, R. Grondin, D. Asber, J. Gingras, and G. Trudel, "Active-power stabilizers for multimachine power systems: challenges and prospects," *IEEE Transactions on Power Systems*, vol. 13, no. 4, pp. 1352–1358, 1998. 3

[11] N. Mithulananthan, C. Canizares, J. Reeve, G. J. Rogers, *et al.*, "Comparison of pss, svc, and statcom controllers for damping power system oscillations," *IEEE Transactions on Power Systems*, vol. 18, no. 2, pp. 786–792, 2003. 3

[12] M. Noroozian and G. Andersson, "Damping of inter-area and local modes by use of controllable components," *Power Delivery, IEEE Transactions on*, vol. 10, no. 4, pp. 2007–2012, 1995. 3

[13] E. V. Larsen, J. J. Sanchez-Gasca, and J. H. Chow, "Concepts for design

of facts controllers to damp power swings," *Power Systems, IEEE Transactions on*, vol. 10, no. 2, pp. 948–956, 1995. 3

[14] M. Zarghami, M. L. Crow, and S. Jagannathan, "Nonlinear control of facts controllers for damping interarea oscillations in power systems," *Power Delivery, IEEE Transactions on*, vol. 25, no. 4, pp. 3113–3121, 2010. 3

[15] H. Wang and F. Swift, "A unified model for the analysis of facts devices in damping power system oscillations. i. single-machine infinite-bus power systems," *Power Delivery, IEEE Transactions on*, vol. 12, no. 2, pp. 941–946, 1997. 4

[16] R. Sadikovic, P. Korba, and G. Andersson, "Application of facts devices for damping of power system oscillations," in *Power Tech, 2005 IEEE Russia*, pp. 1–6, IEEE, 2005. 4

[17] L.-J. Cai and I. Erlich, "Simultaneous coordinated tuning of pss and facts damping controllers in large power systems," *IEEE Transactions on Power Systems*, vol. 20, no. 1, pp. 294–300, 2005. 4

[18] X. Lei, E. N. Lerch, and D. Povh, "Optimization and coordination of damping controls for improving system dynamic performance," *Power Systems, IEEE Transactions on*, vol. 16, no. 3, pp. 473–480, 2001. 4

[19] P. Pourbeik and M. J. Gibbard, "Simultaneous coordination of power system stabilizers and facts device stabilizers in a multimachine power system for enhancing dynamic performance," *Power Systems, IEEE Transactions on*, vol. 13, no. 2, pp. 473–479, 1998. 4

[20] X. Yang and A. Feliachi, "Stabilization of inter-area oscillation modes

through excitation systems," *Power Systems, IEEE Transactions on*, vol. 9, no. 1, pp. 494–502, 1994. 4

[21] M. J. Gibbard, D. J. Vowles, and P. Pourbeik, "Interactions between, and effectiveness of, power system stabilizers and facts device stabilizers in multimachine systems," *Power Systems, IEEE Transactions on*, vol. 15, no. 2, pp. 748–755, 2000. 5

[22] M. E. Aboul-Ela, A. Sallam, J. D. McCalley, and A. Fouad, "Damping controller design for power system oscillations using global signals," *Power Systems, IEEE Transactions on*, vol. 11, no. 2, pp. 767–773, 1996. 5

[23] J. H. Chow, J. J. Sanchez-Gasca, H. Ren, and S. Wang, "Power system damping controller design-using multiple input signals," *Control Systems, IEEE*, vol. 20, no. 4, pp. 82–90, 2000. 5

[24] A. Heniche and I. Kamwa, "Assessment of two methods to select wide-area signals for power system damping control," *Power Systems, IEEE Transactions on*, vol. 23, no. 2, pp. 572–581, 2008. 5, 21

[25] U. Mhaskar and A. Kulkarni, "Power oscillation damping using facts devices: modal controllability, observability in local signals, and location of transfer function zeros," *Power Systems, IEEE Transactions on*, vol. 21, no. 1, pp. 285–294, 2006. 5

[26] A. Hamdan and A. Elabdalla, "Geometric measures of modal controllability and observability of power system models," *Electric power systems research*, vol. 15, no. 2, pp. 147–155, 1988. 5

[27] M. Farsangi, Y. Song, and K. Y. Lee, "Choice of facts device control inputs

for damping interarea oscillations," *Power Systems, IEEE Transactions on*, vol. 19, no. 2, pp. 1135–1143, 2004. 5

[28] A. G. Phadke and J. S. Thorp, *Synchronized phasor measurements and their applications*. Springer Science & Business Media, 2008. 5

[29] A. F. Snyder, D. Ivanescu, N. HadjSaid, D. Georges, and T. Margotin, "Delayed-input wide-area stability control with synchronized phasor measurements and linear matrix inequalities," in *IEEE Power Engineering Society Summer Meeting*, vol. 2, pp. 1009–1014, IEEE, 2000. 6, 36

[30] I. Kamwa, R. Grondin, and Y. Hébert, "Wide-area measurement based stabilizing control of large power systems-a decentralized/hierarchical approach," *IEEE Transactions on Power Systems*, vol. 16, no. 1, pp. 136–153, 2001. 6

[31] H. Ni, G. T. Heydt, and L. Mili, "Power system stability agents using robust wide area control," *Power Systems, IEEE Transactions on*, vol. 17, no. 4, pp. 1123–1131, 2002. 6

[32] D. Dotta, A. S. Silva, and I. C. Decker, "Wide-area measurements-based two-level control design considering signal transmission delay," *IEEE Transactions on Power Systems*, vol. 24, no. 1, pp. 208–216, 2009. 6, 25, 35, 80

[33] Y. Zhang and A. Bose, "Design of wide-area damping controllers for interarea oscillations," *Power Systems, IEEE Transactions on*, vol. 23, no. 3, pp. 1136–1143, 2008. 6

[34] B. C. Moore, "On the flexibility offered by state feedback in multivariable systems beyond closed loop eigenvalue assignment," in *Decision and*

Control including the 14th Symposium on Adaptive Processes, 1975 IEEE Conference on, pp. 207–214, IEEE, 1975. 7, 23

[35] G. P. Liu and R. Patton, *Eigenstructure assignment for control system design*. John Wiley & Sons, Inc., 1998. 7

[36] H. Kimura, "Pole assignment by gain output feedback," *IEEE Transactions on Automatic Control*, vol. 20, no. 4, pp. 509–516, 1975. 7, 23

[37] P.-H. Huang and Y.-Y. Hsu, "Eigenstructure assignment in a longitudinal power system via excitation control," *IEEE Transactions on Power Systems*, vol. 5, no. 1, pp. 96–102, 1990. 7, 28

[38] N. Kshatriya, U. D. Annakkage, F. M. Hughes, and A. M. Gole, "Optimized partial eigenstructure assignment-based design of a combined pss and active damping controller for a dfig," *IEEE Transactions on Power Systems*, vol. 25, no. 2, pp. 866–876, 2010. 7, 8, 24, 26, 28, 29

[39] A. Konara and U. Annakkage, "Robust power system stabilizer design using eigenstructure assignment," *IEEE Transactions on Power Systems*, vol. PP, no. 3, pp. 1–9, 2015. 8, 55, 57

[40] F. Milano, *Power system modelling and scripting*. Springer Science & Business Media, 2010. 12, 18

[41] P. Kundur, *Power system stability and control*, vol. 7. McGraw-hill New York, 1994. 14, 18, 20

[42] J. H. Chow and K. W. Cheung, "A toolbox for power system dynamics and control engineering education and research," *IEEE Transactions on Power Systems*, vol. 7, no. 4, pp. 1559–1564, 1992. 18, 40

[43] P. W. Sauer and M. Pai, "Power system dynamics and stability," *Urbana*, 1998. 18

[44] L. C. Zanetta Jr and J. J. d. Cruz, "An incremental approach to the coordinated tuning of power systems stabilizers using mathematical programming," *IEEE Transactions on Power Systems*, vol. 20, no. 2, pp. 895–902, 2005. 23, 32

[45] R. Jabr, B. C. Pal, N. Martins, *et al.*, "A sequential conic programming approach for the coordinated and robust design of power system stabilizers," *IEEE Transactions on Power Systems*, vol. 25, no. 3, pp. 1627–1637, 2010. 23, 54, 55

[46] T. B. Cunningham, "Eigenspace selection procedures for closed loop response shaping with modal control," in *Decision and Control including the Symposium on Adaptive Processes, 1980 19th IEEE Conference on*, pp. 178–186, IEEE, 1980. 24, 59

[47] Y. Le Gorrec, J. Magni, and C. Chiappa, "Flexible transmission system controlled by modal dynamic feedback," in *1997 European Control Conference (ECC)*, pp. 1779–1784, IEEE, 1997. 24, 29, 32

[48] D. W. Rew, J. L. Junkins, and J.-N. Juang, "Robust eigenstructure assignment by a projection method-applications using multiple optimization criteria," *Journal of Guidance, Control, and Dynamics*, vol. 12, no. 3, pp. 396–403, 1989. 24

[49] J.-N. Juang, K. B. Lim, and J. L. Junkins, "Robust eigensystem assignment for flexible structures," *Journal of Guidance, Control, and Dynamics*, vol. 12, no. 3, pp. 381–387, 1989. 24, 28

[50] H. Wu, K. S. Tsakalis, and G. T. Heydt, "Evaluation of time delay effects to wide-area power system stabilizer design," *IEEE Transactions on Power Systems*, vol. 19, no. 4, pp. 1935–1941, 2004. 25, 36

[51] F. Milano and M. Anghel, "Impact of time delays on power system stability," *Circuits and Systems I: Regular Papers, IEEE Transactions on*, vol. 59, no. 4, pp. 889–900, 2012. 25

[52] B. Chaudhuri, R. Majumder, and B. C. Pal, "Wide-area measurement-based stabilizing control of power system considering signal transmission delay," *Power Systems, IEEE Transactions on*, vol. 19, no. 4, pp. 1971–1979, 2004. 25

[53] W. Yao, L. Jiang, J. Wen, Q. Wu, and S. Cheng, "Wide-area damping controller of facts devices for inter-area oscillations considering communication time delays," *IEEE Transactions on Power Systems*, vol. 29, no. 1, pp. 318–329, 2014. 25, 37

[54] S. Zhang and V. Vittal, "Design of wide-area damping control robust to transmission delay using μ-synthesis approach," in *IEEE PES General Meeting Conference & Exposition*, pp. 1–5, IEEE, 2014. 25, 37

[55] A. Andry, E. Shapiro, and J. Chung, "Eigenstructure assignment for linear systems," *IEEE transactions on aerospace and electronic systems*, vol. 19, no. 5, pp. 711–729, 1983. 27

[56] P. Saraf, R. Hadidi, and E. Makram, "Partial right eigenstructure assignment based mode selective damping in a power system," *2015 North American Power Symposium (NAPS)*, Oct 2015. 32

[57] T. H. S. Abdelaziz, "Parametric eigenstructure assignment using state-

derivative feedback for linear systems," *Journal of Vibration and Control*, vol. 18, no. 12, pp. 1809–1827, 2012. 32

[58] S. Chable, S. Mahieu, and C. Chiappa, "Design and optimisation of restricted complexity controller: A modal approach for reduced-order controllers," *European journal of control*, vol. 9, no. 1, pp. 39–47, 2003. 33, 38

[59] H. G. Far, H. Banakar, P. Li, C. Luo, and B.-T. Ooi, "Damping interarea oscillations by multiple modal selectivity method," *IEEE Transactions on Power Systems*, vol. 24, no. 2, pp. 766–775, 2009. 33

[60] I. Kamwa, A. Heniche, G. Trudel, M. Dobrescu, R. Grondin, and D. Lefebvre, "Assessing the technical value of facts-based wide-area damping control loops," in *IEEE Power Engineering Society General Meeting*, pp. 1734–1743, IEEE, 2005. 33

[61] Y. L. Gorrec, J.-F. Magni, C. Doll, and C. Chiappa, "Modal multimodel control design approach applied to aircraft autopilot design," *Journal of guidance, control, and dynamics*, vol. 21, no. 1, pp. 77–83, 1998. 38, 39

[62] B. Pal and B. Chaudhuri, *Robust control in power systems*. Springer Science & Business Media, 2006. 40

[63] P. Saraf, K. Balasubramaniam, R. Hadidi, and E. Makram, "Design of a wide area damping controller based on partial right eigenstructure assignment," *Electric Power Systems Research*, vol. 134, pp. 134–144, May 2016. 43, 46

[64] C. Zhu, M. Khammash, V. Vittal, and W. Qiu, "Robust power system

stabilizer design using h loop shaping approach," *Power Systems, IEEE Transactions on*, vol. 18, no. 2, pp. 810–818, 2003. 54

[65] B. Chaudhuri and B. C. Pal, "Robust damping of multiple swing modes employing global stabilizing signals with a tcsc," *Power Systems, IEEE Transactions on*, vol. 19, no. 1, pp. 499–506, 2004. 54

[66] B. Ramanathan and V. Vittal, "Small-disturbance angle stability enhancement through direct load control part i-framework development," *IEEE Transactions on Power Systems*, vol. 21, no. 2, pp. 773–781, 2006. 54

[67] D. Ke and C. Chung, "An inter-area mode oriented pole-shifting method with coordination of control efforts for robust tuning of power oscillation damping controllers," *Power Systems, IEEE Transactions on*, vol. 27, no. 3, pp. 1422–1432, 2012. 55

[68] J.-F. Magni, *Robust Modal Control®*. Springer Science & Business Media, 2012. 61, 63, 67

[69] J.-F. Magni, "A toolbox for robust modal control design (rmct)," *CACSD. Conference Proceedings. IEEE International Symposium on Computer-Aided Control System Design (Cat. No.00TH8537)*. 61, 63, 67

[70] J. Magni and A. Manouan, "Robust flight control design by eigenstructure assignment," in *Proc. of the IFAC Symposium on Robust Control, Rio de Janeiro, Brasil*, pp. 388–393, 1994. 63, 66

[71] R. Castellanos, A. Messina, and H. Sarmiento, "A μ-analysis approach to power system stability robustness evaluation," *Electric Power Systems Research*, vol. 78, no. 2, pp. 192–201, 2008. 75, 76

[72] M. Djukanovic, M. Khammash, and V. Vittal, "Application of the struc-

tured singular value theory for robust stability and control analysis in multimachine power systems. part-i: Framework development," *IEEE Transactions on Power Systems*, vol. 13, no. 4, pp. 1311–1316, 1998. 75, 76

[73] G. Ferreres and J.-M. Biannic, "Reliable computation of the robustness margin for a flexible aircraft," *Control Engineering Practice*, vol. 9, no. 12, pp. 1267–1278, 2001. 78

[74] P. M. Young and J. C. Doyle, "Computation of μ with real and complex uncertainties," in *Proceedings of the 29th IEEE Conference on Decision and Control*, pp. 1230–1235, IEEE, 1990. 78

[75] G. Ferreres, J. Biannic, and J.-F. Magni, "A skew mu toolbox (smt) for robustness analysis," in *2004 IEEE International Symposium on Computer Aided Control Systems Design*, pp. 309–314, IEEE, 2004. 78

A.IEEE 68 bus *base-case* system data

Bus no.	Initial bus voltage	Initial bus angle	P_g	Q_g	P_{load}	Q_{load}	Bus type
1	1.0634	7.1886	0	0	2.527	1.1856	3
2	1.0612	8.5706	0	0	0	0	3
3	1.0479	6.4222	0	0	3.22	0.02	3
4	1.034	7.5027	0	0	5	0.736	3
5	1.0338	8.3774	0	0	0	0	3
6	1.0342	8.9999	0	0	0	0	3
7	1.0291	6.9114	0	0	2.34	0.84	3
8	1.0311	6.4639	0	0	5.22	1.77	3
9	1.0441	3.7966	0	0	1.04	1.25	3
10	1.0375	11.182	0	0	0	0	3
11	1.0353	10.431	0	0	0	0	3
12	0.9603	10.378	0	0	0.09	0.88	3
13	1.0355	10.451	0	0	0	0	3
14	1.0345	8.7404	0	0	0	0	3
15	1.0285	7.1708	0	0	3.2	1.53	3
16	1.0412	8.1345	0	0	3.29	0.32	3
17	1.0452	6.9648	0	0	0	0	3
18	1.0448	6.3019	0	0	1.58	0.3	3
19	1.054	12.789	0	0	0	0	3
20	0.9937	11.588	0	0	6.8	1.03	3
21	1.0375	10.516	0	0	2.74	1.15	3
22	1.0532	15.086	0	0	0	0	3
23	1.0477	14.744	0	0	2.48	0.85	3
24	1.0461	8.1757	0	0	3.09	-0.92	3
25	1.0639	9.6436	0	0	2.24	0.47	3
26	1.0602	7.6868	0	0	1.39	0.17	3
27	1.049	6.1244	0	0	2.81	0.76	3
28	1.0534	10.106	0	0	2.06	0.28	3
29	1.052	12.688	0	0	2.84	0.27	3
30	1.0577	6.8518	0	0	0	0	3

Figure A.1.: Bus data

31	1.06	9.2447	0	0	0	0	3
32	1.052	11.494	0	0	0	0	3
33	1.057	7.9358	0	0	1.12	0	3
34	1.0657	2.9585	0	0	0	0	3
35	1.014	2.9166	0	0	0	0	3
36	1.0434	-0.3978	0	0	1.02	-0.1946	3
37	1.0294	-6.6793	0	0	60	3	3
38	1.0574	9.2134	0	0	0	0	3
39	1.0048	-8.3421	0	0	2.67	0.126	3
40	1.0657	14.947	0	0	0.6563	0.2353	3
41	0.9993	44.84	0	0	10	2.5	3
42	0.9991	39.616	0	0	1.5	2.5	3
43	1.0142	-7.5187	0	0	0	0	3
44	1.0136	-7.5503	0	0	2.6755	0.0484	3
45	1.0168	2.7999	0	0	2.08	0.21	3
46	1.0322	10.077	0	0	1.507	0.285	3
47	1.0752	7.2969	0	0	2.0312	0.3259	3
48	1.0763	8.9727	0	0	2.412	0.022	3
49	1.0105	13.357	0	0	1.64	0.29	3
50	1.0097	19.902	0	0	1	-1.47	3
51	1.0207	6.8256	0	0	3.37	-1.22	3
52	0.9931	39.555	0	0	24.7	1.23	3
53	1.045	10.852	2.5	0.6383	0	0	2
54	0.98	16.217	5.45	0.9506	0	0	2
55	0.983	18.023	6.5	1.1464	0	0	2
56	0.997	17.335	6.32	0.9037	0	0	2
57	1.011	16.66	5.052	1.4688	0	0	2
58	1.05	20.152	7	2.0445	0	0	2
59	1.063	22.582	5.6	0.8783	0	0	2
60	1.03	16.054	5.4	-0.2074	0	0	2
61	1.025	19.173	8	-0.0461	0	0	2
62	1.01	15.949	5	0.0941	0	0	2
63	1	18.317	10	-0.3645	0	0	2
64	1.0156	4.8734	13.5	2.4363	0	0	2
65	1.011	0	36.365	9.2781	0	0	1
66	1	46.375	17.85	0.6926	0	0	2
67	1	40.476	10	0.6617	0	0	2
68	1	46.496	30	4.739	0	0	2

Figure A.2.: Bus data continued

From bus	To bus	R	X	B
36	37	0.0005	0.0045	0.32
49	52	0.0076	0.1141	1.16
16	19	0.0016	0.0195	0.304
16	21	0.0008	0.0135	0.2548
21	22	0.0008	0.014	0.2565
22	23	0.0006	0.0096	0.1846
23	24	0.0022	0.035	0.361
16	24	0.0003	0.0059	0.068
2	25	0.007	0.0086	0.146
25	26	0.0032	0.0323	0.531
17	27	0.0013	0.0173	0.3216
26	27	0.0014	0.0147	0.2396
26	28	0.0043	0.0474	0.7802
26	29	0.0057	0.0625	1.029
28	29	0.0014	0.0151	0.249
1	30	0.0008	0.0074	0.48
9	30	0.0019	0.0183	0.29
9	30	0.0019	0.0183	0.29
30	31	0.0013	0.0187	0.333
1	31	0.0016	0.0163	0.25
30	32	0.0024	0.0288	0.488
32	33	0.0008	0.0099	0.168
33	34	0.0011	0.0157	0.202
34	36	0.0033	0.0111	1.45
9	36	0.0022	0.0196	0.34
9	36	0.0022	0.0196	0.34
16	17	0.0007	0.0089	0.1342
31	38	0.0011	0.0147	0.247
33	38	0.0036	0.0444	0.693
41	40	0.006	0.084	1.5
48	40	0.002	0.022	1.28
42	41	0.004	0.06	2.25
52	42	0.004	0.06	2.25
37	43	0.0005	0.0276	0

Figure A.3.: Line data

39	44	0	0.0411	0
43	44	0.0001	0.0011	0
35	45	0.0007	0.0175	1.39
39	45	0	0.0839	0
44	45	0.0025	0.073	0
38	46	0.0022	0.0284	0.43
1	47	0.0013	0.0188	1.31
47	48	0.0025	0.0268	0.4
47	48	0.0025	0.0268	0.4
46	49	0.0018	0.0274	0.27
45	51	0.0004	0.0105	0.72
50	51	0.0009	0.0221	1.62
17	18	0.0007	0.0082	0.1319
3	18	0.0011	0.0133	0.2138
1	2	0.0035	0.0411	0.6987
2	3	0.0013	0.0151	0.2572
3	4	0.0013	0.0213	0.2214
4	5	0.0008	0.0128	0.1342
5	6	0.0002	0.0026	0.0434
6	7	0.0006	0.0092	0.113
5	8	0.0008	0.0112	0.1476
7	8	0.0004	0.0046	0.078
8	9	0.0023	0.0363	0.3804
6	11	0.0007	0.0082	0.1389
10	11	0.0004	0.0043	0.0729
10	13	0.0004	0.0043	0.0729
4	14	0.0008	0.0129	0.1382
13	14	0.0009	0.0101	0.1723
14	15	0.0018	0.0217	0.366
15	16	0.0009	0.0094	0.171
1	27	0.032	0.32	0.41
50	52	0.0012	0.0288	2.06
2	53	0	0.0181	0
6	54	0	0.025	0
10	55	0	0.02	0
19	56	0.0007	0.0142	0
20	57	0.0009	0.018	0
22	58	0	0.0143	0

Figure A.4.: Line data continued

23	59	0.0005	0.0272	0
25	60	0.0006	0.0232	0
29	61	0.0008	0.0156	0
31	62	0	0.026	0
32	63	0	0.013	0
36	64	0	0.0075	0
37	65	0	0.0033	0
41	66	0	0.0015	0
42	67	0	0.0015	0
52	68	0	0.003	0
19	20	0.0007	0.0138	0
35	34	0.0001	0.0074	0
12	11	0.0016	0.0435	0
12	13	0.0016	0.0435	0

Figure A.5.: Line data continued

Exciter type	Machine no.	Tr	KA	TA	Tb	Tc	Vrmax	Vrmin
0	1	0	100	0.01	0	0	5	-5
0	2	0	100	0.01	0	0	5	-5
0	3	0	100	0.01	0	0	5	-5
0	4	0	100	0.01	0	0	5	-5
0	5	0	100	0.01	0	0	5	-5
0	6	0	100	0.01	0	0	5	-5
0	7	0	100	0.01	0	0	5	-5
0	8	0	100	0.01	0	0	5	-5
0	9	0	100	0.01	0	0	5	-5
0	10	0	100	0.01	0	0	5	-5
0	11	0	100	0.01	0	0	5	-5
0	12	0	100	0.01	0	0	5	-5
0	13	0	100	0.01	0	0	5	-5
0	14	0	100	0.01	0	0	5	-5
0	15	0	100	0.01	0	0	5	-5
0	16	0	100	0.01	0	0	5	-5

Figure A.6.: Exciter data

type	machine no.	Kpss	Tw	Tn1	Td1	Tn2	Td2	ymax	ymin
1	1	80	10	0.1	0.02	0.08	0.02	0.2	-0.05
1	2	80	10	0.08	0.02	0.08	0.02	0.2	-0.05
1	3	80	10	0.08	0.02	0.08	0.02	0.2	-0.05
1	4	80	10	0.08	0.02	0.08	0.02	0.2	-0.05
1	5	80	10	0.08	0.02	0.08	0.02	0.2	-0.05
1	6	50	10	0.1	0.02	0.1	0.02	0.2	-0.05
1	7	80	10	0.08	0.02	0.08	0.02	0.2	-0.05
1	8	80	10	0.08	0.02	0.08	0.02	0.2	-0.05
1	9	100	10	0.08	0.03	0.05	0.01	0.2	-0.05
1	10	80	10	0.1	0.02	0.1	0.02	0.2	-0.05
1	11	50	10	0.08	0.03	0.05	0.01	0.2	-0.05
1	12	80	10	0.1	0.02	0.1	0.02	0.2	-0.05

Figure A.7.: PSS data

turbine model	machine no.	speed set-point	1/R	Tmax	Ts	Tc	T3	T4	T5
1	1	1	20	1.1	0.2	0.1	0	2.5	8
1	2	1	20	1.1	0.2	0.1	0	2.5	8
1	3	1	20	1.1	0.2	0.1	0	2.5	8
1	4	1	20	1.1	0.2	0.1	0	2.5	8
1	5	1	20	1.1	0.2	0.1	0	2.5	8
1	6	1	20	1.1	0.2	0.1	0	2.5	8
1	7	1	20	1.1	0.2	0.1	0	2.5	8
1	8	1	20	1.1	0.2	0.1	0	2.5	8
1	9	1	20	1.1	0.2	0.1	0	2.5	8
1	10	1	20	1.1	0.2	0.1	0	2.5	8
1	11	1	20	1.1	0.2	0.1	0	2.5	8
1	12	1	20	1.1	0.2	0.1	0	2.5	8

Figure A.8.: turbine-governor data

svc no.	bus no.	svc base MVA	Bcvmax	Bcvmin	Kr	Tr	Tb	Tc
1	40	200	1	-1	10	0.02	0	0
2	50	200	1	-1	10	0.02	0	0

Figure A.9.: Static Var compensator data

B.Implementing controller design in PST

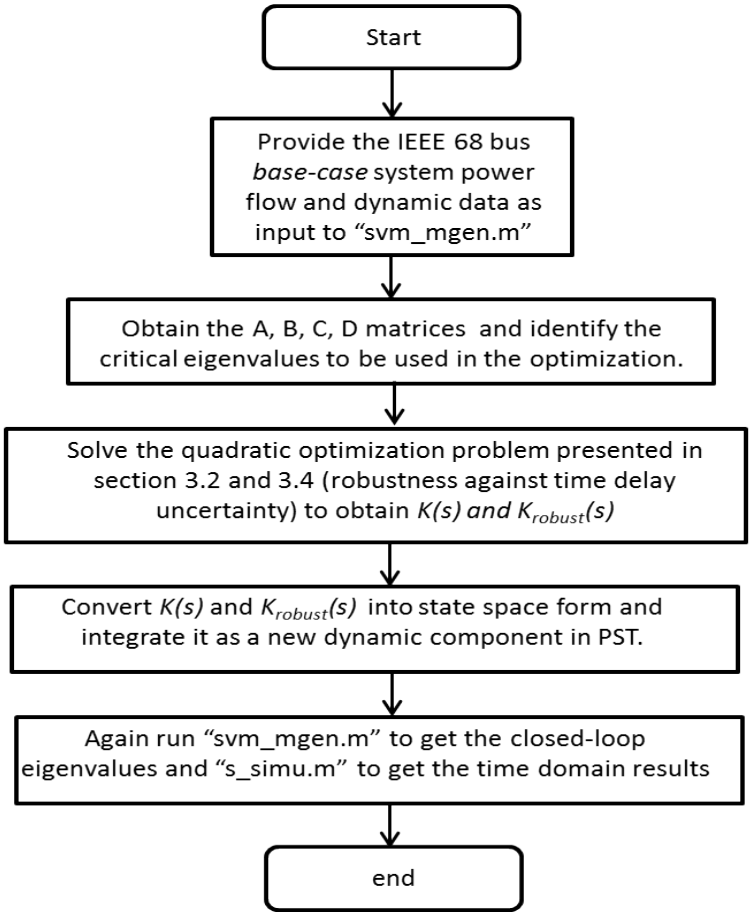

Figure B.1.: Flowchart representing the steps to be followed to obtain the controller

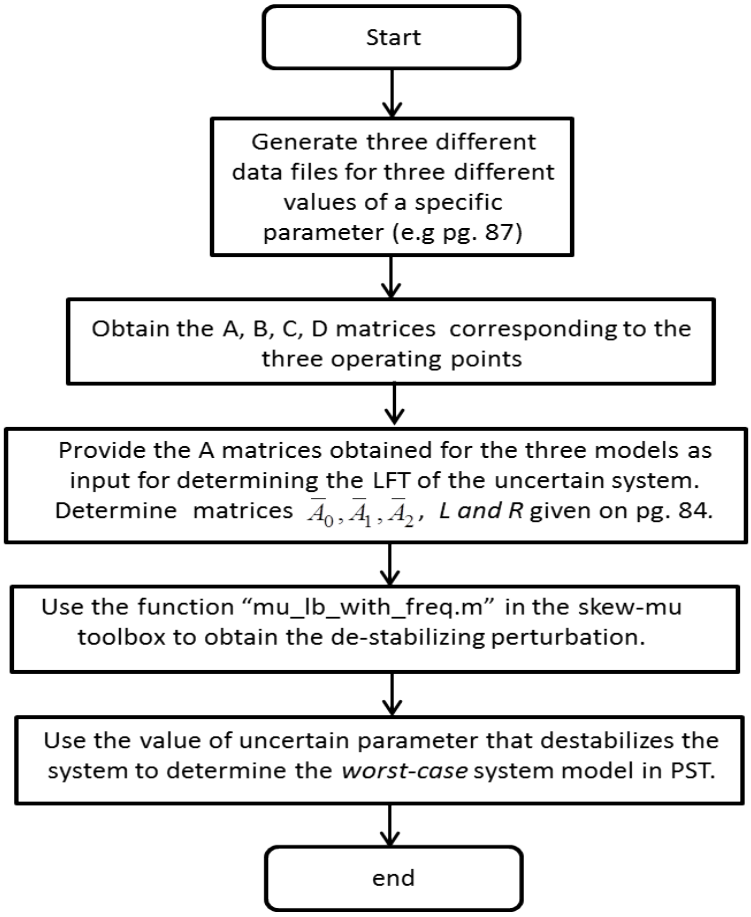

Figure B.2.: Steps to be followed to determine the *worst-case* model

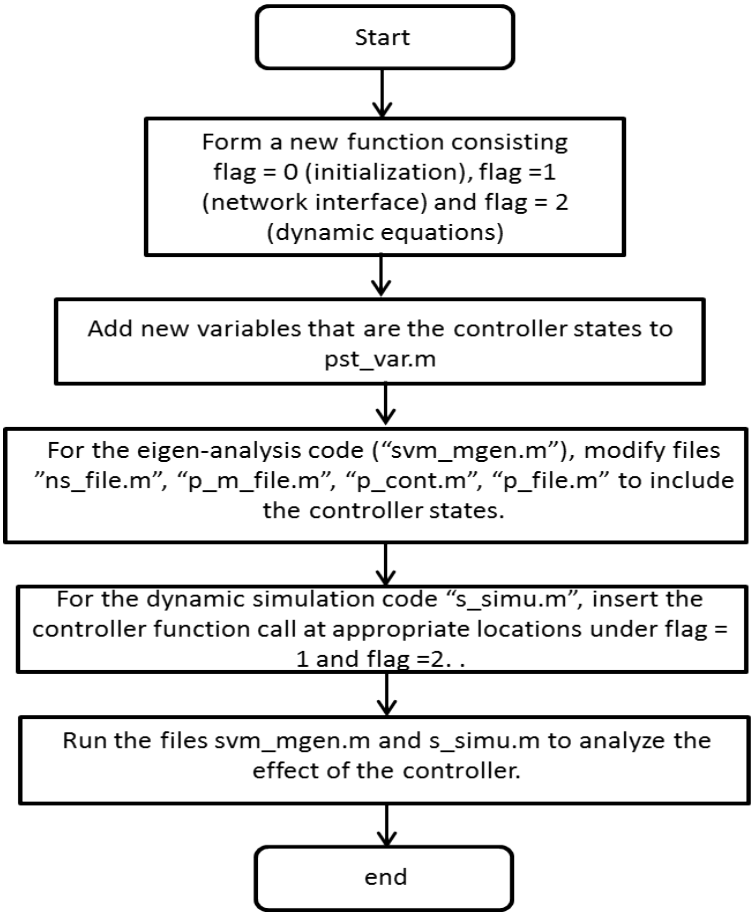

Figure B.3.: Adding the controller to PST